Univerzita Karlova v Praze
Matematicko-fyzikální fakulta

DIPLOMOVÁ PRÁCE

Helena Munzarová

Anisotropie svrchního pláště pod Severními Apeninami z dat mezinárodního experimentu RETREAT (Itálie)

Katedra geofyziky

Vedoucí diplomové práce: RNDr. František Gallovič, Ph.D.
Konzultant diplomové práce: RNDr. Jaroslava Plomerová, DrSc.

Studijní program: Geofyzika

Praha 2011

Charles University in Prague
Faculty of Mathematics and Physics

MASTER THESIS

Helena Munzarová

Anisotropy of the upper mantle under the Northern Apennines based on data from the international experiment RETREAT (Italy)

Department of Geophysics

Supervisor of the master thesis: RNDr. František Gallovič, Ph.D.
Consultant of the master thesis: RNDr. Jaroslava Plomerová, DrSc.

Study programme: Geophysics

Prague 2011

First of all, I would like to thank Jaroslava Plomerová who introduced me to the issue of seismic anisotropy. She was always determined to help me with emerging problems, to discuss them and to give me useful advice. Of course, I can't forget to thank her for the persistence, with which she read and corrected my English writing.

Further, I would like to thank Luděk Vecsey for pre-processing of the dataset and for his assistance while using softwares Autopick and Seismic Handler. I also express my thanks to Hanka Karousová for her great help with the part of the thesis concerning the seismic tomography, Jiří Bok for his constant readiness to help us resolving various difficulties with software, Vladislav Babuška and František Gallovič for the time spent by reading the thesis and for their useful comments.

Last but not least, I thank to my beloved family and to my dear Radek for their support.

I declare that I carried out this master thesis independently, and only with the cited sources, literature and other professional sources.

I understand that my work relates to the rights and obligations under the Act No. 121/2000 Coll., the Copyright Act, as amended, in particular the fact that the Charles University in Prague has the right to conclude a license agreement on the use of this work as a school work pursuant to Section 60 paragraph 1 of the Copyright Act.

In Prague, 28 July 2011 Helena Munzarová

Název práce: Anisotropie svrchního pláště pod Severními Apeninami z dat mezinárodního experimentu RETREAT (Itálie)

Autor: Helena Munzarová

Katedra / Ústav: Katedra geofyziky

Vedoucí diplomové práce: RNDr. František Gallovič, Ph.D.
Katedra geofyziky

Konzultant diplomové práce: RNDr. Jaroslava Plomerová, DrSc.
Geofyzikální ústav, Akademie Věd ČR

Abstrakt: V této diplomové práci zpracováváme data mezinárodního pasivního seismologického experimentu RETREAT (2003-2006) ve snaze přispět k poznání struktury svrchního pláště pod Severními Apeninami. V Severních Apeninách dochází k aktivní kolizi mezi Tyrhénskou a Adriatickou litosférickou deskou (zanořující se západním směrem). Kolize je doprovázená zpětným pohybem kolizního příkopu ve východním směru. Směrová závislost odchylek v časech šíření vln P, společně se změnami polarizací rychlých štěpených střižných vln indikují, že pozorovaná anisotropie seismických rychlostí je odrazem fosilní anisotropie uvnitř plášťové litosféry a anisotropie, vznikající v důsledku aktuálního tečení v astenosféře. Kontinentální Adriatickou desku je možné rozdělit přinejmenším na dvě oblasti s vlastní fosilní orientací anisotropní struktury. Rovněž jsme vyhodnocovali provázanost seismické anisotropie a heterogenit, zde reprezentovaných vysokorychlostní zanořující se Adriatickou deskou. Vyšetřování seismické anisotropie vyžaduje přesná měření časů příchodů prostorových vln. Poloautomatický program, který dokáže rychle a spolehlivě odečítat časy příchodů jednotlivých vln v rozsáhlých datových souborech, je nezbytným nástrojem nahrazujícím obvyklé manuální zpracování seismogramů. Na části dat získaných během experimentu RETREAT jsme proto otestovali a porovnali tři poloautomatické programy. Software *Autopick* byl vyhodnocen jako nejvhodnější a použili jsme ho ke změření časů příchodu vln P z kompletního souboru dat experimentu RETREAT.

Klíčová slova: anisotropie rychlostí seismických vln; prostorové vlny; svrchní plášť; Severní Apeniny; poloautomatický program na měření časů příchodu seismických vln

Title: Anisotropy of the upper mantle under the Northern Apennines based on data from the international experiment RETREAT (Italy)

Author: Helena Munzarová

Department: Department of Geophysics

Supervisor of the master thesis: RNDr. František Gallovič, Ph.D.
Department of Geophysics

Consultant of the master thesis: RNDr. Jaroslava Plomerová, DrSc.
Institute of Geophysics, Czech Academy of Sciences

Abstract: In this master thesis, we process data recorded during the passive seismic experiment RETREAT (2003-2006) in the Northern Apennines with the aim to explore the upper mantle structure in the region. Active orogeny in the Northern Apennines relates to the collision of the Tyrrhenian and Adriatic (subducting westward) plates and is accompanied by an eastward retreat of the trench. Directional dependences of P-wave travel-time deviations together with variations of the fast split polarization azimuths of teleseismic SKS waves are derived from data recorded during experiment RETREAT. Both the fossil anisotropic structure in the mantle lithosphere and the anisotropy due to the present-day flow in the sub-lithospheric mantle are sources of the observed velocity-anisotropy patterns. Thick continental Adriatic plate can be divided into at least two sub-regions with their own fossil fabrics. We have also tried to evaluate effects of the well known trade-off between large-scale anisotropy derived from body-wave anisotropic parameters and a heterogeneity represented here by the high-velocity subducting Adriatic slab. Investigation of seismic anisotropy of the upper mantle requires precise measuring of teleseismic body-wave arrival times. A (semi-)automatic software (picker) for a fast and reliable processing of extensive datasets is a welcome alternative to a standard manual picking procedure. Therefore, we tested three semi-automatic pickers on subsets of the RETREAT data and selected the most precise and effective picker, the Autopick software, to measure the P-wave arrival times for the whole RETREAT dataset.

Keywords: velocity anisotropy; seismic body waves; upper mantle; Northern Apennines; semi-automatic picking software

Contents

Preface

Detailed analysis of the upper mantle structure, based on deviations of teleseismic body-wave propagation, requires a high-quality processing of a large number of data. In this study we evaluate data recorded during the passive seismic experiment RETREAT in the Northern Apennines and explore the upper mantle structure in the region of colliding Tyrrhenian and Adriatic plates.

The presented thesis consists of two parts. Part I deals with evaluating body-wave anisotropy and inferring the upper mantle structure beneath the Northern Apennines. Part II is devoted to application and testing of three different semi-automatic softwares to measure arrival times recorded by an array of seismic stations and benefits partly from results of a bachelor thesis of Munzarová (2009). The P-wave travel-time deviations represent crucial material for detailed analysis of lateral changes of anisotropic structure of the mantle lithosphere and for a joint interpretation along with the shear-wave splitting analysis.

PART I

Anisotropy of the upper mantle beneath the Northern Apennines

I.1. Introduction

I.1.1. Seismic anisotropy

Seismic anisotropy is inherent physical property of rock-forming minerals that influences all types of seismic waves - longitudinal (P), shear (S) and also surface (Love and Rayleigh) waves. In anisotropic media, velocities of seismic waves depend on direction of propagation and their polarization depends not only on the type of the wave but also on the local symmetry of anisotropic medium. Whereas in case of P waves, only the directional characteristics of recorded waves bring information about anisotropy, S waves provide another evidence of anisotropy - shear wave splitting. In isotropic material, only one shear wave propagating in a direction exists. As soon as the shear wave enters anisotropic medium, it splits into two quasi-shear waves with mutually perpendicular polarizations (Babuška and Cara, 1991).

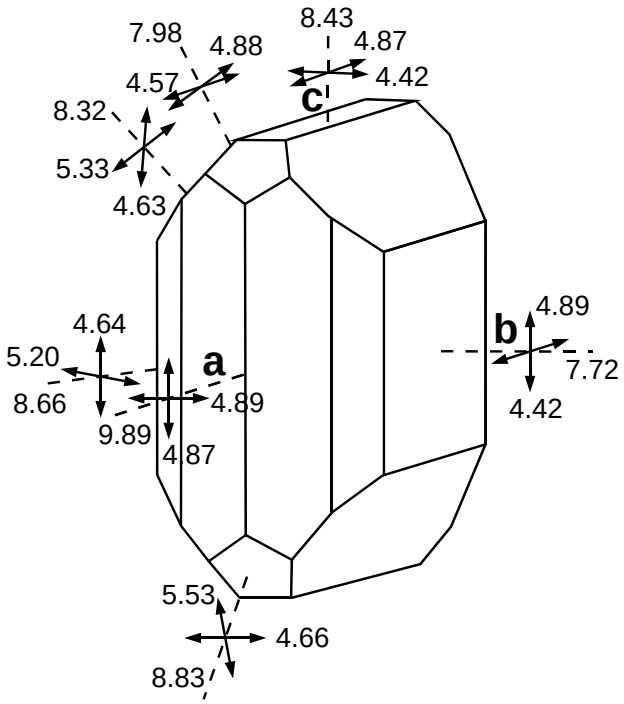

Figure I.1.1 Compressional and shear-wave velocities in a monocrystal of olivine (Kumazawa and Anderson, 1969; Babuška and Cara, 1991). The velocities are given in km/s and **a**, **b**, **c** are the crystallographic axes.

Anisotropy is generally caused either due to preferentially oriented isotropic heterogeneities (e.g., stack of isotropic layers, cracks potentially filled with fluid) or due to the preferred orientation of microscopic features in the material (intrinsic anisotropy). The effect of oriented isotropic heterogeneities can be found particularly in the crust, while the lattice preferred orientation (LPO) of mineral crystals,

especially olivine (*Fig. I.1.1*), which is the dominant component of the Earth upper mantle rocks (~ 75%), is generally accepted as the principal cause of the observed anisotropy in the subcrustal lithosphere (Babuška and Cara, 1991). The olivine crystals are of orthorhombic symmetry and the coefficients of anisotropy are about 25% and 22% for P- and S-waves, respectively. However, other minerals present in the upper mantle, such as pyroxene and garnet, which together with olivine form peridotite rock, have diluting effects on the overall upper-mantle anisotropy. Moreover, only a part of olivine crystals in the upper mantle is oriented in the same direction, therefore the overall large-scale anisotropy is not as strong as anisotropy of the pure olivine crystals (Christensen, 1984). Babuška et al. (1993) proposed two models of anisotropic symmetries of peridotite aggregate in the continental lithosphere on the basis of geological and petrological concepts:

- fabric with orthorhombic symmetry possessing the coefficients of anisotropy 9% and 4% for P- and S-waves, respectively
- fabric with hexagonal symmetry with low velocities along the symmetry axis and with P and S anisotropic coefficients equal to 5%.

I.1.2. Three-dimensional (3D) anisotropic models of the mantle lithosphere

The 3D modelling of seismic anisotropy of the continental mantle lithosphere has been developed in the Geophysical Institute in the 80' (Babuška et al., 1984a; 1984b; 1993; Babuška and Plomerová, 1992; 1993; Plomerová et al., 1996; Šílený and Plomerová, 1996). The research of seismic anisotropy, especially mapping lateral variations of its 3D orientation, found out that the mantle lithosphere consists of domains with differently oriented frozen-in anisotropic structures, often with plunging symmetry axes, that reflect preferred orientation of olivine created during an active stress field. Formation of frozen-in anisotropic fabric can be related to the stress field of the last mantle-lithosphere deformation (Silver and Chan, 1991; Savage, 1999) or it has preserved information about olivine preferred orientation formed in the stress field in time of the lithosphere origin (Babuška and Plomerová, 1989). Sharp boundaries between the domains, related to changes of anisotropic-symmetry orientation, suggest that the anisotropic fabric was formed during an original stage of formation of micro-continents. Processes like successive subductions and accretions of lithospheric fragments to a continental core may govern the observed anisotropic structure (Plomerová and Babuška, 2010). Seismic anisotropy thus represents an efficient tool for deciphering and understanding the development of continental lithosphere.

To model orientation of anisotropic symmetry in individual lithospheric blocks a great amount of high-quality data with a good azimuthal distribution of the earthquake foci is necessary. Therefore, passive seismic experiments with a dense station network covering a large area must be organized. Here, we

present examples of passive seismic experiments which the Geophysical Institute in Prague organized, cooperated or processed the acquired dataset during the last two decades. First of them was organized by co-operating Czech, French and Swedish scientific groups and took place in south-central Sweden in 1991 (Plomerová et al., 2001). The stations were installed on both sides of a prominent suture, the Protogine Zone, where standard tomography showed similar velocities in both lithospheric blocks. However, the 3D self-consistent anisotropic model, derived by inversion and joint interpretation of P-residual spheres and shear-wave splitting, revealed anisotropy with high-velocity foliation plane convergently dipping to the Protogine Zone in each lithospheric block and thus mapped the suture.

The next passive seismic experiment was organised in the Bohemian Massif in 1992 (Plomerová et al., 1998; Babuška and Plomerová, 2000; 2001). A 3D model with divergently dipping anisotropic structures of Saxothuringian and Moldanubian was suggested and a model of continental collision proposed. Furthermore, it was proved that studying only azimuthal instead of generally 3D oriented dependence of shear-wave splitting (Vinnik et al., 1994; Bormann et al., 1996; Brechner et al., 1998; Makeyeva et al., 1990) does not detect the boundary between divergently dipping structures in Saxothuringian and Moldanubian (Plomerová et al., 1998). This occurs because the average azimuths of the fast split shear waves are approximately parallel in both tectonic units.

Another experiment, MOSAIC (1998-1999), was deployed again in the Bohemian Massif and in other two Variscan massifs, namely the Armorican Massif (Judenherc et al., 2002) and the French Massif Central (Babuška et al., 2002). The results showed that each of the Variscan massifs is divided into at least two domains of the mantle lithosphere with differently oriented dipping anisotropic structures.

Two large international field measurements were organised within the EUROPROBE (ESF supported) program - the TOR experiment (1996-1997) focused on studying the lithospheric structure around the Trans European Suture Zone (TESZ) located in the north-western part of Europe, separating the Precambrian and Phanerozoic parts of Europe, and the SVEKALAPKO experiment (1998-1999) focused on the lithosphere structure of the Proterozoic and Archean units of the eastern part of the Fennoscandia (Bock and SSTWG, 2001). Modelling the seismic anisotropy around the TESZ delimited three lithospheric domains (Plomerová et al., 2002) which are in a remarkable agreement with the isotropic P-wave tomography (Gregersen et al., 2002) and the surface-wave modelling (Cotte et al., 2002).

All the field experiments mentioned above were deployed in stable Precambrian or Phanerozoic continental regions without any active subductions. Together with experiment RETREAT (field measurements: 2003-2006), held in the Northern Apennines in Italy, was great opportunity to test the method for determining the 3D anisotropic structures in the area with an active subduction (for details about the RETREAT experiment see *chapter I.2.*), where anisotropy due

to the present-day flow in the sub-lithospheric mantle can play more distinct role than in stable continental regions. Moreover, it is evident that modelling anisotropic structure of the upper mantle beneath the Northern Apennines will be more difficult than beneath the tectonically stable regions due to the distinct velocity heterogeneity (active subducting slab). The method applied to a geologically young region requires potential modifications with the aim to bring new information about forming the mantle lithosphere in active tectonic settings and to contribute to better understanding how the present-day continents were formed.

I.1.3. Geodynamic settings of the Northern Apennines

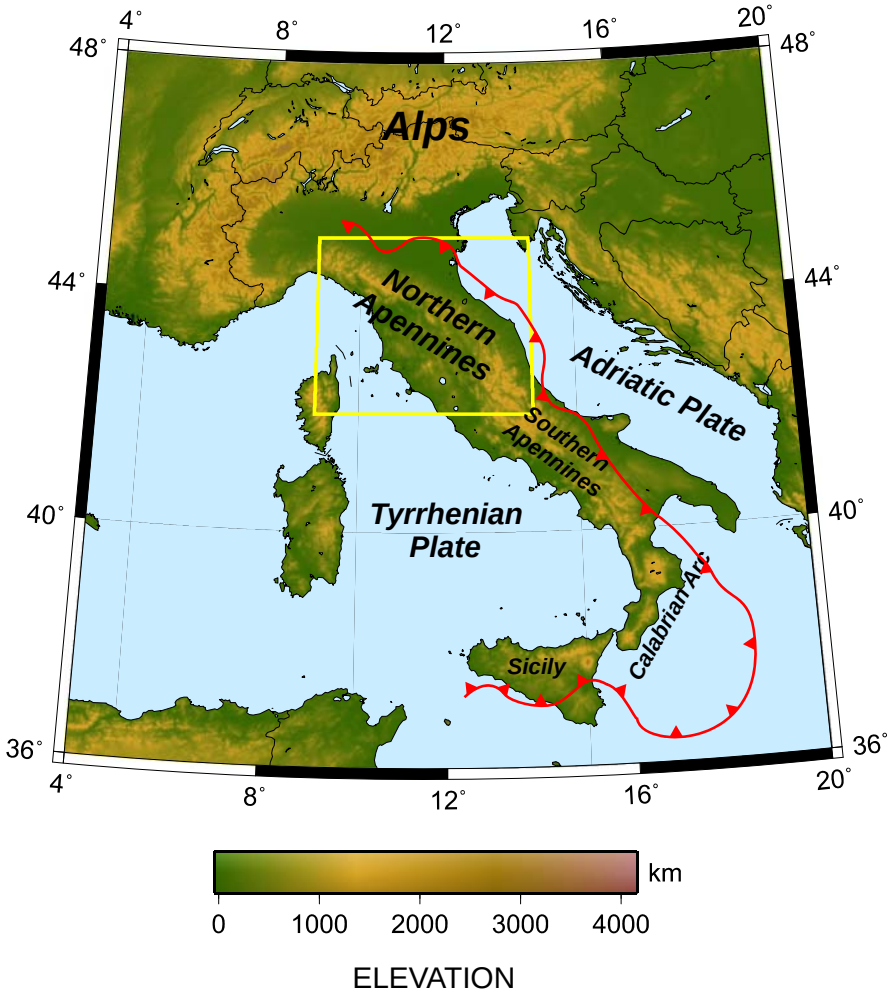

Figure I.1.2 Relief map of Italian peninsula and its surroundings, the approximate location of the main thrust front (red curved line; e.g., Benoit et al. 2011) associated with the convergence of the Adriatic and Tyrrhenian plates and the region of experiment RETREAT (yellow rectangle, in detail shown in *Fig. I.2.1*).

The Northern Apennines mountain belt is located in the central Mediterranean region (*Fig. I.1.2*). Its development started in the Late Cretaceous due to the slow collision of the African and the European plates (Stampfli and Borel, 2002) which

also led to westward subduction of the Adriatic and the Ionian microplates beneath the European plate (Doglioni, 1991). 35 My ago, a continuous trench oriented NE-SW, from the Ligurian region to the southern Iberia, was active (Dewey et al., 1989). It is estimated that rates as large as 5 cm/y occurred in the Apennines convergence zone during isolated periods during the last 30 My (Faccenna et al., 2003). From the Late Miocene, the trench geometry was strongly affected by development of the Tyrrhenian Basin where extensional process was initiated. Consequently, the Apennine orogeny started moving eastward and the slab rollback of the Adriatic subtucting plate begun (Faccenna et al., 2003). This movement of the contact between the retro-plate (Tyrrhenian plate) and the pro-plate (Adriatic plate) in the direction opposite to the subduction is often denoted as 'trench retreat'.

At present, the Apennines orogeny is separated into two main arcs - the Northern Apennines and the region beginning in the Southern Apennines, continuing to the Calabrian Arc and ending in the Sicily (see *Fig. I.1.2*). Whereas the Calabrian Arc has exhibited characteristics of an active subduction zone until present, e.g., volcanism (Aeolian Islands) and seismicity down to 600 km depth, in the Northern Apennines none of these two features is present. Serpelloni et al. (2005) estimates the convergent movement in the Northern Apennines of less than 1 mm/y. It may indicate that the subduction has stopped there. Other studies propose that some portions of the Apennines slab begun to detach from the surface plate (Wortel and Spakman, 2000).

The distribution of seismic anisotropy in the upper mantle, thickness of the crust and of the lithosphere, as well as the geometry of the Adriatic slab should help clarify mantle dynamics in the region. Previous profile measurements, the Northern Apennines Profile (NAP, 1994), held in the southern part of the RETREAT experiment showed orogen-parallel polarization of the fast split shear waves in the mountain crest that rotated to orogen-normal in the Tyrrhenian zone (Margheriti et al., 1996; 2003). This could imply 2D orogen-parallel sublithospheric flow beneath the Adriatic plate due to the slab rollback and orogen-normal flow beneath the Tyrrhenian plate associated with the extension in the back-arc basin (Park and Levin, 2002). Shear-wave splitting measurements from the RETREAT experiment after one year of its duration indicate different situation in the region located northward of the mentioned profile (Plomerová et al., 2006b). The orientation of the fast split-wave polarization, i.e., orogen-normal and orogen-parallel in the Adriatic and the Tyrrhenian plate, respectively, with visible dependence on back-azimuth does not permit the same explanation as in the southern part of the Northern Apennines, i.e., mantle anisotropy assigned exclusively to the mantle flow (Plomerová et al., 2006b; Margheriti et al., 2006). The different behaviour could be caused, e.g., by 3D mantle flow in this part of the Apennines or the splitting polarizations might reflect anisotropy in the mantle lithosphere instead of the mantle flow. The situation seems to be very complex in the Northern Apennines and analyzing the full dataset of the RETREAT experiment should bring detailed information about the region.

I.2. Passive seismic experiment RETREAT (Northern Apennines)

International passive seismic experiment RETREAT (REtreating-TRench, Extension and Accretion Tectonics) was held in the Northern Apennines (Italy) during the years 2003 and 2006 (http://earth.geology.yale.edu/RETREAT/). The RETREAT is a multidisciplinary project, in which the Geophysical Institute of the Czech Academy of Sciences (GFÚ AV ČR) cooperated with the Italian Istituto Nazionale di Geofisica e Vulcanologia (INGV, Rome), the Yale University and other institutions. The project was funded by the United States National Science Foundation (NSF), the INGV and the Grant Agency of the Czech Academy of Sciences (GAAV). The main goal of the RETREAT experiment is to develop our knowledge about the upper mantle beneath the Northern Apennines – crustal and lithospheric thicknesses, the location and geometry of the Adriatic slab, and the distribution of seismic anisotropy in the lithosphere and asthenosphere (Plomerová et al., 2006b; Margheriti et al., 2006).

I.2.1. Station array

Up to 50 seismic stations with three-component (NEZ) seismometers were deployed in stages during the experiment (*Fig. I.2.1* and *Attachment 1*). In October 2003, 10 portable broadband seismic stations (BARR, CSNR, MCUR – later moved to MASR, PIIR, RAVR, RSMR, SCUR, SFIR, VOLR and ZOCR) belonging to the seismic pool of the GFÚ AV ČR were installed in the region as a back-bone during the whole duration of the experiment. All the stations from GFÚ were equipped with an STS-2 broadband sensor and a GAIA data acquisition system (DAS, designed by GFÚ). Continuous data were recorded with 20Hz sampling frequency and with 100Hz in trigger mode. Besides the stations provided by GFÚ, medium period (5s sensor) and broadband (30s sensor) permanent stations of the Italian National Network (sampled at 100Hz) were included into the RETREAT array and together with the GFÚ stations formed a base of the array. In October 2004, 25 additional stations (ANZR, CAIR, CLLR, CORR, CRER, CSTR, CUTR, ELBR, FIRR, FOSR, GABR, GUSR, MNGR, MSTR, MTVR, PDCR, PIZR, PNTR, POPR, PRUR, PTCR, RONR, SASR, USOR and VRGR) from the IRIS PASSCAL Instrument Centre were deployed mostly in a narrow band perpendicular to the Northern Apennines mountain belt. Stations from the PASSCAL pool were equipped with the STS-2 or CMG-40T sensor and the REFTEK-130 DAS. The sampling frequency was 50Hz at all PASSCAL stations. Permanent broadband station VLC (STS-2 sensor, 20Hz sampling frequency) from the MedNet was also included in the array.

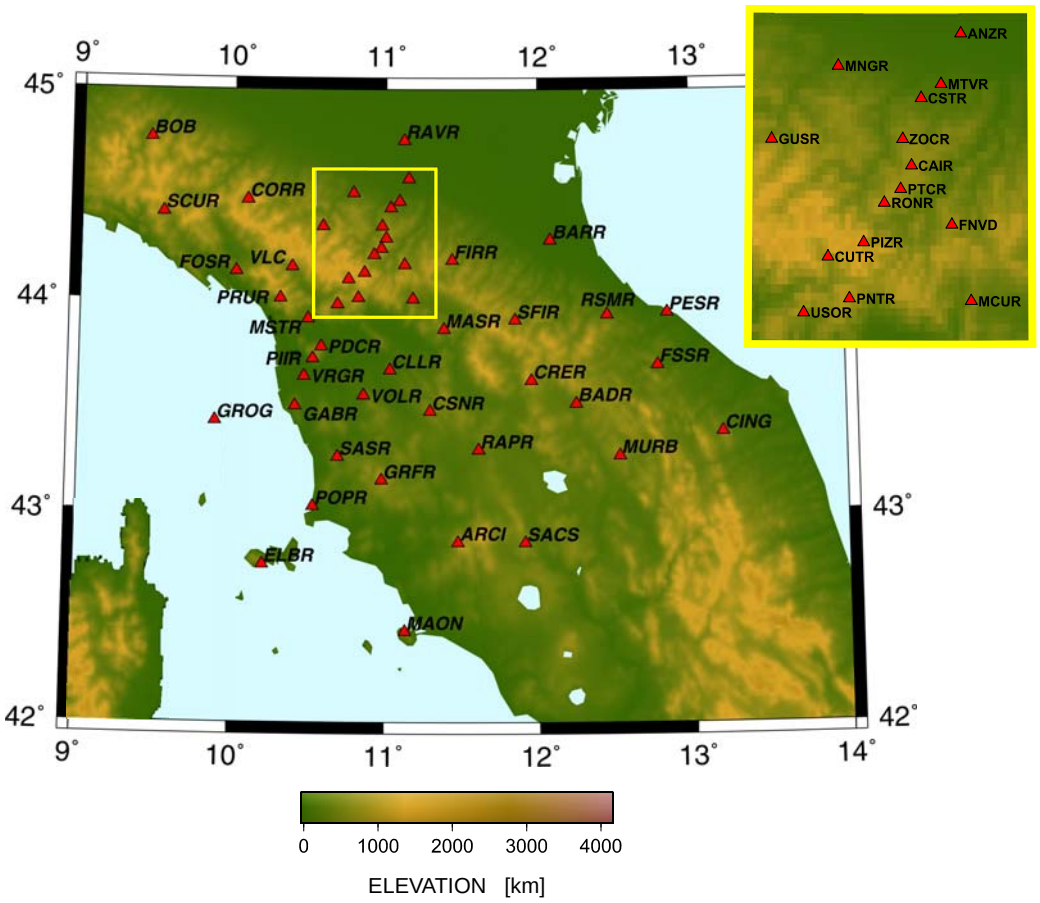

Figure I.2.1 Map of the RETREAT stations located in the Northern Apennines. For the location of the RETREAT region see *Fig. I.1.2*.

I.2.2. Data

Continual data, recorded during the three-year operation in the Northern Apennines, are stored in the IRIS data centre in miniseed format and can be provided to the scientific groups participating in the project. An event-oriented database, containing recordings of 938 teleseismic events, was created for the purpose of teleseismic tomography. The event-oriented database was restored to CMG-40T sensor response with 20Hz sampling frequency. The CMG-40T response is a broadband sensor characteristic which allows processing both the longitudinal and the shear phases.

In order to analyze the P-wave travel-time residuals from the RETREAT experiment, which is one of the main tasks of this study, we needed to pick the P wave arrival times (for details of picking procedure see *Part II*). Thus, we filtered the waveforms, contained in the event-oriented database, using the WWSSN-SP (World Wide Standard Station Network - Short Period) response with the corner frequencies 0.80Hz and 1.33Hz to magnify the 1Hz frequency corresponding to the P waves (Bormann, 2002). Hence, we had two different datasets (broadband CMG-40T and short period WWSSN). In case of longitudinal P waves, we processed

only the Z component of the three-component seismograms. We tested different picking procedures on the RETREAT dataset (see *Part II*). However, regardless of the picking method used, only about one third of the whole dataset of 938 events provided reliable measurements of the P-wave arrival times. *Fig. I.2.2* shows locations of 312 suitable events (see also *Attachment 2* for more information about the earthquakes). The P-arrival times were measured with the picker described in *chapter II.4.* The travel-time residuals derived from this set of measurements were used for analysis of the P-wave anisotropy in the region (see *chapter I.4.2.*).

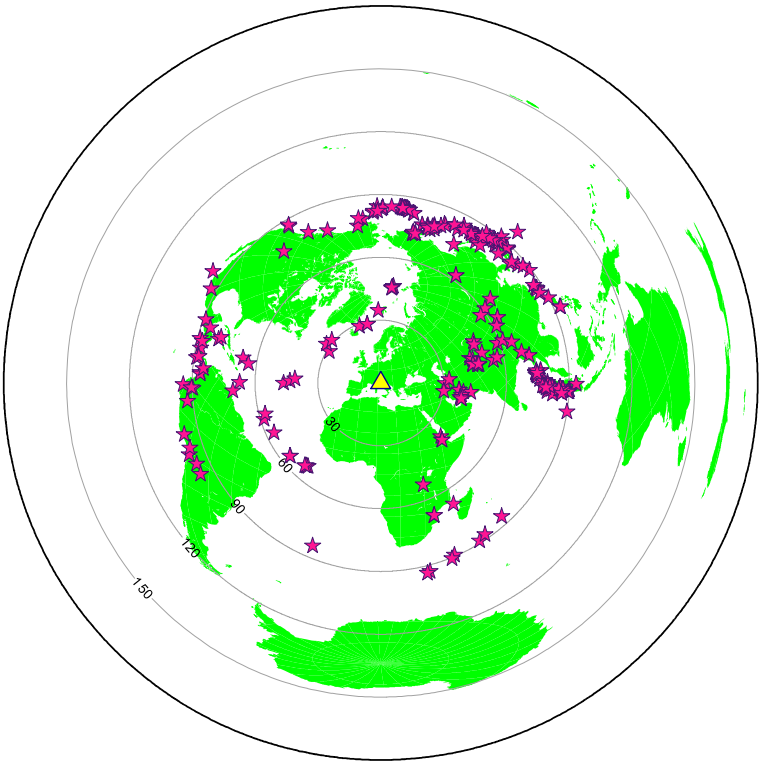

Figure I.2.2 Locations of 312 teleseismic earthquakes used for directional analysis of P-wave travel-time residuals.

I.3. Body-wave seismic anisotropy (Methods)

The shear-wave splitting (see *chapter I.3.2.*) is considered as a plausible evidence of seismic anisotropy in the medium. But both types of the body waves - longitudinal and shear waves - are affected by the anisotropic structures through which they propagate. Directional dependence of the P-wave travel-time residuals (see *chapter I.3.1.*) is not caused only by the velocity heterogeneities, which used to be considered as a unique source of dependence of P-wave velocity on direction of propagation, but also by the seismic velocity anisotropy which is present in the upper mantle (Christensen, 1984). Nevertheless, the trade-off between the heterogeneities and the anisotropy complicates the analysis of directional dependence of the P-wave travel-time residuals and it must be taken into account.

I.3.1. P-wave anisotropy

In early 80' Babuška et al. (1984a; 1984b) developed a set of programs for analysis of the travel-time residuals of P waves (Babuška et al.,; 1993; Babuška and Plomerová, 1992; 1993; Plomerová et al., 1996; Šílený and Plomerová, 1996). The programs are written in FORTRAN 77 and are intended to separate, in several successive steps, the isotropic part and the directionally dependent components of the relative travel-time residuals.

The input data file, entering into the travel-time residuals analyzing procedure, contains the P-wave arrival times measured at each station, where the quality of the recording enabled to pick the arrival time (for details about the picking procedure see *Part II*). The arrival times at individual stations are written successively for all measured earthquakes in the input data file and earthquake specifications (type of the wave; origin date and time; depth, latitude and longitude of the earthquake; and sum of stations with picked arrival times) are also added before the arrival times of respective event.

1) ***The first step – Absolute travel-time residuals*** $AbsRes_{ij}$

The absolute travel-time residuals $AbsRes_{ij}$ are computed according to formula

$$AbsRes_{ij} = O_{ij} - C_{ij} \tag{I.3.1}$$

where O_{ij} is the observed travel time, i.e., the difference between the arrival time measured on the seismogram and the origin time of the event, and C_{ij} is a calculated (theoretical) travel time according to a reference radial velocity model. Index i stands for a station and index j represents an event. In current version of the procedure, the calculated travel time C_{ij} is evaluated by a subroutine derived from program TTime with use of the IASP91 velocity model (Kennett, 1991). Corrections for the crust and the sediments are also applied (see *chapter I.4.1.*).

2) ***The second step – Clustering of events***

In this step, the events can be clustered according to epicentral distances and back-azimuths. To construct segments, we divide epicentral distances R and back-azimuths Baz into sections from $R_{\min}$ (usually 10º) to $R_{\max}$ (usually 100º) after R_{step} (usually 10º) and $Baz_{\min}$ (0º by default) to $Baz_{\max}$ (360º by default) after Baz_{step} (usually 20º). Each segment is defined by the epicentral distance and the back-azimuth of its centre relative to the centre of the array. The clustering of events helps balance the unequal distribution of the earthquake foci (usually, majority of events from the NE; see *Fig. I.2.2*) and thus reach a more homogeneous azimuth-distance coverage of rays illuminating the studied volume.

3) ***The third step – Normalization*** $Norm_j$

In this step, a normalization value for each event is calculated as an average of the absolute residuals of the event. The normalization $Norm_j$ of the event (index j) is defined as

$$Norm_j = \frac{1}{N_{ref}} \sum_{i=1}^{N_{ref}} AbsRes_{ij} \qquad \text{(I.3.2)}$$

For the normalization we use the mean absolute residual computed either from all stations that recorded the event or from a subset of stations of the array represented by the high-quality and well distributed stations with the highest number of observations. N_{ref} is number of the reference stations.

The normalization value is calculated to eliminate effects from deeper mantle and focal areas, i.e., those originated out of the investigated volume beneath the array and assumed to influence all the teleseismic rays similarly.

4) ***The fourth step – Relative residuals*** $RelRes_{ij}$ **(*for event*) *or*** $RelRes_{ik}$ **(*for segment*)**

In the fourth step, a relative travel-time residual for each event/segment-station pair is determined.

$$\begin{aligned} RelRes_{ij} &= AbsRes_{ij} - Norm_j \\ RelRes_{ik} &= \sum_{j=1}^{Nk} RelRes_{ij} \end{aligned} \qquad \text{(I.3.3)}$$

Index k numbers the segments and N_k is number of events in the k-th segment. The effects from the deeper paths and source regions, including mislocations, are minimized by subtracting the normalization values from the absolute travel-time residuals.

5) ***The fifth step – Directional means*** $DirMean_i$ ***and Static terms***

In the fifth step, either a static term or a directional mean is computed from the relative residuals at each station. First, azimuthal means are calculated and then a representative value for each station as a mean from them is evaluated. This step and the next one should suppress the uneven distribution of foci/segments. The static terms are means calculated preferably from the steep rays and are used to estimate the lithosphere thickness. The directional mean $DirMean_i$ is defined as a mean regardless of epicentral distance and considered as a value quantifying the isotropic velocities below the station.

6) ***The sixth step – Directional terms*** $DirTerm_{ij}$ **(*for event*)** $DirTerm_{ik}$ **(*for segment*)**

In the sixth step, the directional terms $DirTerm_{ij}$ for each event/segment-station pair are calculated from the relative residuals $RelRes_{ij}$ by subtracting the directional mean of the station i.

$$\begin{aligned} DirTerm_{ij} &= RelRes_{ij} - DirMean_i \\ DirTerm_{ik} &= \sum_{j=1}^{Nk} DirTerm_{ij} \end{aligned} \qquad \text{(I.3.4)}$$

The directional terms express the directionally dependent components of the observed travel-time residuals.

7) ***The seventh step – P-residual spheres***

Finally, the smoothed directional terms at each station are visualized in a lower hemisphere stereographic projection (P sphere) as a function of azimuth and angle of propagation (measured from the vertical) within the mantle lithosphere. Positive directional terms (delayed arrivals relative to isotropic velocity) indicate low-velocity directions, while negative values (relatively early arrivals) signify high-velocity directions.

Distribution of P-sphere patterns can reveal consistent fabrics within the mantle lithosphere often extending over large continental provinces (e.g., Plomerová et al., 2001, 2002, 2006a; Babuška and Plomerová, 2006; Babuška et al., 2008; Eken et al., 2010). Directional variations of P-wave velocity below the stations, extracted from the P-wave travel-time residuals, provide complementary information to shear-wave splitting analysis.

I.3.2. Shear-wave anisotropy

I.3.2.1. Shear-wave splitting

The shear waves converted at the core-mantle boundary from the P waves, e.g., SKS, SKKS, PKS phases, travelling through isotropic medium should exhibit SV polarization, i.e., linear polarization in the Q-L plane of LQT ray-parameter coordinate system (L - longitudinal component in the ray direction; Q - component in the plane of the ray and perpendicular to L; T - component perpendicular to the plane of the ray). A general shear wave can be described in the LQT coordinate system according to Vecsey et al. (2008) as

$$Q_1(t) = A_0 f(t)$$
$$T_1(t) = B_0 f(t) \tag{I.3.5}$$

$Q_1(t)$ and $T_1(t)$ are two time dependent components of the shear wave in isotropic medium. $f(t)$ represents the time function of the signal. A_0 and B_0 are the amplitudes. In case of core-mantle refracted shear waves, the polarization is linear in the ray-path plane, therefore the T component is zero ($B_0 = 0$). While propagating through anisotropic medium, the shear wave splits into two quasi-shear waves with mutually perpendicular polarizations and different velocities, resulting in a time difference δt between the fast and slow waves at the end of the anisotropic region. Then, the Q and T components can be described as

$$Q_2(t) = A\cos\psi f(t) - B\sin\psi f(t-\delta t)$$
$$T_2(t) = A\sin\psi f(t) + B\cos\psi f(t-\delta t) \tag{I.3.6}$$

Coefficients A and B are

$$A = A_0\cos\psi + B_0\sin\psi$$
$$B = -A_0\sin\psi + B_0\cos\psi \tag{I.3.7}$$

The polarization ψ of fast split shear-wave is defined as an angle in the Q-T plane from the interval (0°; 360°) which is oriented downward. Geometrically, it is defined by two Euler angles φ (azimuth) and θ (inclination measured from the vertical Z axis oriented downward). For the definition of the angle ψ see also *Fig I.3.1*.

Different methods aim at evaluating splitting parameters - time difference δt and the fast shear-wave polarization ψ - from the three-component waveforms as a measure of anisotropy of a medium. The linearly polarized wave that propagated through the isotropic medium before entering the anisotropic region can be gained

by rotating the coordinate system in the Q-T plane by angle ψ and shifting the two shear-wave components in this coordinate system by δt .

Dealing with teleseismic shear waves passing through the anisotropic upper mantle, the dominant periods of the phases are about one order larger than the observed delay time δt (Vecsey et al., 2008). It means that the two split shear waves interfere and can not be separated in time easily. Thus, they exhibit elliptical polarization observed in the Q-T plane.

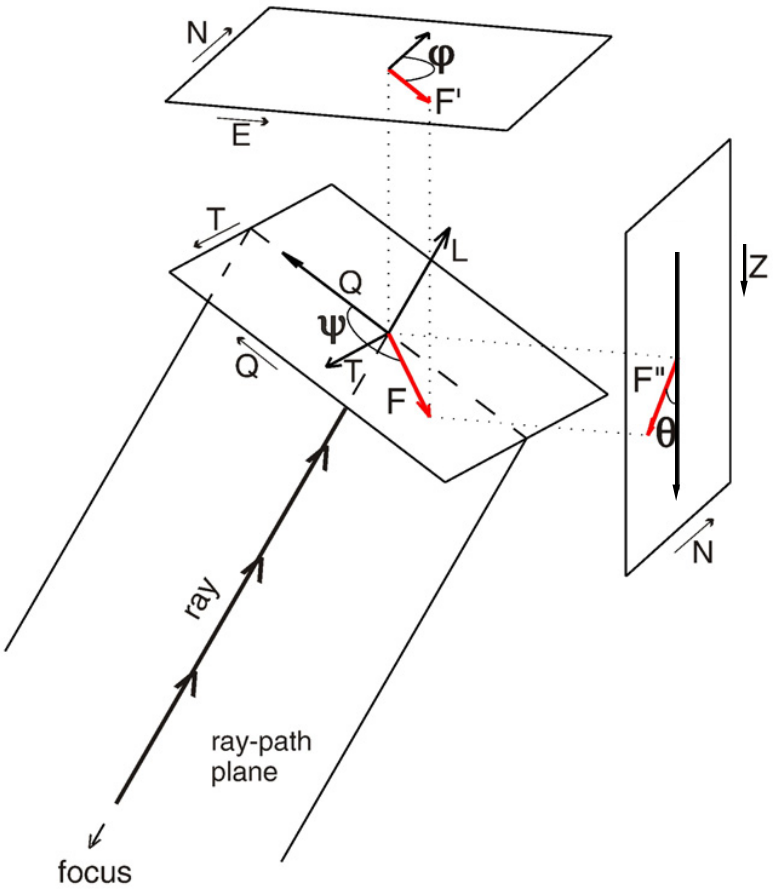

Figure I.3.1 Evaluation of shear-wave splitting in the ray-parameter coordinate LQT system (Vecsey et al., 2008). The fast polarization direction **F** lies in the Q-T plane and its orientation in this plane is given by polarization angle ψ measured from the Q axis. The polarization directions can be also given by two Euler angles - azimuth φ (measured from the N axis in the horizontal plane) and inclination θ (measured from the Z axis oriented downward in the vertical plane).

I.3.2.2. Different approaches and methods to evaluate splitting parameters

The polarization of the fast shear wave with nearly vertical incidence angle is often assumed to be in the horizontal plane. Horizontal polarization is directly associated with the direction of the fast olivine axis of a model mantle structure (see *chapter I.1.1.*). In case of horizontal symmetry axis, the direction of the fast split-wave polarization does not depend on back-azimuth which is not in agreement with numerous observations (Plomerová et al., 1998; Plomerová et al., 2001; Plomerová et al., 2006b; Eken et al., 2010). Therefore, two or more anisotropic layers with differently oriented horizontal fast symmetry axis were proposed in an attempt to explain the back-azimuth dependence of the fast shear waves (Silver and Savage, 1994). For applications of multi-layer anisotropic models with horizontally oriented fast symmetry axis in the shear-wave splitting studies see, e.g., Silver (1996), Savage (1999), Park and Levin (2002).

Models with inclined symmetry axes represent another approach to fit the azimuthal variations of the fast shear-wave polarization (Šílený and Plomerová, 1996). Moreover, anisotropic models with dipping symmetry axes generally oriented in 3D meet directional dependence of P waves, often expressed by bipolar P-residual pattern. Such a bipolar pattern is impossible to resolve with a multi-layer model of anisotropy with horizontal fast symmetry axis (Babuška et al., 1993; Plomerová et al., 1998).

In this work, we analyze the SKS splitting parameters evaluated by Salimbeni et al. (2008) and discuss them along with the directional dependence of P-wave travel-time residuals in the Northern Apennines (see *chapter I.4.*). To evaluate the splitting parameters, Salimbeni et al. (2008) uses the computer code SPLITshear written by Luděk Vecsey (GFÚ) available at http://www.ig.cas.cz/en/personal-pages/ludek-vecsey/split.

The SPLITshear code (Vecsey et al., 2008) allows to evaluate the splitting parameters, i.e., delay time δt between the fast and slow split waves and the fast polarization direction ψ sought generally in the ray-normal plane (Q-T plane), by three different methods - the cross-correlation method (Ando, 1984; Levin et al., 1999), the eigenvalue method (Silver and Chan, 1991) and the transverse minimization (Savage and Silver, 1993). The first two methods are based on the similarity between the fast and slow components of the waveform in weakly anisotropic medium and is applicable to SKS and S waves which are linearly polarized before arriving into the anisotropic region. On the contrary, the second method can be applied only to SKS waves because the method assumes a linear polarization in the ray-path plane before the wave enters the anisotropic medium - no energy on the T component.

A misfit function can be computed for all possible angles and delay times for each of the three methods. The searched pair of splitting parameters ψ and δt is

retrieved at the minimum of the misfit function. The misfit function of the transverse energy-minimization method, which was used for evaluation of the splitting parameters (Salimbeni et al., 2008) and discussed in this work, corresponds to auto-correlation of the recovered T component at the bottom of the anisotropic layer. The minimum of the misfit corresponds to the minimum of energy on the T component of non split shear wave. Therefore, the transverse minimization is applicable only to core-mantle refracted waves.

The bootstrap method (Sandvol and Hearn, 1994) appears as the efficient method to estimate errors of the splitting parameters. It consists of multiple calculations of the splitting parameters from simulated data, i.e., original data mixed with different noise. Errors of the splitting parameters are calculated as standard deviations of the simulated data.

Joint interpretation of P-residual pattern (see *chapter I.3.1.*) and splitting parameters of the shear waves allows us to recover anisotropic structure of individual domains of the mantle lithosphere with symmetry axes generally oriented in 3D, assuming the structure is homogeneous within each domain (Šílený and Plomerová, 1996).

I.4. Anisotropy in the Northern Apennines (Results)

The main purpose of this work is to retrieve anisotropic structure in the upper mantle beneath the Northern Apennines, particularly in the mantle lithosphere. We work with P and SKS waves collected during passive seismic experiment RETREAT (see *chapter I.2.*) and analyze dependences of P-wave travel-time residuals and the fast shear-wave polarizations on back-azimuth and incidence angle at individual stations. The detailed P-wave residual analysis, results of which we interpret by the upper mantle structures, requires elimination (minimization) of effects originating in the crust. Thus, we applied crustal corrections to the P-wave travel-time residuals before the directional analysis itself (see *chapter I.4.1.*).

I.4.1. Crustal corrections

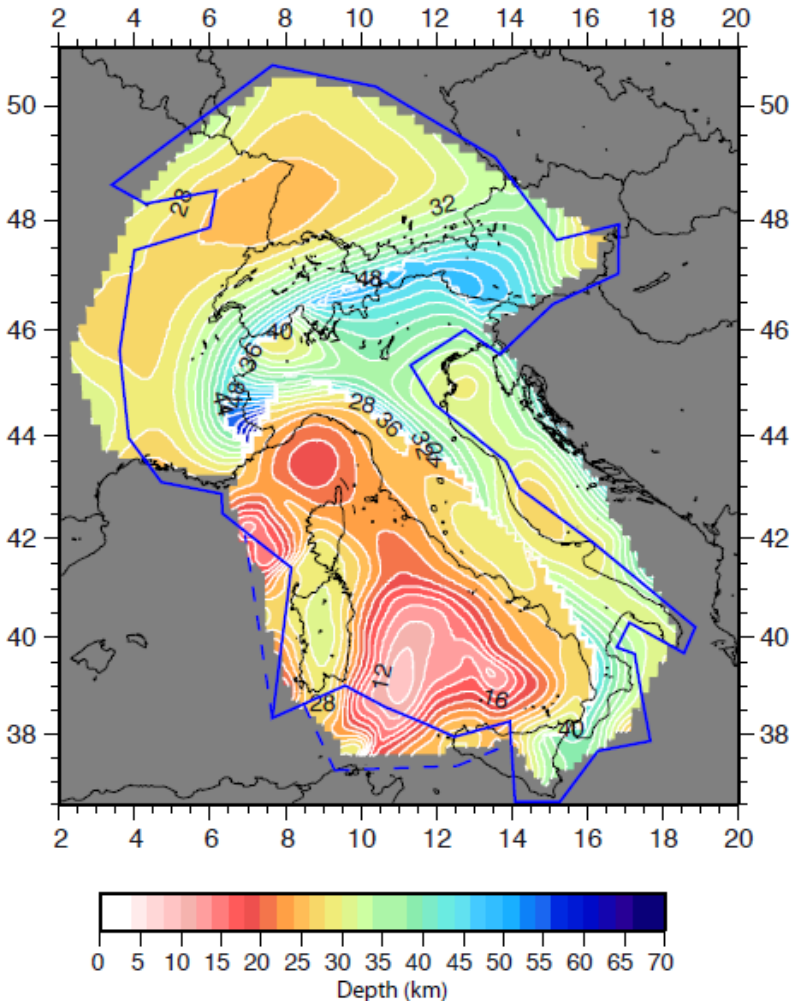

Figure I.4.1 Topography and contour lines (every 2 km depth) describing the Moho geometry of the European, Adriatic and Tyrrhenian plate units (Di Stefano et al., 2011).

Three lithospheric plates - the European, the Adriatic promontory of the African plate and the Tyrrhenian - collide beneath Italy and thus the geometry of the Moho discontinuity is complicated. Di Stefano et al. (2011) developed a new and original Moho map beneath Italy by integrating controlled-source seismic and teleseismic receiver function data (*Fig. I.4.1*).

There is a distinct sudden step in Moho depths beneath the Northern Apennines, where the RETREAT stations were deployed (*Fig. I.4.2*). The crust is very thin (~ 25 km) in the Tyrrhenian plate in the southwest, while to the northeast, in the Adriatic plate, the crust is thick (~ 45 km in the vicinity of the Moho step). Therefore, it was necessary to apply carefully the crustal corrections to remove the effects of the crust. With a permission of the authors, we use the crustal model by Di Stefano et al. (2011). We derived Moho depths beneath each station of the RETRAT array by linear interpolation of the values in the model grids neighbouring the stations. As an average velocity in the crust, we adopted values of 6.1 km/s and 6.2 km/s for the stations in the Tyrrhenian and the Adriatic plates, respectively.

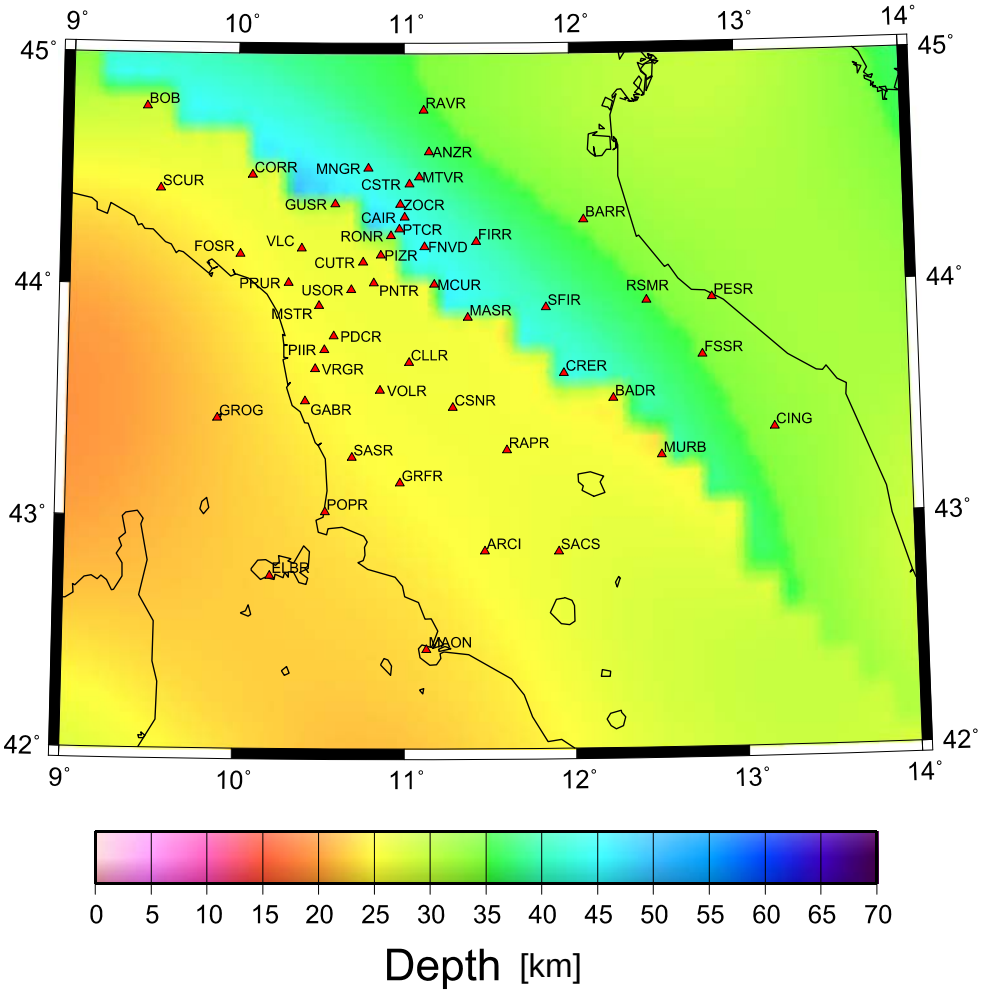

Figure I.4.2 Moho depths in the Northern Apennines, based on Di Stefano et al. (2011). Red triangles represent the RETREAT stations.

We had to pay special attention to the stations situated in a narrow band of approximately 50 km width above the Moho step. At these stations, the crustal corrections should differ for the rays coming from the southwest, passing through the thin Tyrrhenian crust, and from the northeast, propagating through the thick Adriatic crust. The step in the Moho depth directly affects stations as follows: BADR, BOB, CAIR, CORR, CRER, CUTR, FNVD, GUSR, MASR, MCUR, MURB, PIZR, PNTR, PTCR, RONR and ZOCR. We estimated strike of the boundary between the two plates from *Fig. I.4.2* at a range of 115° - 135°. The thicknesses of the two crusts as well as the corresponding velocities in the Tyrrhenian and the Adriatic plates, were determined for the stations named above.

I.4.2. Directional dependence of P-wave travel-time residuals

We measured arrival times of teleseismic P waves on the recordings of seismic experiment RETREAT (see *chapter I.2.*) with semi-automatic software Autopick (see *chapter II.4.*). The final dataset consists of 312 teleseimic events (see *Fig. I.2.2* and *Attachment 2)* which resulted in 7378 individual arrival-time measurements. We checked the time stability of the travel-time residuals at individual stations to prevent working with incorrectly recorded arrival times due to operation problems. We evaluated the directional terms of the P-wave travel-time residuals as described in *chapter I.3.1.*

The directional terms are directionally dependent components of the relative travel-time residuals normalized further to the station directional mean (see *chapter I.3.1)* and we show them in the lower hemisphere stereographic projection, i.e., the P-residual sphere (*Fig. I.4.3*). The outer circle of the spheres represent the incidence angle of 50°, which corresponds to angles of incidence at the Moho from epicentral distances of ~ 20°.

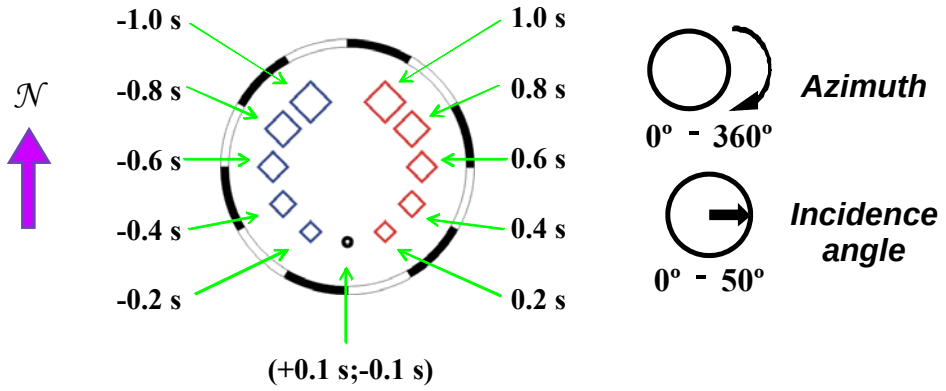

Figure I.4.3 Explanatory example of P-residual sphere imaging the directional terms of a station in lower-hemisphere stereographic projection.

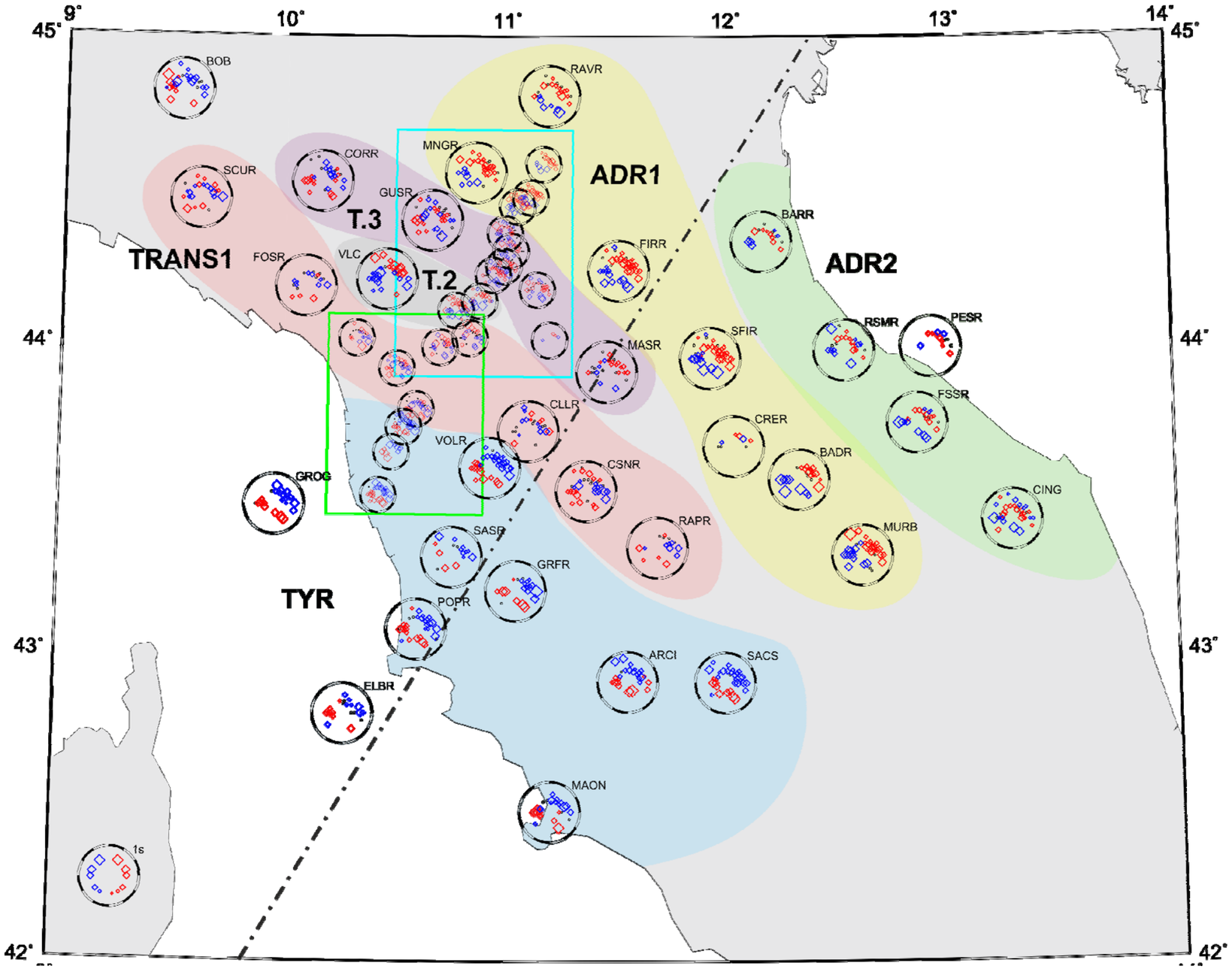

Figure I.4.4 a) Map of the RETREAT array with P-residual spheres at individual stations. Domains with similar P-sphere patterns are coloured. Two details (green and blue rectangles) are imaged in *Figs. I.4.4b* and *c*. Dot-and-dashed line indicates location of the vertical cross-section in *Fig. I.4.13*. **T.2** and **T.3** stand for **TRANS2** and **TRANS3**, respectively.

The directional terms are represented by a blue or red diamond of different size or a small black circle (see *Fig. I.4.3*). Blue colour stands for negative values, range of (-1.0 s; -0.1 s), while positive values are in red, range of (0.1 s; 1.0 s). Small black circles stand for the values around zero, range of (-0.1 s; 0.1 s). The size of the diamond is proportional to the value of the directional term. Negative directional terms (blue diamonds) indicate relatively early arrival times (high-velocity directions), while positive values (red diamonds) reflect relatively delayed arrival times (low-velocity directions). The high- or low-velocity directions relate to an isotropic velocity approximation in the upper mantle beneath each station represented by its directional mean.

To map the anisotropic structure of the upper mantle, we plot the P-residual spheres for the individual stations of the RETREAT array (*Fig. I.4.4*). Distribution of the diamonds in each sphere creates a pattern which varies across the array. Stations with a similar pattern form groups and divide the whole region into several domains with consistent P-sphere pattern in each of them.

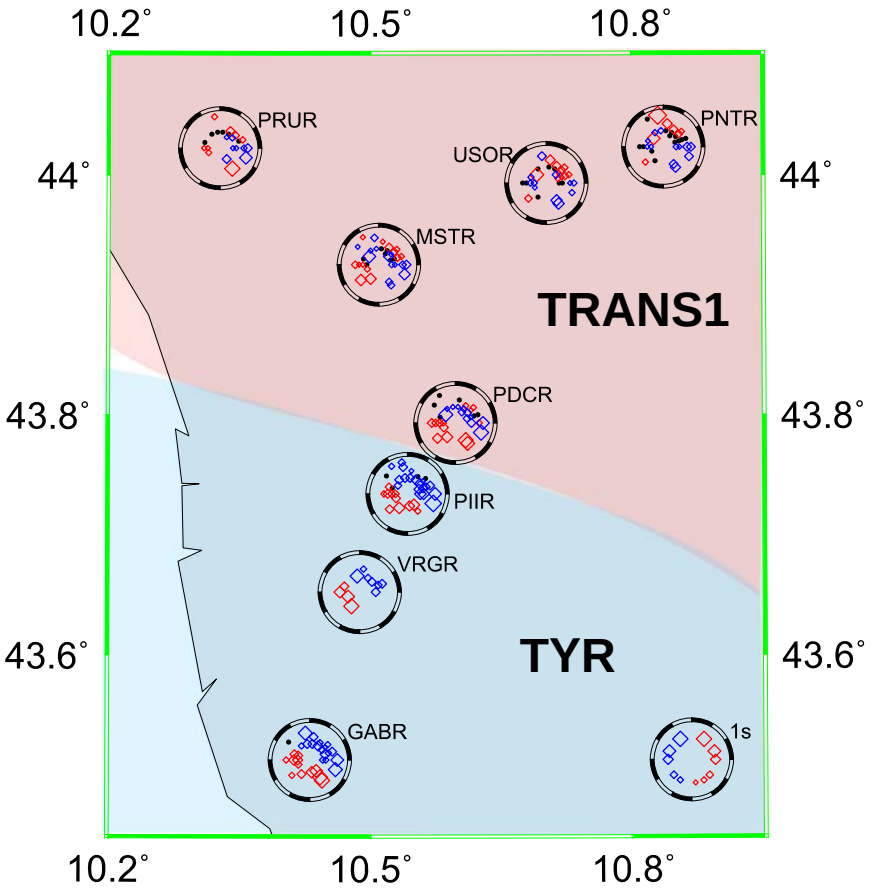

Figure I.4.4 b) Detail of the lower part of the dense station profile, located in *Fig. I.4.4a*, with P-residual spheres at individual stations. Domains with similar P-sphere patterns are coloured.

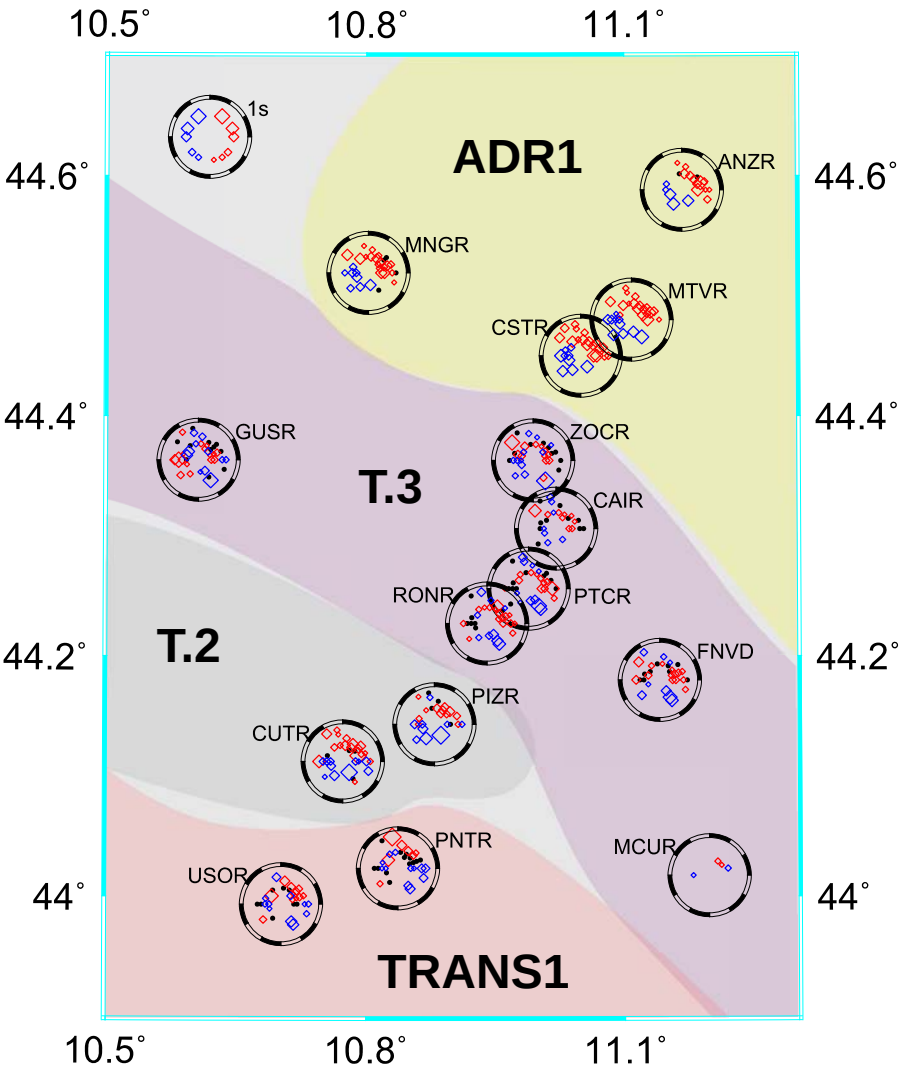

Figure I.4.4 c) Detail of the upper part of the dense station profile, located in *Fig. I.4.4a*, with P-residual spheres at individual stations. Domains with similar P-sphere patterns are coloured. **T.2** and **T.3** stand for **TRANS2** and **TRANS3**, respectively.

In the Tyrrhenian region, there is only one group of stations with similar P-sphere pattern - ARCI, ELBR, GABR, GRFR, GROG, MAON, PIIR, POPR, SASR, SACS, VOLR and VRGR. We denominate this domain as TYR (*Figs. I.4.4* and *I.4.5*). The directional terms of waves arriving from the SW are positive (red diamonds), while those arriving from the NE, they are negative (blue diamonds) in this domain. This means that the rays coming from the SW are relatively slower than those arriving from the NE. This characteristic type of P-sphere pattern - one half positive and one half negative - is called bipolar pattern.

In the Adriatic part of the RETREAT experiment, the situation is more complex. At some stations, the bipolar pattern is also obvious - ANZR, BADR, CSTR, FIRR, MNGR, MTVR, MURB, RAVR and SFIR. Station CRER is also close to this area but the measurements are scarce there, so it is impossible to assign

the CRER station to a domain. These stations form a narrow band (ADR1 domain) where the P-sphere pattern is clearly bipolar, but reverse in comparison with the pattern in the TYR domain (see *Figs. I.4.4* and *I.4.5*). The negative terms (blue) are in the SW and the positive terms (red) are on the other side of the P spheres, i.e., in the NE.

Stations in the most eastern part of the array - BARR, CING, FSSR, PESR and RSMR (ADR2 domain) have a similar pattern to the stations of the ADR1 domain. Waves from the SW are relatively fast (blue) and those from the NE are mostly slow (red). Nevertheless, the pattern in the ADR2 domain is not as clearly bipolar as the pattern in the TYR and ADR1 domains. There is a difference between the residuals for shallow and steep rays from the NE. The waves arriving at incidence angles around 30° from the NE are fast (blue), while the steeper rays from the NE azimuths are slow (red) at all the stations of the ADR2 domain. Though the directional distribution of the data is not very good for these stations (no rays from SE - SW at PESR and BARR), the P-sphere pattern is consistent across that domain.

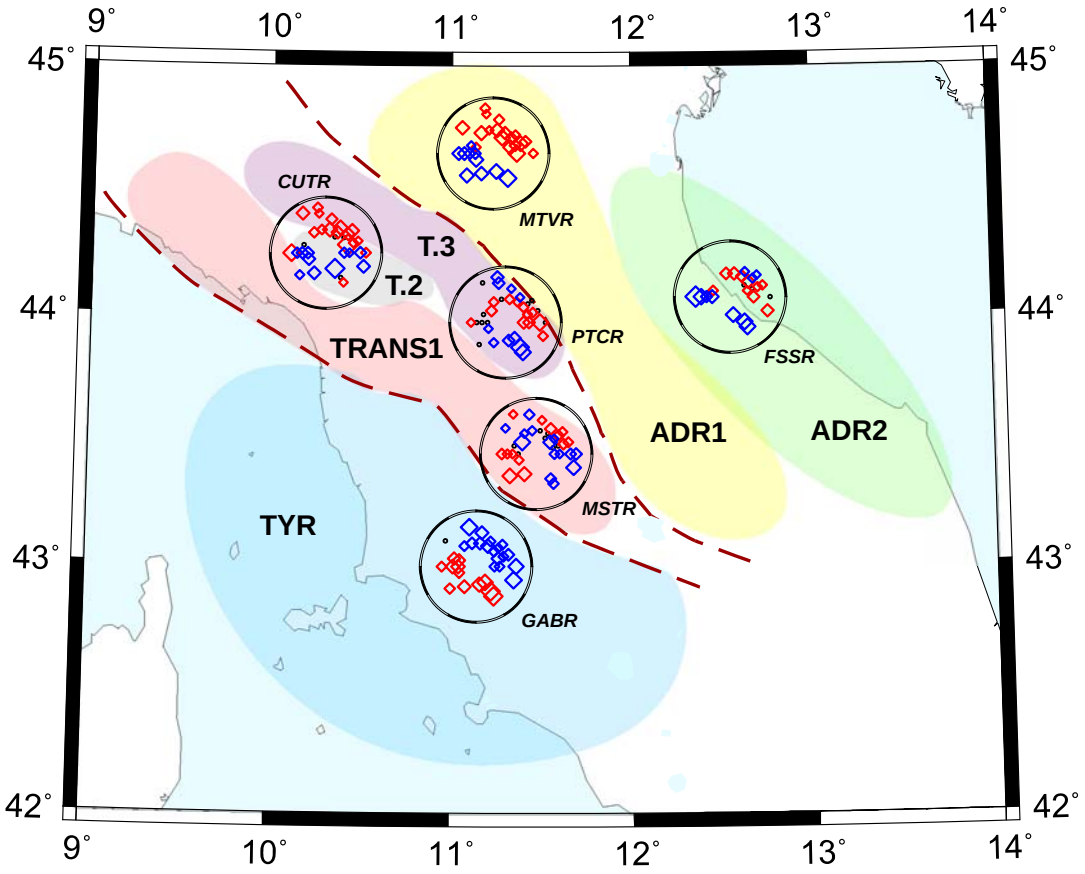

Figure I.4.5 Location of the six domains, derived according to the similarity of the P-sphere pattern at individual stations, with a characteristic P sphere representing each domain. The boundaries between the Tyrrhenian region, transitional zone and the Adriatic region are marked with dashed brown lines. **T.2** and **T.3** stand for **TRANS2** and **TRANS3**, respectively.

Approximately one half of the RETREAT stations lies in a transition zone between the TYR domain and the ADR1 and ADR2 domains in the Northern Apennines mountain range above the boundary between the Tyrrhenian and the Adriatic plates. The P-sphere pattern varies significantly from one station to another particularly when crossing the transition zone perpendicularly to the strike of the mountain chain. The stations near the western edge of the belt of the transition zone show slow propagations (red) from the SW and the NE, particularly for relatively shallow incidences, while the waves from the NW and SE are fast (blue) for all the incidence angles. Thus, we delimit a region (TRANS1 domain) corresponding to this P-sphere pattern - stations CLLR, CSNR, FOSR, MSTR, PDCR, PNTR, PRUR, RAPR, SCUR and USOR.

On the other side of the transition zone, the P-sphere pattern is approximately reversed in comparison with the pattern in the TRANS1 domain. The waves arriving at shallower incidences from the SW and the NE are fast (blue) and the waves from the rest of the directions are slow (red). Nevertheless, the pattern is not very consistent among the stations in this zone and changes rapidly. Stations CAIR, CORR, FNVD, GUSR, MASR, MCUR, PTCR, RONR and ZOCR are included in this domain which we call as TRANS3.

Four stations between the TRANS1 and TRANS3 domains yet remain unclassified. Station MCUR comprises very few data due to a very short period of registration of this station. On the other hand, the P-sphere pattern at stations CUTR, PIZR and VLC is very similar to the bipolar pattern at the ADR1 domain, i.e., fast from the SW and slow from the NE. We denote this domain as TRANS2. Surprisingly, the amplitudes in the P spheres of the TRANS2 domain are larger than those of the stations in theTRANS1 and TRANS3, where there are plenty of near zero values (black small circles).

We can see a transformation of the P-sphere pattern from the TYR bipolar to the ADR1 bipolar type, which are reversed, through the stations in the transition zone (see *Fig. I.4.5*). In the TRANS1 domain, the fast (blue) waves come from the NW, SE and steep incidences, while in the TYR domain, the ‘fast directions’ are moved more to the NE, involving the shallower incidences which become slow (red) in the TRANS1. In the TRANS2 domain, the ‘fast directions’ are shifted to the SW in comparison with the TRANS1 and form a very clear bipolar pattern. This trend seems to continue in the TRANS3. The relatively slow waves are shifted from the NE in the TRANS2 to the steeper incidences in the TRANS3 and fast waves arrive from the north and NE in the TRANS3. Further to the NE, in the Adriatic plate, the pattern of the ADR1 is again bipolar like in the TRANS2 domain.

I.4.3. Regional variations of SKS splitting parameters

Due to the trade-off between effects of heterogeneities and anisotropy, we analyse also results of the shear-wave splitting, whose appearance is considered as an undoubted proof of existence of anisotropy as the shear-wave splitting appears when shear-waves travel through an anisotropic medium. Therefore, analyzing splitting parameters (see *chapter I.3.2.*), along with the results from P-residual analysis (see *chapter I.3.1.*), is a very powerful tool to evaluate anisotropic properties of the Earth. Salimbeni et al. (2008) studied shear-wave splitting for 27 teleseismic earthquakes (see *Fig. I.4.6* and *Attachment 3*) recorded during the RETREAT experiment (see *chapter I.2.*). For each station-event pair, Salimbeni et al. (2008) determined the splitting parameters according to the method described in Šílený and Plomerová (1996) using the computer code SPLITshear written by Luděk Vecsey and available at http://www.ig.cas.cz/en/personal-pages/ludek-vecsey/split (see *chapter I.3.2.*).

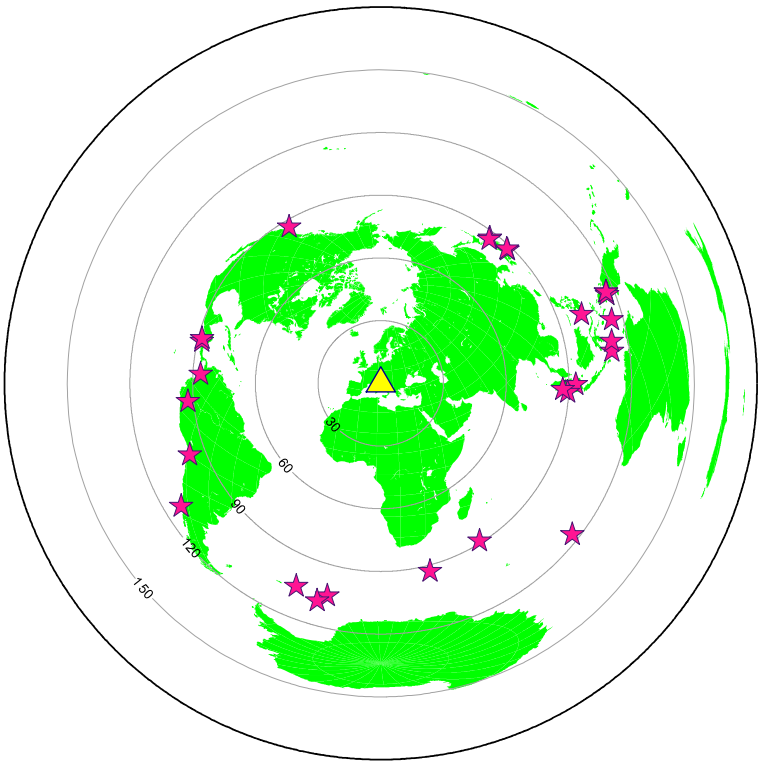

Figure I.4.6 Locations of 27 teleseismic earthquakes used for evaluation of SKS splitting parameters in Salimbeni et al. (2008).

Polarizations of the fast split shear waves (orientation of a bar) and the time difference between the fast and slow waves (length of a bar) evaluated by Salimbeni et al. (2008) are shown at piercing points of 80 km depth in *Fig. I.4.7*. Presentation of the fast shear-wave polarizations at piercing points attributes the anisotropy to a chosen depth and to the position with respect to the epicentre location. We

decided to show the polarizations at 80 km deep piercing points, in which we might expect the main sources of the observed anisotropy - sub-lithospheric mantle flow beneath the Tyrrhenian plate and mantle lithosphere in the Adriatic region. Thus, we can see how much the splitting parameters vary at individual stations and also whether they become consistent somewhere in the region.

We analyze the dependence of the fast shear-wave polarization azimuth on back-azimuth, therefore, we distinguish two intervals of back-azimuths with colours (red - waves from -45° to 135°; blue - waves from 135° to 315°) for a better azimuth distinction. The orientation of the boundary between the two intervals is parallel to the Northern Apennines mountain chain, which separates the Adriatic and the Tyrrhenian plates.

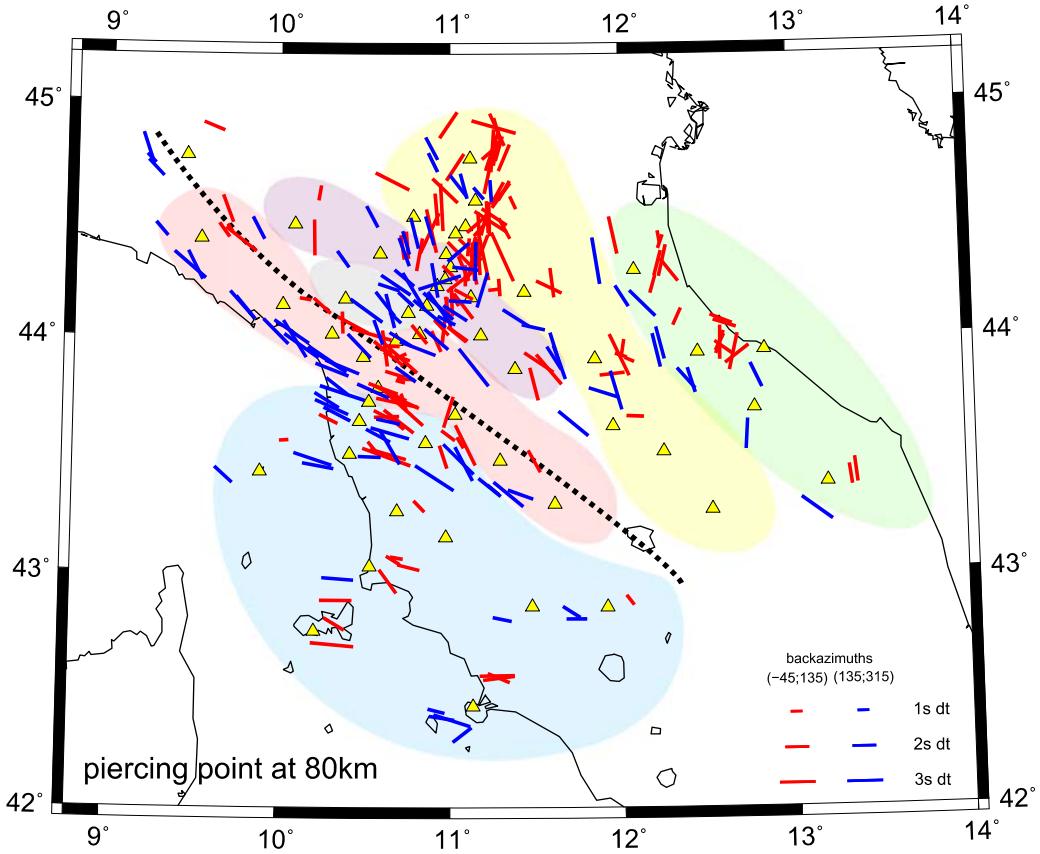

Figure I.4.7 Map of the splitting measurements for eastern (red) and western back-azimuths (blue), derived by Salimbeni et al. (2008). Individual measurements are represented with a line oriented in the direction of the fast-polarization azimuth and scaled with the delay time. The measurements are projected into piercing points at a depth of 80 km. Approximate boundary between the polarization azimuths independent of back-azimuth and those dependent on back-azimuth is shown by dotted black line. Six domains, derived according to the similarity of the P sphere pattern at individual stations, are coloured. Yellow triangles represent the stations.

The azimuths of the fast shear waves are dominantly NW-SE, in the Tyrrhenian region, and tend to E-W directions in its southernmost part. The fast-wave polarizations show no dependence on back-azimuth at individual stations and are very consistent in the Tyrrhenian region. The time differences vary in the range (0.6 s; 3.3 s) and the average value is 1.8 s (Salimbeni et al., 2008).

The fast-wave polarizations pertaining to the stations above the Adriatic plate are not as homogeneous as those in the Tyrrhenian region and the splitting parameters vary with back-azimuth. The red bars (for waves from the east and the northeast) are oriented predominantly in the N-S and NE-SW directions, while the blue bars (waves from the west and the southwest) are mostly oriented in the (N)NW-(S)SE directions. We can see a tendency of a slight clock-wise rotation of the fast-wave polarization azimuths from the stations located in the mountain range to those in the eastern Adriatic coast. The split delay times are similar both in the Adriatic and in the Tyrrhenian provinces.

According to the fast shear-wave polarization azimuths, the region of the RETREAT experiment can be roughly divided into two main domains - Tyrrhenian (very consistent polarization directions with back-azimuth) and the Adriatic (back-azimuth dependence of the polarizations), though, additional three sub-regions were delineated in the Adriatic province (Plomerová et al., 2006b). The P-residual analysis also identified at least six regions of the upper mantle beneath the Northern Apennines according to a consistent P-sphere pattern in each of them (see *chapter I.4.2.*). Finer clustering of the stations solely according to the splitting parameters is difficult also due to a smaller amount of data in comparison with the P-residuals. Therefore, we decided to analyze the splitting parameters separately in domains determined according to the P-sphere patterns (see *chapter I.4.2.).*

The general characteristic of the splitting parameters is the dependence of the fast shear-wave polarization azimuth on a back-azimuth. We show this dependence in *Fig. I.4.8* for each of the six domains defined from the P-sphere analysis. At first glance, the dependences for individual domains look very similar. There are two main groups of points which are totally separated one from the other. The dependence of the polarization azimuths on the back-azimuth becomes more and more complex while moving from the western domains to the eastern areas, particularly as far as the eastern back-azimuths are concerned.

The fast S-polarization azimuths (in full 0°-360° range) form two bands of points for each domain and they are separated by a broad empty band. We remind that the fast-polarization direction is evaluated in the Q-T plane and oriented downward (see *chapter I.3.2.1.*). Thus, there is the 180° interval for each back-azimuth, from which we cannot obtain an azimuth angle φ.

To emphasize variability of individual polarizations, we show also rose diagrams for all the six domains (*Fig. I.4.9*). To keep the full back-azimuth dependences, i.e., 0°-360°, the polarizations are divided into two groups according

to their back-azimuth, and thus, two rose diagrams are plotted for each domain. The left diagrams contain information for the back-azimuths from 210° to 30° and the right diagrams belong to the back-azimuths from 30° to 210°. The back-azimuth of 210° approximately separates the two groups of data points in *Fig. I.4.8*.

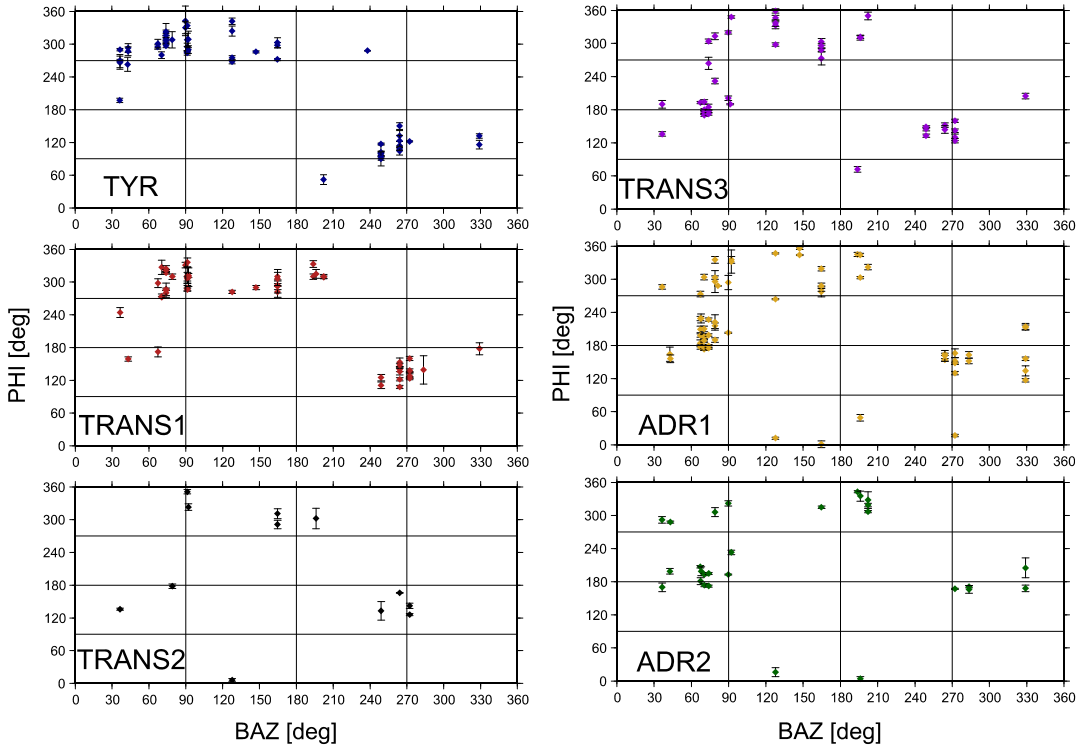

Figure I.4.8 Dependence of the fast shear-wave polarization azimuths on back-azimuth for six domains derived according to the P-sphere pattern.

The rose diagrams illustrate frequency of occurrence of the fast shear-wave polarization azimuths in 18° fans. To be compatible with commonly used evaluation of the splitting azimuth only from the horizontal components of the seismograms and to emphasize differences in variations, we present also φ + 180° azimuth (in light colours) in the rose diagrams.

Though of different orientation, one dominant azimuth of the polarizations exists for each domain for the western back-azimuths. On the contrary, the rose diagrams for the eastern back-azimuths are 'scattered' and differ significantly among the domains. In the TYR domain, azimuths around 280° prevail, while in the TRANS1 domain a separation into two sectors occurs (see *Fig. I.4.9a*). The most frequent azimuths are around 315° and azimuths around 280° are also very frequent for the eastern back-azimuths. The TRANS2 domain comprises only few data.

TRANS3, ADR1 and ADR2 domains are very complicated for the eastern back-azimuths (see *Fig. I.4.9b*). Azimuths around 180° are very dominant in the TRANS3 domain and also a wide group of N and WNW azimuths occurs.

The ADR1 rose diagram for eastern back-azimuths is in general similar to that of TRANS3. The most frequent azimuths are again around 180°, but in this case the interval is larger. Other very frequent azimuths are around 290°. In the ADR2 domain, there are two prevailing azimuths as well. One of them is around 190° and the second is around 315° for waves arriving from the east. The interval around 190° is more scattered than the interval around 315°.

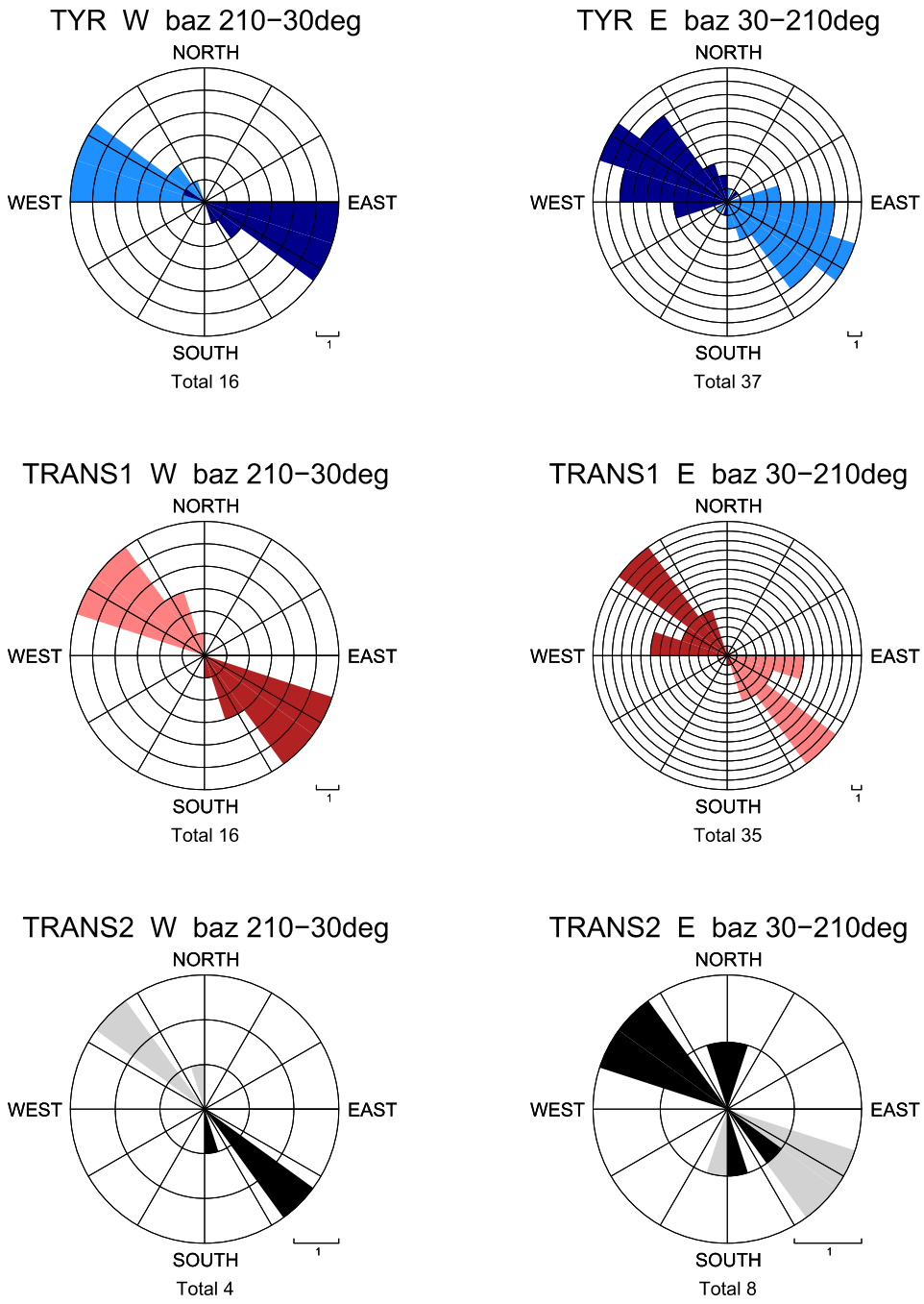

Figure I.4.9 a) Rose diagrams representing the frequencies of polarization azimuths (dark colour) at the TYR, TRANS1 and TRANS2 domains for the western back-azimuths (210° - 30°, left diagrams) and those for the eastern back-azimuths (30° - 210°, right diagrams). Opposite azimuths are shown in light colour.

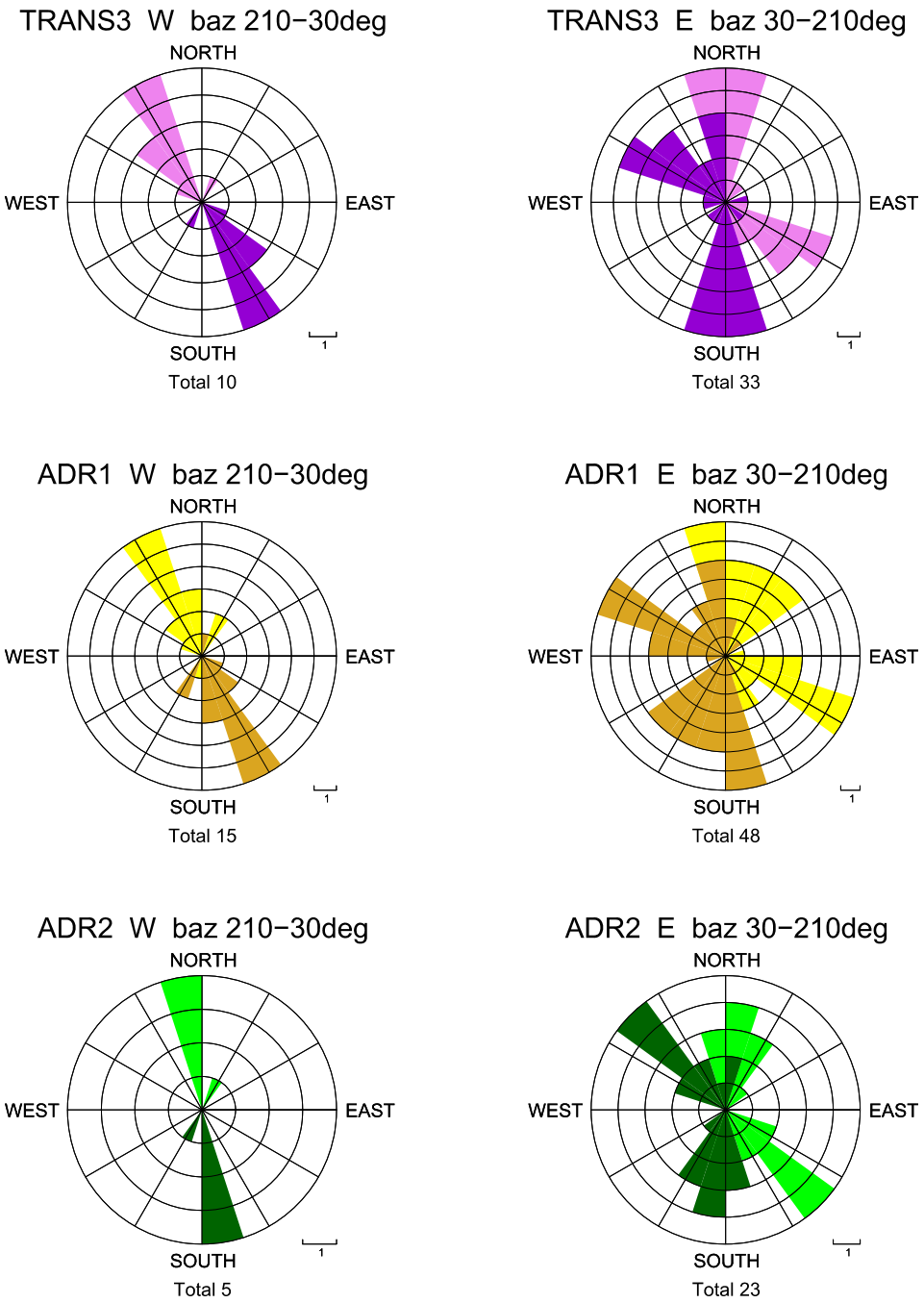

Figure I.4.9 b) Rose diagrams representing the frequencies of polarization azimuths (dark colour) at the TRANS3, ADR1 and ADR2 domains for the western back-azimuths (210° - 30°, left diagrams) and those for the eastern back-azimuths (30° - 210°, right diagrams). Opposite azimuths are shown in light colour.

Only in the TYR domain (see *Fig. I.4.9a*), the polarization azimuths do not show any back-azimuthal dependence – the most frequent azimuths are around 110° (290°) for the western (eastern) back-azimuths. The two rose diagrams in the TYR domain differ slightly only in the shape – the rose diagram for the eastern azimuths is more scattered than that one for the western back-azimuths. The situation is similar in the TRANS1 domain, for which the azimuths from the eastern back-azimuths

cover approximately the same azimuths as those of the western back-azimuths. Nevertheless, the shape of the frequencies of individual sectors differ. This difference becomes more significant in the TRANS3, ADR1 and ADR2 domains (see *Fig. I.4.9b*), in which none of the distinct polarization azimuths for the eastern back-azimuths finds its equivalent in the most frequent azimuths in the diagrams for the western back-azimuths.

Moving from the Tyrrhenian coast through the transition zone to the Adriatic coast, a slight clock-wise rotation of the polarization azimuths is apparent (see *Figs. I.4.9* and *I.4.7*). The rotation can be seen particularly in the rose diagrams for the western back-azimuths, because those diagrams are simpler. The most frequent azimuths in the individual domains from the western back-azimuths are as follows: TYR - 110°; TRANS1 - 130°; TRANS2 - 140°; TRANS3 - 150°; ADR1 - 160° and ADR2 - 170° (see *Fig. I.4.9*).

When evaluating differences or similarities in polarization azimuths, one has to keep in mind that the total number of measurements presented in the rose diagrams differ (mentioned below each diagram). For the western back-azimuths, the number of measurements is only one third to one half of those for the eastern back-azimuths. Nevertheless, in the TYR, TRANS1, TRANS3 and ADR1, there is a sufficient number of measurements, respectively. It is thus enough to reveal general features of the western back-azimuths in the domains.

I.4.4. Anisotropy vs. heterogeneity ?

The Northern Apennines lie in an active tectonic region of the subducting Adriatic plate and above assumed horizontal flows in the sub-lithospheric mantle (e.g., Margheriti et al., 2003). Therefore, the upper mantle anisotropy, originated both in the lithosphere and below it, together with the velocity heterogeneities, manifested mainly by the subduction, affect propagation of seismic waves. Velocity perturbations due to isotropic heterogeneities and due to anisotropy are comparable in their amplitudes, though difficult to separate. Nevertheless, modelling upper mantle structures in 3D and combining different methods allow us to unravel the problem.

Standard methods of imaging velocities or velocity perturbations in the upper mantle, consider only isotropic propagations. However, neglecting the anisotropy can cause false or distorted artefacts in the isotropic tomographies (e.g., wrong amplitudes of the heterogeneities, or, false heterogeneities; Sobolev et al., 1997). On the other hand, also the P-residual spheres which bear the information about the anisotropy (see *chapter I.4.2.*) might also be affected by uncorrected heterogeneities.

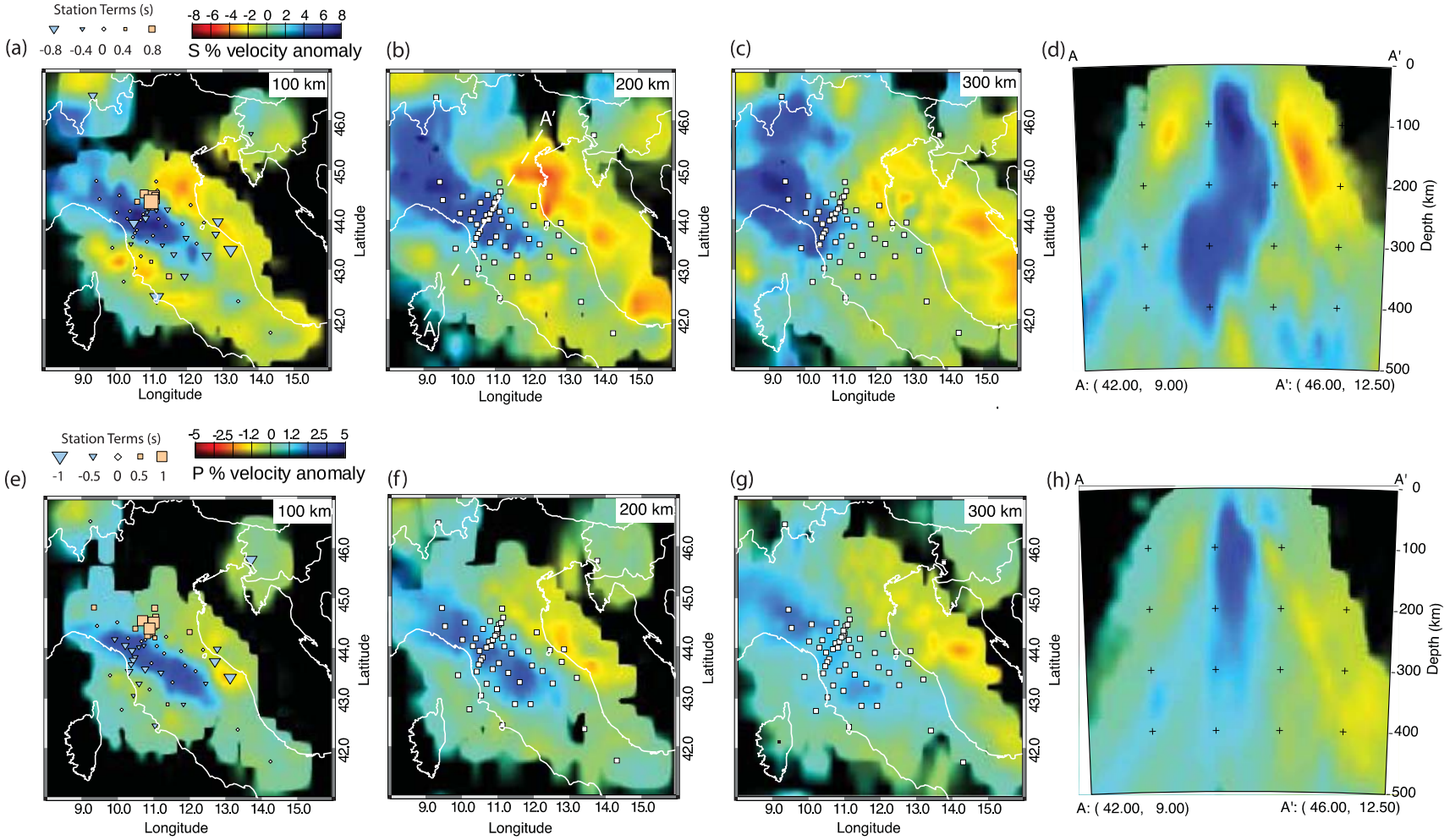

Figure I.4.10 Horizontal and vertical cross-sections sliced trough the S-velocity perturbation (a-d) and P-model (e-h). After Benoit et al. (2011).

Several tomographic images of velocity perturbations in the upper mantle below the Northern Apennines have been published (e.g., *Babuška and Plomerová, 1990*; *Lucente et al., 1999*; *Piromallo and Morelli, 2003*; *Spakman and Wortel, 2004*; *Cimini and Marchetti, 2006*; *Koulakov et al., 2009*). All of them imaged an inclined or nearly vertical high-velocity heterogeneity that is associated with the subducting Adriatic lithosphere. We capitalize on a recent body-wave tomography (Benoit et al., 2011) calculated from the RETREAT teleseismic data which results in the P- and S-velocity perturbation models. Both models image a short steeply sinking slab (*Fig. I.4.10*) similar to that of Lucente et al. (1999), derived from teleseismic data of the Italian National Network. We decided to compute P-wave travel times in the tomographic model of Benoit et al. (2011) for waves recorded during the RETREAT experiment, to perform the same analysis (described in *chapter I.3.1*.) of directional dependence of the synthetic P-wave travel-time residuals and to compare them with the observed ones (see *chapter I.4.2.*).

We evaluated the synthetic travel-time residuals as differences between the times spent in the tomographic model and in the IASP91 model (Kennet, 1991). This new synthetic time residuals were analyzed in the same manner as the real observed P-wave travel-time residuals (*chapter I.4.2.*), but without applying the crustal corrections according to Di Stefano (2011), as the authors of the tomography corrected their data for the crustal effects and related the perturbations only to the upper mantle.

The synthetic P-residual spheres, based on tomography from Benoit et al. (2011) can be divided into two groups (*Fig. I.4.11*). Most of the stations show the bipolar pattern of the P spheres with negative (blue - early) residuals from the western and southern directions and positive (red - delayed) residuals from the eastern and northern directions. This characteristic pattern was found in all the stations in the transition zone (TRANS1, TRANS2 and TRANS3 domains) and the Adriatic zone (ADR1 and ADR2 domains). The P spheres in the TYR domain differ as they exhibit positive (red - delayed) values for the western and southern directions and negative terms (blue - early) in the eastern and northern directions. But in addition to that, the directional terms of waves arriving from the NE back-azimuths tend to positive values.

The TYR domain has the same extent according to both the synthetic (*Fig. I.4.11*) and the observed P-sphere patterns (*Fig. I.4.4*). It consists of identical stations, with exception of station PIIR, the synthetic P sphere of which differs from the others in the TYR domain. However, though mutually similar among the stations, the synthetic and the observed P-patterns in the TYR domain differ. The patterns of the synthetic P spheres in the Tyrrhenian part of the RETREAT array are less distinct than the patterns of the observed P-spheres. Moreover, the synthetic patterns become weaker, i.e., the difference between the positive and negative residuals is gradually decreasing, across the TYR domain with the lateral distance from the slab.

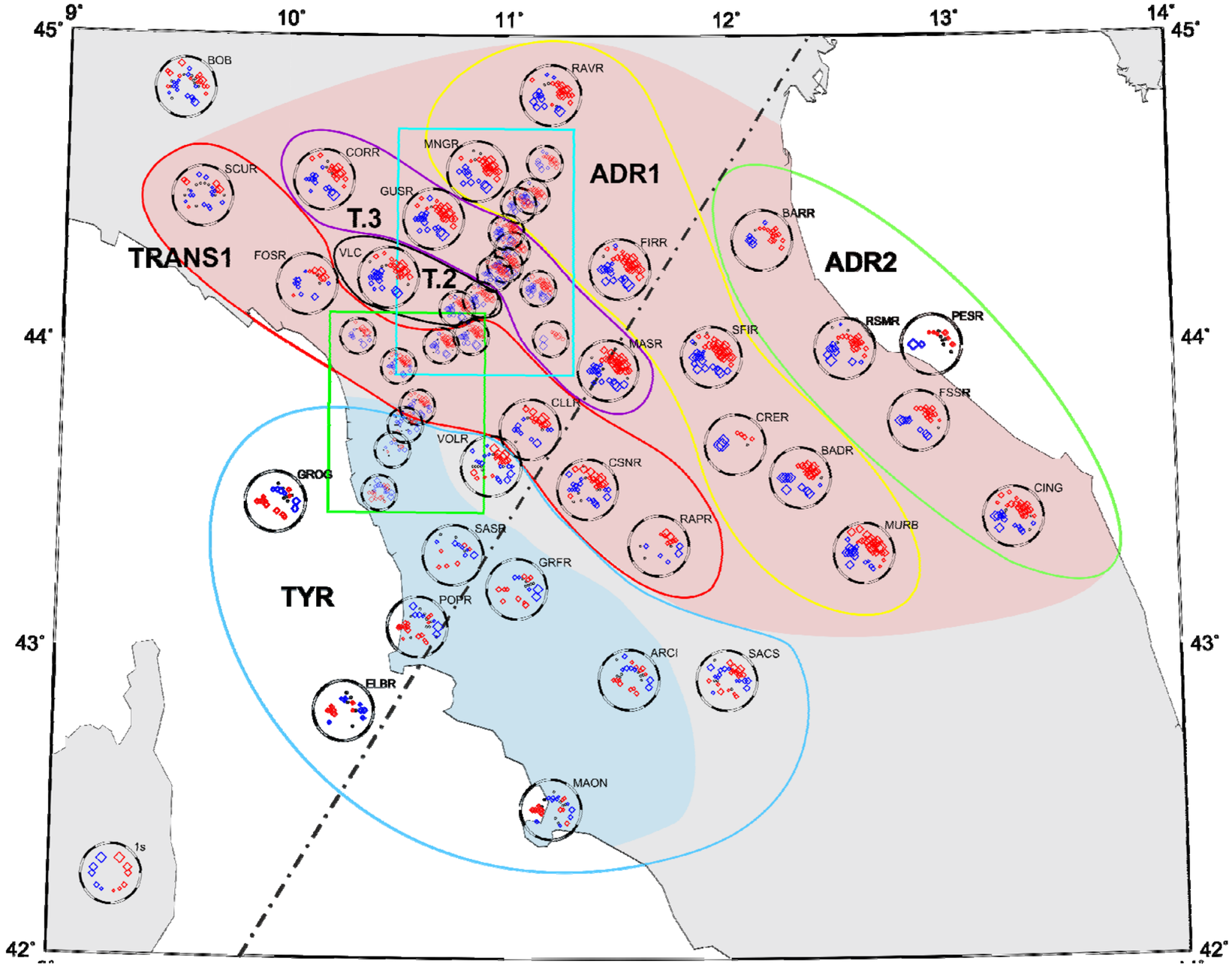

Figure I.4.11 a) Map of the RETREAT array with P-residual spheres at individual stations derived from the tomography model of Benoit et al. (2011). Domains with similar patterns in the synthetic P-spheres are coloured. The boundaries between the domains according to the observed P spheres (see *Fig. I.4.4*) are delineated with coloured lines. Two details (green and blue rectangles) are imaged in *Figs. I.4.11b* and *c*. Dot-and-dashed line indicates location of the vertical cross-section in *Fig. I.4.13*. **T.2** and **T.3** stand for **TRANS2** and **TRANS3**, respectively.

Out of the Tyrrhenian domain, we distinguished five regions (TRANS1, 2, 3, ADR1 and 2) according to the observed P-sphere patterns (see *Fig. I.4.4*). On the other hand, the synthetic P spheres are all consistent there (south and west - blue; north and east - red) and do not allow any detailed delimination of the transition and the Adriatic regions.

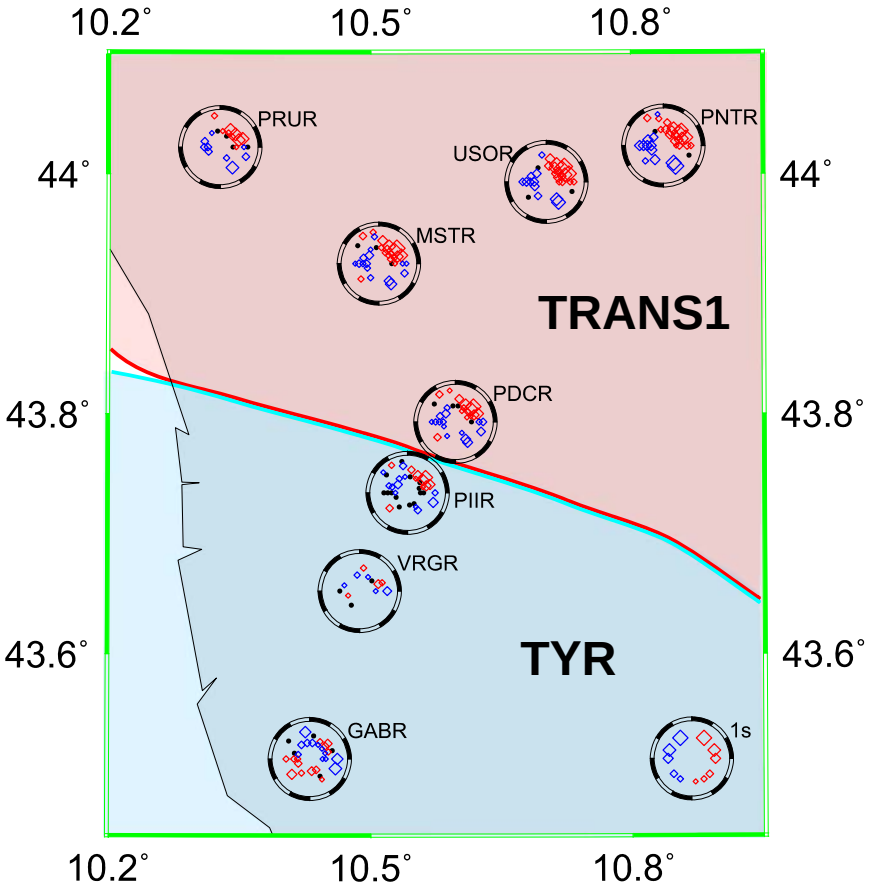

Figure I.4.11 b) Detail of the lower part of the dense station profile, located in *Fig. I.4.11a*, with synthetic P-residual spheres at individual stations derived from the tomography model of Benoit et al. (2011). Domains with similar patterns in the synthetic P-spheres are coloured. The boundaries between the domains according to the observed P spheres (see *Fig. I.4.4*) are delineated with coloured lines.

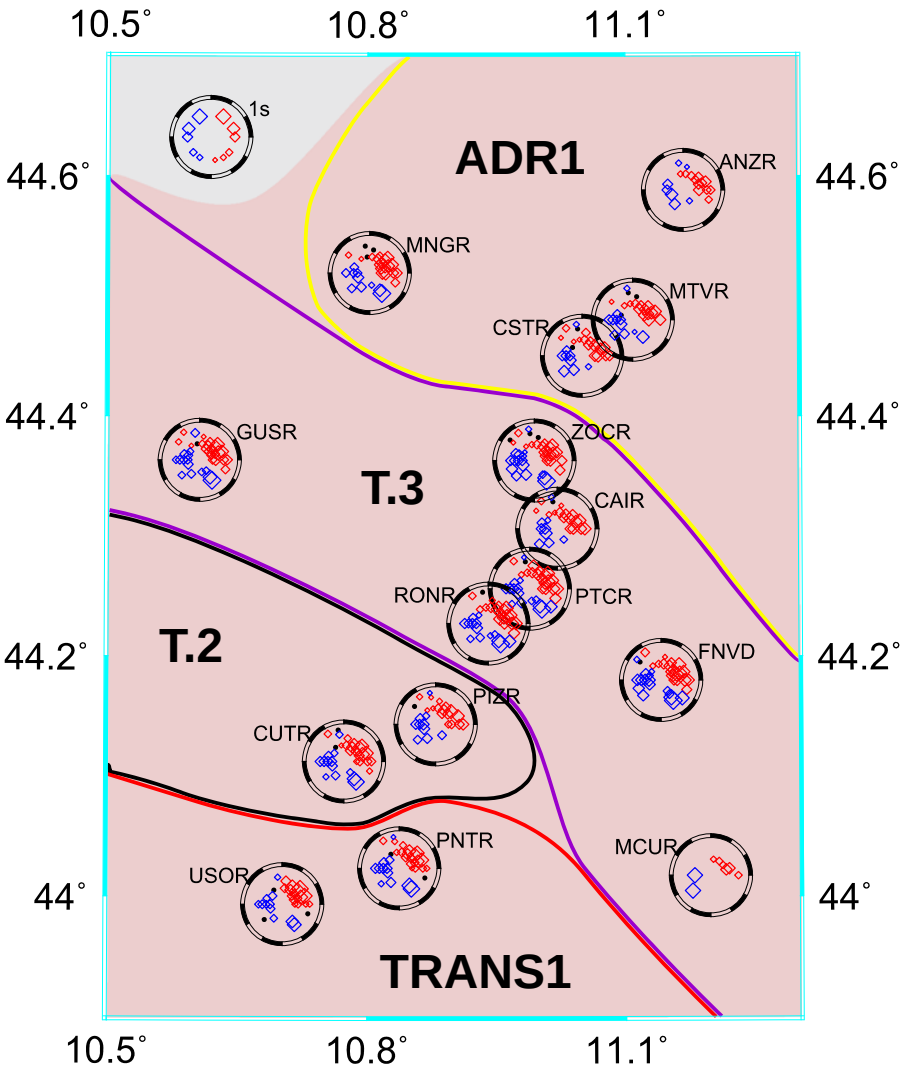

Figure I.4.11 c) Detail of the upper part of the dense station profile, located in *Fig. I.4.11a*, with synthetic P-residual spheres at individual stations derived from the tomography model of Benoit et al. (2011). Domains with similar patterns in the synthetic P-spheres are coloured. The boundaries between the domains according to the observed P spheres (see *Fig. I.4.4*) are delineated with coloured lines. **T.2** and **T.3** stand for **TRANS2** and **TRANS3**, respectively.

To understand better the differences between the synthetic and observed P spheres, we selected several stations, for which the P spheres differ significantly (*Fig. I.4.12*). We divided each P sphere into 6 azimuth bins in such a way that the azimuth separating the early and delayed arrivals is also one of the line segments that separate the 6 azimuth sectors. Then, we calculated average values of the directional terms in each of the bins.

The highest resemblance between the synthetic and observed P patterns is documented on the P spheres of the MURB and RAVR stations (*Fig. I.4.12a*), though the differences *dt* between the negative and positive directional terms slightly differ, e.g., *dt* = 1.1 s for MURB (observed) and *dt* =1.8 s for MURB

(synthetic). Similarly, $dt = 0.8$ s for RAVR (observed) and $dt = 1.1$ s for RAVR (synthetic). Both the MURB and RAVR stations lie in the ADR1 domain, eastward of the slab. Probably, the slab in the tomography made the waves from the west faster than those from the east and thus increased the time difference dt.

The P- spheres of stations PIIR and FOSR (*Fig. I.4.12b*) were selected to demonstrate the reversed patterns. The observed bipolar pattern at station PIIR and a pattern with a tendency to the bipolar at FOSR are almost completely reversed in the synthetic P spheres. FOSR is located in the TRANS1 domain and PIIR lies in the TYR domain near the boundary with TRANS1. The observed directional dependence of the relative travel-time residuals, with characteristic bipolar pattern, is impossible to retrieve at stations PIIR and FOSR with the isotropic tomography model.

Another difference between the synthetic and observed patterns is demonstrated in station pair SACS and VOLR (*Fig. I.4.12c*). The clear bipolar pattern from the observed data changes into the quadruple pattern of the synthetic spheres. Other stations in the TYR domain tend to this quadruple pattern as well. The quadruple pattern can signify that stations SACS and VOLR are located just above the slab imaged in the isotropic tomography. The SW and the NE rays pass through the high-velocity heterogeneity in the direction perpendicular to the NW-SE strike of the slab and therefore, they are relatively slower in comparison with the rays from the NW and the SE, which spent much more time within the high-velocity slab. The observed P spheres do not exhibit such behaviour at all. The tomography thus probably mixes the time delays due to the anisotropy and due to the heterogeneity that could even result in a mislocation of the slab.

The last two pairs of examples of the observed and synthetic P spheres (*Fig. I.4.12d*) demonstrate a change of the bipolar patterns into chaotic ones (no P pattern). The MAON station exhibit the bipolar pattern for the observed P sphere, while pattern of the synthetic P spheres is chaotic. On the other hand, the bipolar pattern of the synthetic P sphere of station CAIR changes into ‘no pattern’ in the observed sphere. ‘No pattern’ is also reflected in the average values close to zero.

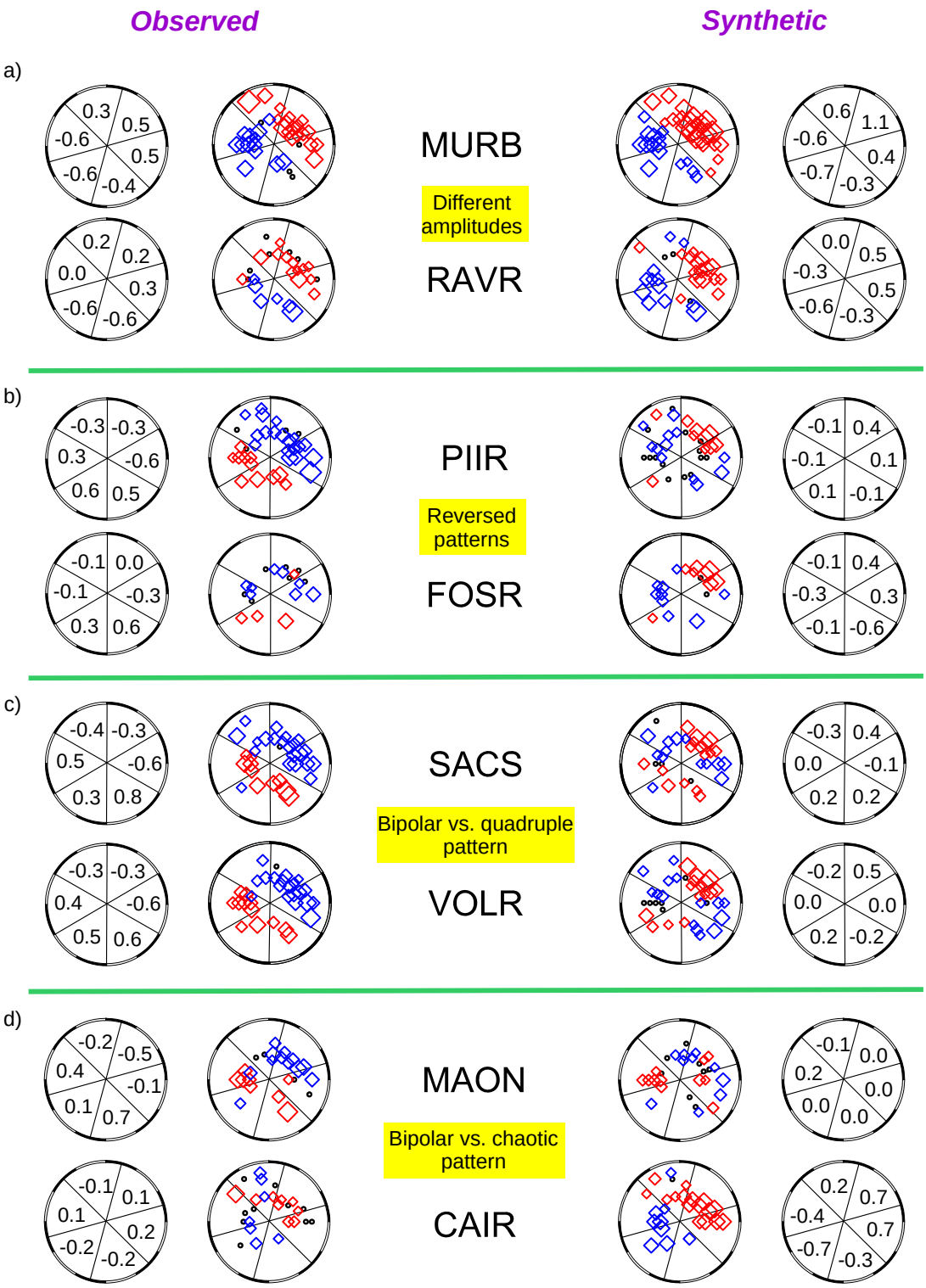

Figure I.4.12 Comparison of the observed (left column) and the synthetic (right column) P spheres at selected stations to represent differences between the P sphere patterns. Average directional terms are calculated for each of the six sectors in the P spheres.

A vertical cross-section through the tomography (for location of the profile see *Fig. I.4.11*) and a ray tracing to four stations for epicentral distances of 40° and 80° are imaged in *Fig. I.4.13*. The VOLR station is located just above the high-velocity heterogeneity imaged by the inversion, which results in the quadruple pattern of the synthetic P-sphere, as mentioned above. The other stations, further to the NE (CSNR, SFIR and BARR), show the bipolar pattern in the synthetics with the negative terms in the SW, where the slab is located according to the tomography.

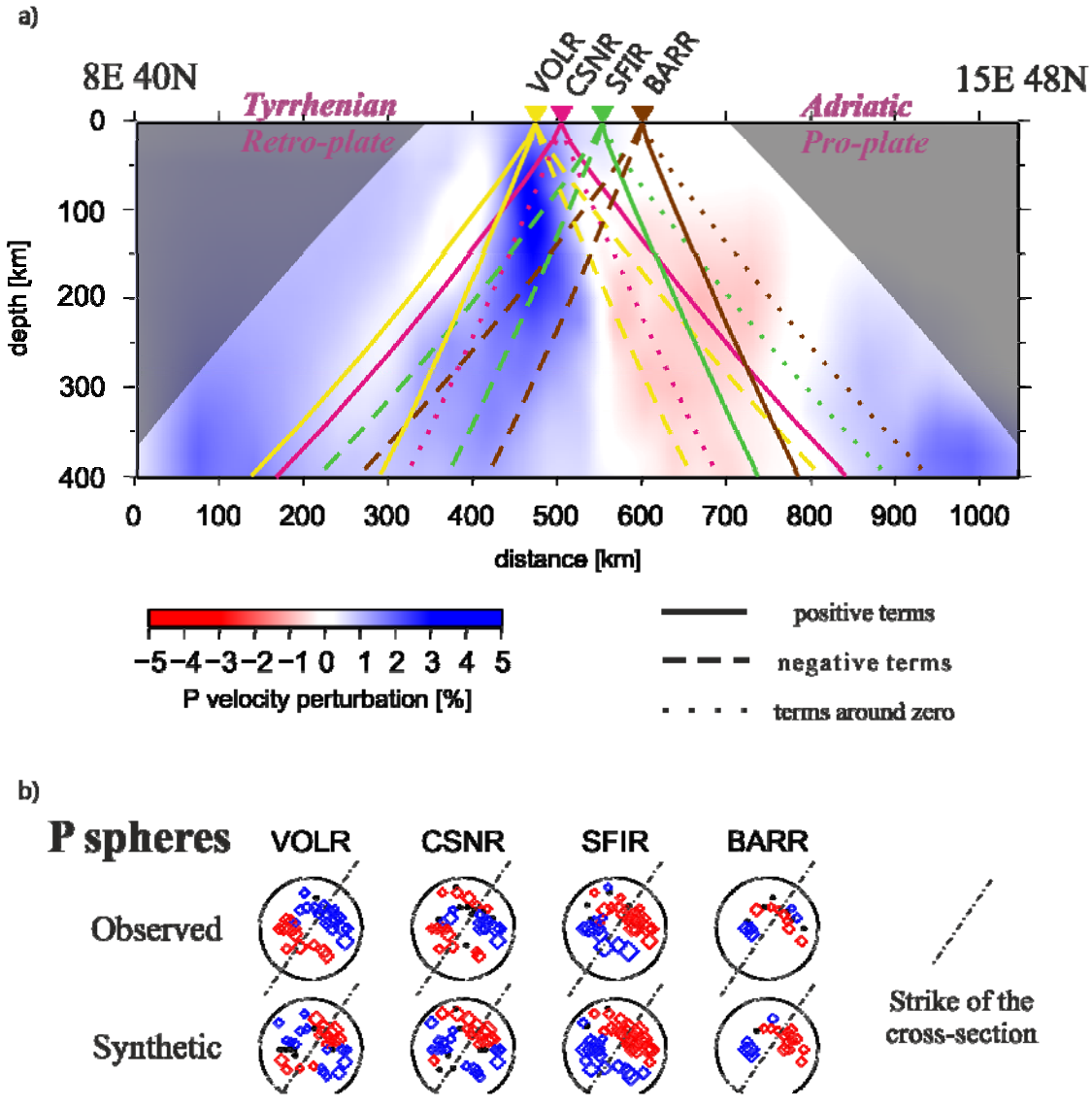

Figure I.4.13 *a)* Vertical cross-section through the P-wave tomographic model of Benoit et al. (2011) along the profile marked, e.g., in *Fig. I.4.11a*. Rays from epicentral distances of 40° and 80° to four stations superimpose the velocity model. Different styles of the ray curves indicate whether the corresponding observed directional term is positive (full curve), negative (dashed curve) or around zero (dotted curve). *b)* Observed and synthetic P-residual spheres at the four selected stations.

Except for the SFIR station, there are distinct differences between the synthetics and the spheres calculated from the observed data. Assuming the slab heterogeneity is located as shown in the inversion, the applied residual procedure eliminates its effect and the observed sphere of the VOLR with the early arrivals from the NE and delayed arrivals from the SW can be associated with mainly anisotropic propagation. On the other hand, the P sphere of the SFIR station can be affected by a part of uncorrected effects due to the high-velocity heterogeneity and effects of anisotropy and heterogeneity might be mixed there. However, the synthetic travel times calculated for the isotropic velocity-perturbation model (Benoit et al., 2011) cannot, in general, explain the patterns of the observed P-residual spheres evaluated from the data of the RETREAT experiment and associated with anisotropic structure of the upper mantle (compare *Figs. I.4.4* and *I.4.11*). It is obvious that the synthetic P spheres reflect the vertical heterogeneity (see *Fig. I.4.13*) and that other effects, e.g., those resulting from anisotropy or smaller-size heterogeneities, are blurred in the tomography.

I.5. Discussion

In principle, it is difficult to separate effects of anisotropy and heterogeneity on seismic wave propagation. Nevertheless, if the anisotropy is absolutely neglected in large-scale studies of the upper-mantle structure, then a part of the travel-time residual caused by anisotropy can be misinterpreted as heterogeneity or can affect location of isotropic velocity heterogeneities. The analysis of directional dependence of P-wave travel-time residuals has been successfully applied in several continental regions of different geological ages, from Precambrian to Phanerozoic (see *chapter I.1.2.*), for which the assumption that the P-wave directional terms beneath the station array were produced by anisotropy was justified. Tectonic situation beneath the Northern Apennines is more complicated in comparison with tectonically stable provinces. Under the RETREAT array, the Adriatic plate subducts beneath the Tyrrhenian plate as a result of ongoing collision between the Eurasian and African plates.

Elimination of the contribution of the heterogeneity to the travel-time residuals is crucial for retrieving the P-wave anisotropy signal. It is not obvious whether and how much we have already excluded effects of the slab from the observed P spheres by the two-step normalization of the absolute travel-time residuals. If all the rays for an event have the same length path within the slab, the time, spent in the heterogeneity, would be completely removed from the residuals by the first step of normalization, which subtracts the part of residuals common to all the rays. Isotropic part of the relative travel-time residuals (directional mean), reflecting the average velocity structure beneath the individual stations, is eliminated from the directional dependence of the residuals by the second step of normalization, i.e., by subtracting the directional mean from the relative travel-time residuals. However, a heterogeneity, such as that represented by a slab, can hardly be removed completely by subtracting the directional means, in general. Nevertheless, the effects of a vertical slab might be minimized in case of the stations lying just above the slab (e.g., VOLR).

According to the P-sphere pattern, we distinguished several domains in the Northern Apennines (see *Fig. I.4.4*). The domains form bands approximately parallel to the mountain range. The TYR domain in the Tyrrhenian part of the array is also clearly evident from the fast split shear-wave polarization measurements (see *Figs. I.4.7* and *I.4.9*). North-eastward of the Tyrrhenian region, we observed the transitional zone of about 80 km width, forming approximately three sub-regions (TRANS1, TRANS2 and TRANS3), where the P pattern changes suddenly (see *Fig. I.4.4*). Further to the east and north, in the Adriatic region, the P-sphere patterns are more stable and we separated them into two domains (ADR1 and ADR2). However, station clustering according to the shear-wave polarizations is not so evident there (*Fig. I.4.7)*.

In general, we observed a rotation of the polarization azimuths of the fast shear waves across the RETREAT array from its western part to the eastern part. The rotation is apparent especially for the westerly arriving waves in *Fig. I.4.9*, where the rose diagrams are simpler. While, the changes of the P-pattern are more abrupt and the P-residual spheres are consistent in the individual domains, especially in the TYR, ADR1 and ADR2, the change of the polarization azimuths from the Tyrrhenian domain to the Adriatic domain is gradual. The lower sensitivity of the S-waves on the changes in structure could be caused by different wavelengths of P and S waves. Considering 1 s and 8 s as dominant periods and velocities in the upper mantle about 8 km/s and 4.5 km/s for P and S waves, respectively, we estimate the P and S wavelengths approximately at about 8 km and 36 km. Thus the P waves are able to detect smaller-size lateral variations than the shear waves.

Simultaneous extension in the Tyrrhenian Sea and an eastward slab roll-back of the subducting Adriatic plate (e.g., Margheriti et al., 2003) probably induce a very complicated flow in the sub-lithospehric mantle. Each of generally accepted models for extension in convergent orogens implies a sub-lithospheric flow that should be detectable by the large-scale LPO anisotropy (Silver, 1996; Savage, 1999). The observed anisotropic behaviour of both the P and S waves can originate either in the mantle lithosphere (namely due to the frozen-in anisotropy) or in the sub-lithospheric mantle, where the fast axis of olivine orients along the flow direction. In case of horizontal mantle flow and sub-vertically incident SKS waves, the azimuth of the fast S-wave polarizations can be thus directly associated with the direction of the asthenospheric flow.

Regardless the direction from which the SKS wave arrives, the polarization azimuths of the fast shear waves are oriented NW-SE for majority of the stations in the Tyrrhenian region. The Tyrrhenian plate is probably thin (see also the thin crust in the model by Di Stefano et al., 2011) and the thickness of the mantle lithosphere there hardly exceeds the wavelengths of the shear-wave signals. Therefore, a source of the major part of the evaluated anisotropic signal in the Tyrrhenian region is most probably located in the sub-lithospheric mantle and can be attributed to the present-day flow in the mantle. As model of syn-convergent extension is usually proposed in the Northern Apennines, anisotropy with the fast symmetry axis perpendicular to the trench would be expected in the sub-lithospheric mantle wedge in the Tyrrhenian region. Such behaviour of the fast shear-wave polarizations was retrieved from data of the Northern Apennines Profile experiment (NAP), located in the southern part of the RETREAT array (Margheriti et al., 1996; 2003), and it is partly confirmed by the results of Salimbeni et al. (2008). The west-east trend of the polarizations at the southernmost RETREAT stations in the Tyrrhenian region is apparent in *Fig. I.4.7*. However, the polarizations at majority of the stations further to the north are oriented in the SE direction which parallels the trench, far from being perpendicular to the mountain chain (see *Figs. I.4.7* and *I.4.9*). Therefore, a horizontal slab-parallel flow in the asthenospheric wedge is generally accepted as an explanation of the observed shear-wave

polarization pattern in the Tyrrhenian domain (e.g., Salimbeni, 2008). The westward rotation of the fast S polarizations in the southernmost stations might be related to a potential slab window in the central Apennines, between the Northern and Southern Apennines mountain chains (Margheriti et al., 2003; Lucente et al, 2006; Civello et al., 2004).

On the other hand, the P-sphere pattern characteristic for the TYR can be likely associated with the structure of the mantle lithosphere. The reason is that the distinct observed bipolar pattern differs from the synthetic one calculated for the tomographic model. The pattern is consistent over the large province without changes of the size of the individual terms in the observed spheres in dependence on the lateral distance from the slab as it is in the synthetics. Moreover, the observed pattern can hardly reflect a horizontal anisotropy due to a flow in the sub-lithospheric mantle, because teleseismic P waves arrive under steep incidences and thus the anisotropy with a horizontal symmetry axis would affect their travel times negligibly. Nevertheless, the effect of anisotropy with a tilted symmetry axis can be, in general, significant (Plomerová et al., 2001).

Contrary to the Tyrrhenian domain, the fast shear-wave polarization azimuths in the Adriatic region vary at individual stations significantly. The complexity of this area is demonstrated in the rose diagrams of the polarizations (*Fig. I.4.9),* where two dominant azimuths – to the NW and S prevail for propagations from the east, while waves from the west polarize predominantly to the S-SSE. The three dominant polarization azimuths can reflect either a double-layer anisotropic structure, e.g., in the mantle lithosphere and in the sub-lithospheric mantle, or, an inclined anisotropy in the mantle lithosphere, or both. The continental Adriatic plate is thicker than the Tyrrhenian plate, and therefore, the SKS waves can be more affected by anisotropy in the Adriatic mantle lithosphere. In analogy with other continental regions (e.g., Babuška and Plomerová, 2001; Eken et al., 2010; Plomerová and Babuška, 2010), we can expect a fossil anisotropy with a dipping symmetry axis in the Adriatic plate. In addition to that, a contribution of the anisotropy located in the sub-lithospheric mantle, due to the present-day flow, into the overall anisotropic signal has to be considered as well.

Salimbeni et al. (2007, 2008) concentrated in their analysis on lateral changes of the shear-wave splitting across the dense transect of stations perpendicular to the Northern Apennines chain. The authors divided the whole array into three domains - the Tyrrhenian (Tuscany) domain in the SW, the Adriatic (Adria) domain in the northeast, and the Transitional zone (~ 30 km wide) in between. The authors evaluated the averaged and most frequent polarization azimuths at each station, which are very similar at the stations in the Tyrrhenian and Adriatic domains. The Transitional zone comprises stations, where the averaged azimuth differs from the most frequent polarizations azimuth at individual stations.

Plomerová et al., (2006b) recognized three domains in the Adriatic plate – the Southern domain of the Northern Apennines (SA), the Ferrara arc domain (FER)

in the central part of the region and the Alps-Apennines Transition domain in the north, each with different characteristics of the fast shear-wave polarizations. Polarizations parallel the mountain chain in the Southern domain, whereas they turn to chain perpendicular in the Ferrara arc domain. The null splits dominate in the Alps-Apennines Transition domain, interpreted as a result of wave propagation trough structures with different anisotropy (Babuška and Plomerová, 2006). At a first glance, we do not see such a clear difference in the SKS polarizations (see *Fig. I.4.7*). Therefore, we re-grouped stations in the Adriatic plate according to the division of the Adriatic plate into the Ferrara arc domain (FER) and the Southern domain of the Northern Apennines (SA) in *Fig. I.5.1*, to understand better the two components with almost comparable frequencies of the azimuths in the rose diagrams of the polarizations in the ADR1 and ADR2 domains (see *Fig. I.4.9*). It is evident (*Fig. I.5.2*) that the shear-wave polarizations in the Ferrara region (dominantly southward polarizations) differ from the polarizations in the Southern Adriatic domain (predominantly WNW polarizations). This can mean that the thicker continental Adriatic plate has its own fabric, which changes laterally, and thus the continental Adriatic plate consists likely from individual domains (Plomerová et al., 2006b).

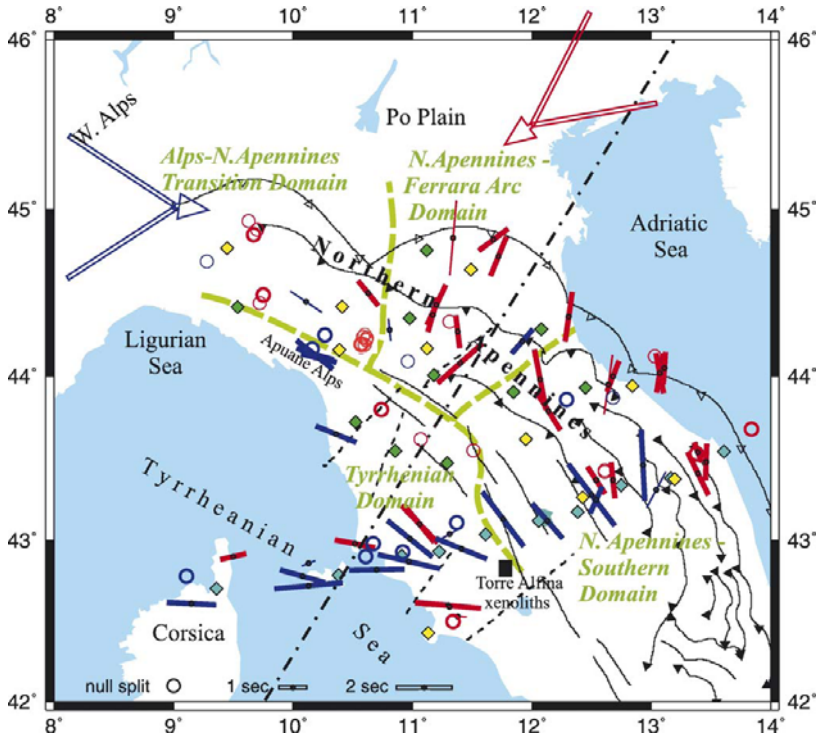

Figure I.5.1 Shear-wave birefringence estimates for teleseismic data recorded by the RETREAT station array (green and yellow diamonds) and the NAP (Northern Apennines Profile - blue diamonds) plotted at piercing points at depths of 100 km. The big arrows on the top indicate the western (blue) and the NE (red) back-azimuths of arriving shear waves. Dashed green curves delimit domains deduced from variations of the splitting parameters (Plomerová et al., 2006b).

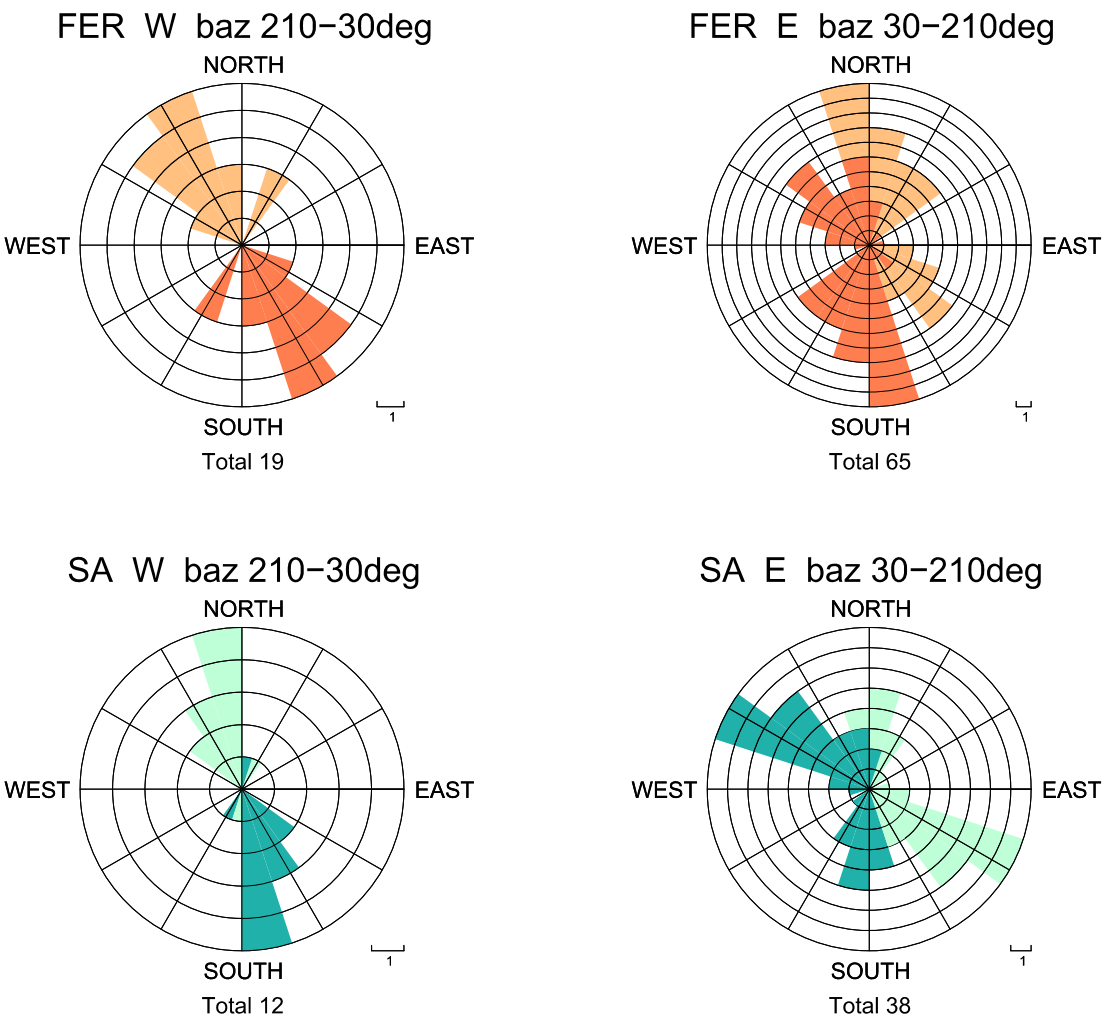

Figure I.5.2 Rose diagrams showing frequencies of the fast shear-wave polarization azimuths for the NW back-azimuths (left diagrams) and those for the SE back-azimuths (right diagrams) of the Ferrara domain (FER, upper pair of diagrams) and the Southern domain of the Northern Apennines (SA, lower pair of diagrams). The stations of the FER and SA domains are grouped according to the *Fig. I.5.1*.

I.6. Conclusions

Based on analysis of directional terms of relative travel-time P-wave residuals and shear-wave splitting, evaluated from recordings of the passive seismic experiment RETREAT (2003 - 2006), we map anisotropic structure of the upper mantle beneath the Northern Apennines. We recognize regions of different fabrics in the mantle lithosphere and also in the sub-lithospheric mantle. Joint analysis of the two different and independent data sets (P-wave travel-time residuals and shear wave splitting) allows us to infer anisotropic structures oriented generally in 3D with inclined symmetry axes.

According to the P-residual sphere pattern at individual stations, the territory of the Northern Apennines and its surroundings can be divided into six domains. A very consistent bipolar P-sphere pattern was found in the Tyrrhenian region. In the Adriatic region, we delimited two domains. The domain closer to the Apennines crest exhibits a very homogeneous bipolar pattern, whereas the easternmost domain shows a tendency to the bipolar pattern. Approximately one half of the stations is situated between the Tyrrhenian and the Adriatic regions. P patterns at those stations indicate a transitional zone of about 80 km wide between the Adriatic and Tyrrhenian regions. We divided the transition zone into 3 additional sub-regions, where the P-sphere patterns differ from the simple bipolar one and where the plotted directional terms are smaller in absolute values in comparison with the pattern at the stations outside of the transition area.

Test of the well-known trade-off between the heterogeneity and anisotropy showed differences between the synthetic P spheres calculated for the standard tomographic model of isotropic velocity perturbations in the upper mantle beneath the Northern Apennines (Benoit et al., 2011) and the observed P spheres. Therefore, the observed directional dependences of the directional terms of the relative travel-time residuals beneath individual stations of the RETREAT array cannot be explained solely by heterogeneities and have to be also associated with effects of anisotropic propagations.

Similarly, detected shear-wave splitting and distinct variations in the analysed fast shear-wave polarizations confirm anisotropic structure of the upper mantle in the Northern Apennines. The polarizations slightly rotate clock-wise from the western coast through the transition zone to the eastern coast. In the Tyrrhenian region, the polarization azimuths are oriented NW-SE for all back-azimuths, while in the transition and the Adriatic region, the polarization azimuths show a great variability with the back-azimuth; at least two different dominant polarization azimuths exist for easterly propagating waves in each of the eastern domains.

Mantle lithosphere fabric in the Tyrrhenian plate, thinner in comparison with the Adriatic one, seems to be detected only in the anisotropic parameters of P waves, which indicate the easterly dipping high velocities there. In the wedge

beneath the Tyrrhenian plate and above the subducting Adriatic plate, the shear-wave polarizations prefer a horizontal slab-parallel flow in the sub-lithospheric mantle to the slab perpendicular flow, which might be expected in the extension zone.

Large-scale structure of both the lithospheric and sub-lithospheric mantle in the Adriatic region is complex. We detected laterally varying anisotropic signal which we associate with changes of a fabric of the lithospheric plate and based on that we delimited sub-regions of the thicker continental Adriatic plate. We also admit effects reflecting probable deviations (rotation?) in a slab-parallel corner flow in the asthenosphere.

Further modelling of anisotropic structures is necessary, but it exceeds the extent of the thesis. Our future research aims at developing a code for a simultaneous inversion for both isotropic and anisotropic velocity perturbations, which will also consider results of shear-wave splitting analyses.

PART II

Semi-automatic picking softwares

II.1. Introduction to semi-automatic picking softwares

In case of teleseismic datasets from dense seismic arrays, a huge amount of seismograms is usually collected. Thousands of waveforms need to be looked through and carefully processed at earliest possible time. Owing to this effort of rapid manipulation with data, many seismological teams try to develop a (semi-)automatic programs (called pickers) which would exceed the manual elaboration of seismograms. How surprising it might seem, manual picking still appears to be the most accurate way of data manipulation.

The difference between an automatic and a semi-automatic picking program is that the automatic programs do not require any manual intervention. For example, the ratio of the Short-Time Average to the Long-Time Average of the seismic signal, STA/LTA (Bormann, 2002), is an automatic method that can detect an event (a sudden increase of the amplitude) and it is mostly used to trigger the data recordings. On the other hand, the semi-automatic programs need an assistance of a person who, for example, sets some parameters or selects an option during the running procedure.

One of the main principles, which semi-automatic programs may be based on, is the correlation (Van Decar, Crosson, 1990). When two signals are correlated, we obtain a correlation coefficient that expresses the level of similarity between the signals. To prosper from the correlation algorithm in case of seismic datasets, an important characteristic of event recordings is that they should consist of very similar waveforms across the array which are only slightly shifted in time one to each other after applying an epicentral distance correction (moveout). This requirement is usually well satisfied in case of the teleseismic data recorded during a seismic passive experiment.

The crucial procedure of a (semi-)automatic picking program is moving each waveform a little bit along the time axis and search for the time correction, for which the correlation coefficient of the moved waveform and a reference waveform is the highest. In other words, the picking programs based on correlation try to align a selected part of seismograms around the first onset. Then, directly the first onset or a correlated extreme after the first onset is picked on each seismogram and finally an output file containing the travel times or the time corrections needed to make the alignment is created.

II.2. Semi-automatic picker XPICK

Munzarová (2009) tested a semi-automatic picker XPICK developed by F.P. Lucente and D. Piccinini (INGV Rome) on a subset of data from the RETREAT experiment by picking the arrival times of the P-waves. The XPICK program has not been published yet and it was provided to the GFÚ within the RETRAT experiment cooperation (for details about the experiment see chapter I.2.). The XPICK is a semi-automatic program written in MatLab and intended for picking the arrival times of different phases at seismograms from passive teleseismic experiments using the cross-correlation method (Van Decar, Crosson, 1990).

II.2.1. Work environment

The XPICK program works in the MatLab programming environment by typing corresponding orders in the command window (*Fig. II.2.1*). All orders (at individual steps provided) are listed there, so the program itself leads us through the picking procedure intuitively. Typing one of the following commands '*xpick p*', '*xpick s*' or '*xpick sks*', we choose which phase is to be picked (P-, S- and SKS-wave, respectively). No other phases are enabled. We select the event in the automatically opened directory containing the data files and the program displays the Z components or performs rotation to LQT coordinate system and displays the T or Q components for all the stations in agreement with the selected phase P, S or SKS, respectively, in a new window, named 'Figure 1' (see *Fig. II.2.1*). The theoretical arrival times for the selected phase are also calculated, using 1D spherical velocity model IASP91 (Kennett, 1991), and marked in different colours in the seismograms (P - red, S - green, SKS - violet).

Before the main picking procedure, we might filter or zoom the data or quit the unloaded event, if the signal is weak. As soon as the waveforms are pre-processed sufficiently, we select a reference seismogram. If possible, there should be a high signal-to-noise ratio and a clearly visible first onset with a distinct amplitude in the reference seismogram. The selected seismogram growths larger so we can look in detail at the signal around the theoretical arrival time. Then, we indicate the real onset of the phase with a mouse click. Apart from that, we also mark the end of the period right after the onset of the phase. This interval is automatically enlarged to both sides by 3 s or 10 s in case of P-wave and shear waves, respectively. This is the correlation window. At that moment, the seismograms are correlated with the correlation window of the reference seismogram in order to identify a part of each seismogram that is similar to the correlation window and mark the arrival time there. According to the correlation coefficient, a quality number from 0 – for the highest-quality pick – up to 4 – the lowest-quality pick, later rejected - is assigned to each seismogram.

In addition to the 'Figure 1' window, displaying the seismograms with both the theoretical arrival times and the arrivals coming from the correlation (observed times), another window, named 'Figure 2', appears. The 'Figure 2' window shows the seismograms aligned to the picked arrival times, but unfortunately without filtering. In spite of that, it is clearly visible in the 'Figure 2' window whether all the arrivals are picked well or not. Now, there are several possibilities what to do next. We can perform the whole correlation again, in case of totally bad results,

repick or directly exclude some seismograms manually, if only a few traces seem to be picked inaccurately or the quality number is inadequate, or state the marked arrival times good and finish the picking procedure by saving the observed arrival times.

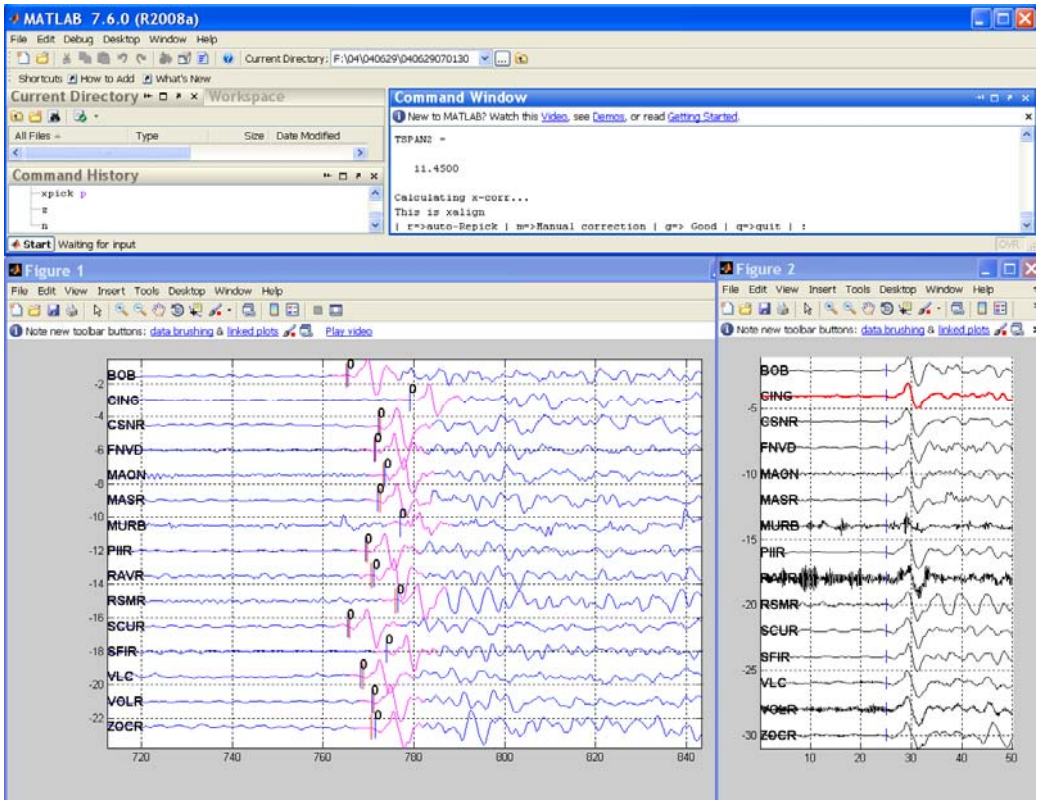

Figure II.2.1 Work environment of the XPICK semi-automatic picker. Event No. 0406290701 is loaded. 'Figure 1' window shows theoretical arrival times of the P waves (red bars), arrival times coming from the correlation (blue bars) and the quality numbers. 'Figure 2' window represents the aligned traces.

II.2.2. Application of the XPICK software on a subset of the RETREAT dataset

We tested semi-automatic picking program XPICK on a subset of data recorded during experiment RETREAT (see *chapter I.2.*). The subset contains only the events from the year 2004. The XPICK processes data in the SAC format (Bormann, 2002). The seismograms were broadband records (CMG-40T) with 20Hz sampling frequency. Finally, we managed to pick the P-wave arrival time of 57 events with the XPICK program and three of them (*Tab. II.2.1*) are discussed in this section.

One of the well-aligned events is event No. 0406290701 (see *Fig. II.2.1*) which illustrates the work environment of XPICK in *chapter II.2.1*.

Table II.2.1 **List of discussed events picked with XPICK**

DAY – number of days from the start of recording; **EVENT** – event code compiled of the origin date and time; **DATE** – origin date [yy/mm/dd]; **OT** – origin time [hhmmss.ss]; **LAT** – latitude [°]; **LON** – longitude [°]; **D** – depth [km]; **MAG** – moment magnitude; **BACK** – back-azimuth [°]; **DIST** – epicentral distance [°]

DAY	EVENT	DATE	OT	LAT	LON	D	MAG	BAZ	DIST
251	0406290701	04/06/29	070130.90	10.74	-87.04	9	6.3	283.0	88.0
271	0407190801	04/07/19	080149.46	49.62	-126.97	23	6.4	333.6	79.6
319	0409051007	04/09/05	100707.82	33.07	136.62	14	7.2	42.6	88.8

As an example of a bad alignment, see *Fig. II.2.2*, representing seismograms of the event No. 0407190801. Station SCUR was chosen as a reference station in this case (red trace in *Fig. II.2.2b*). In *Fig. II.2.2b*, we see that some seismograms (BOB, CING, CSNR, MAON, MASR, MURB, PIIR, VLC and VOLR) are aligned quite well with the SCUR station. It is really a rough alignment where the distinct amplitudes are aligned better than the first onsets (e.g., CING, MAON and MASR). However, the rest of the stations is hardly aligned at all and it was necessary to repick the concerned stations manually (RSMR, SFIR and ZOCR) or exclude them completely from the measuring of the event (BARR and RAVR).

The signal from event No. 0407190801 (*Fig. II.2.3*) is stronger and the first onsets are more obvious in each seismogram than in the example above. Despite high quality of the record, the aligning process failed. Not a single station was aligned correctly with the reference station (red trace in *Fig. II.2.3b*). It was needful to repeat the whole picking procedure manually.

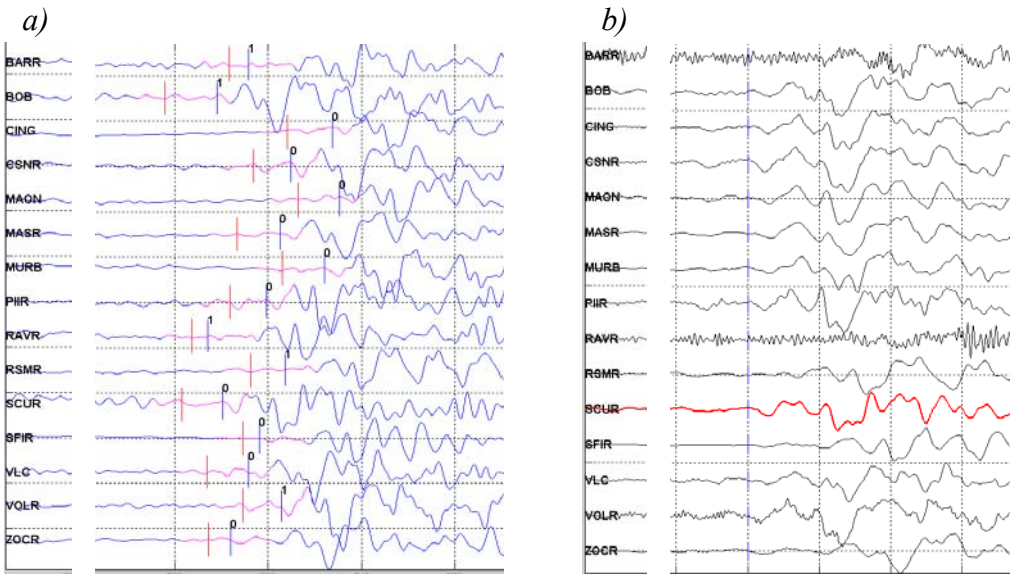

Figure II.2.2 Seismograms of event No. 0407190801 with the theoretical arrival times (red bars), the arrival times coming from the correlation (blue bars) and the quality numbers (a). Traces are aligned according to the first onsets (b).

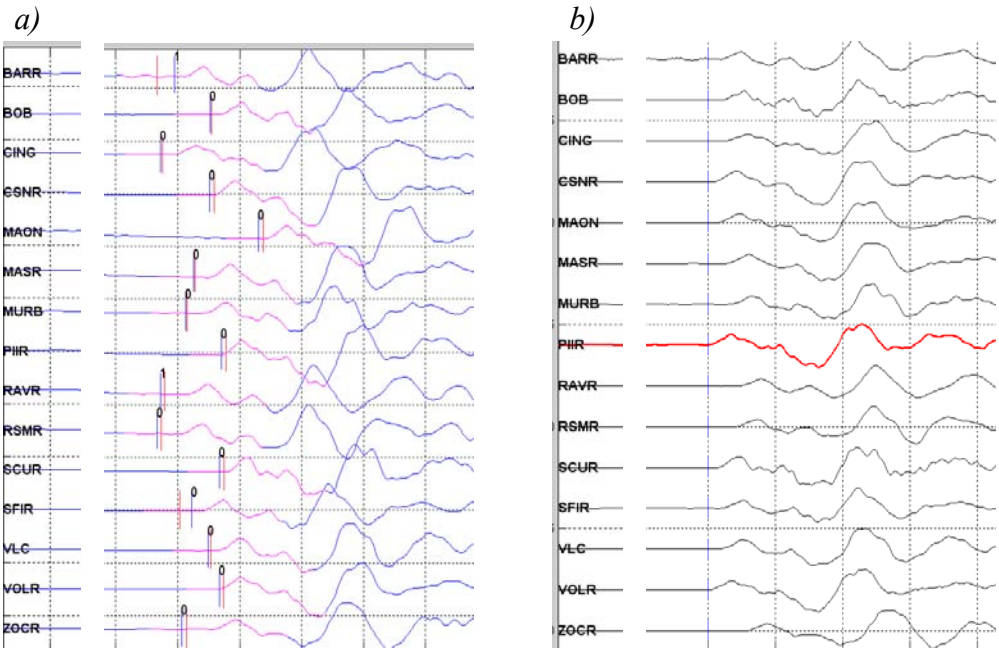

Figure II.2.3 Seismograms of event No. 0409051007 with the theoretical arrival times (red bars), the arrival times coming from the correlation (blue bars) and the quality numbers (a). Traces are aligned according to the first onsets (b).

II.2.3. Discussion about the XPICK software

The XPICK picker is a recent program and thus, there has not been much time for development and stepwise improving of the method and the work environment. The picker is very simple and no extra guide is needed to apply it. But the simplicity of the program also means that the possibilities of usage for different purposes are limited.

Program XPICK is intended just for picking the arrivals of P-, S- and SKS-waves (see *chapter II.2.1.*). The theoretical arrival times are computed only for the three waves mentioned above and only the Z-, T- or Q-components are shown for each type of wave, respectively (T and Q after rotation to LQT coordinate system). Therefore, it is impossible, for instance, to display T-component while picking SKS, which is required, e.g., for analyzing SKS splitting.

For the convenience and also accuracy of the picking procedure itself, several improvements and modifications of the program would help notably, such as, for example, the present state of the XPICK work environment, see *Fig. II.2.1*. One of the useful improvements would certainly be a possibility of scrolling the window, in which the seismograms are displayed. The seismograms are shown all at once, regardless of their number. Thus, the more stations recorded the event, the smaller the amplitudes are in the monitor. Further, a detail window in which we could view a part of a seismogram is not available. And finally, a possibility of displaying the traces in a different manner (e.g., according to the epicentral distance) than in alphabetical order, which does not make any physical sense, would also facilitate the picking routine.

The idea of correlating the waveforms and aligning them according to the first onsets is very effective and it could make faster and easier the picking routine indeed. However, many factors contribute to uncertainties in the alignment, especially differences among the waveforms at the stations (unequal width of the signals as a consequence of dispersion, different signal-to-noise ratios, etc.). But even the requirement of selecting one reference station might induce problems in aligning the traces with sufficient accuracy. It is fundamental that the signal recorded at the reference station includes characteristics typical for other stations in the array. This requirement is not satisfied automatically because each a-priori chosen seismogram has its own peculiarities that are typical just for the reference trace. Even the feature of a high quality might be a characteristic belonging only to a few traces (including the reference trace) and therefore, potentially causing difficulties in correlating the reference seismogram with a noisy or weak record.

II.2.4. Conclusions on the XPICK software

Approximately only every fifth event was picked with the sufficient accuracy by the XPICK program itself, so that it was not necessary to repick any trace of the event manually. The arrival times in seismograms from other events (~ 80%) needed to be corrected manually. Along with the not a user-friendly designed work environment, the picking procedure with the XPICK program was neither faster nor more accurate in comparison with the standard manual picking routine.

II.3. Adaptive Stacking

II.3.1. Theory of the Adaptive Stacking method

How can we avoid the complication of selecting only one reference waveform? Rawlinson and Kennett (2004) published an 'Adaptive Stacking' approach as a new semi-automatic picking method, based on the similarity among the waveforms through a seismic array. In contrast with the previous picker, the Adaptive Stacking does not require the a-priori selection of a reference station. The waveform which is compared with signals at other stations is computed by the picker. This waveform is called 'linear stack' $V_l(t)$ and is evaluated according to formula:

$$V_l(t) = \frac{1}{N}\sum_{i=1}^{N} u_i\left(t - t^c{}_i\right) \qquad \text{(II.3.1)}$$

$u_i(t)$ is the signal at the time t at the i-th station, $t^c{}_i$ is the time moveout correction derived from a specific velocity model and N is number of stations. Great advantage of this procedure is that the linear stack represents a typical waveform across the array, not only a waveform from a single station which potentially comprises some characteristics representative just for this single station. And in addition, the signal, which comes to all stations, is intensified, whereas the noise, which is casual at each station, is suppressed in the linear stack.

Besides the linear stack, a quadratic stack $V_q(t)$ is evaluated as well:

$$V_q(t) = \frac{1}{N}\sum_{i=1}^{N} u_i{}^2\left(t - t^c{}_i\right) \qquad \text{I.3.2)}$$

The quadratic stack expresses the spread in alignment between the stations.

Next step in the Adaptive Stacking procedure is a comparison of each trace with the linear stack and a direct search over time-shift τ to minimize the L_p measure of misfit, defined for i-th station as:

$$P_p{}^i = \sum_{j=1}^{M} \left| V_l(t_j) - u_i\left(t_j - t^c{}_j - \tau\right)\right|^p \qquad \text{(II.3.3)}$$

M is number of samples in the trace segment.

Before the calculation, we have to specify a time interval, in which the time correction τ is searched. The interval should be only a few seconds wide, thus evaluating the misfit for all discrete time-shifts τ located in the time interval is not time consuming. The time-shift τ_i at the i-th station is located in the selected interval, in the minimum of the misfit $P_p{}^i$.

Having the set of time corrections $\{\tau_i\}$, a new and more precise linear stack $V_l(t)$ can be estimated from the shifted traces $u_i\left(t - t^c{}_i - \tau_i\right)$ according to formula (II.3.1). Then the alignment procedure is repeated for each station using the improved stack and a new set of time corrections $\{\tau_i\}$ is evaluated. The process is repeated iteratively, until a stable alignment is obtained. The final time corrections $\{\tau_i\}$ are written into an output file *.ttr (see *chapter II.3.2.*).

II.3.2. Adaptive Stacking in practice

The Adaptive Stacking program, called *tcas,* is written in ForTran77 programming language by Nick Rawlinson and Brian Kennett (Research School of Earth Sciences, Australian National University, Canberra). The theoretical background of this picking procedure is elucidated in the paper 'Rapid estimation of relative and absolute delay times across a network by Adaptive Stacking' (Rawlinson and Kennett, 2004).

Program *tcas* processes data saved in format AQ (see *chapter II.3.3.*). The *tcas* program requires also an input file *tcas.cmd* which contains several parameters for the calculation:

(a) *number of iterations* – 5 iterations should be enough for a strong signal
(b) *index for phase stack* – called p in formula (II.3.3), the value recommended by the authors is 3 (L_3 norm)
(c) *coefficient for pick error and max, min error limits* – influencing the error estimates
(d) *stack window* – start and length of the window desired to be stacked (in seconds)
(e) *event file* – name of the AQ file with the data, e.g., *RE0411150906.aq* ('*RE*' is the abbreviation of the experiment RETREAT and next numbers indicate the event)
(f) *max and min diff time* – allowed interval for the travel-time residuals; for teleseismic events ±(1.0 s; 2.0 s) should be sufficient

As soon as the file with data in AQ format (see *chapter II.3.3.*) and the input file *tcas.cmd* are prepared, program *tcas* can be run just by typing '*tcas*' in the command line. The program writes the lowest value of the trace misfit measure (related to the sought set of the time corrections $\{\tau_i\}$) on the screen after each iteration and generates three output files: *asi0411150.aq*; *asf0411150.aq*; *RE0411150.ttr*.

The file *asi0411150.aq* contains the data of the initial alignment of the traces (after the moveout correction) and *asf0411150.aq* contains the final alignment (after all iterations). Both files *.aq are essentially the same as the AQ input file *RE0411150906.aq*, except that the data of two traces were added at the end of the **.aq* files. The first added trace is the linear stack (zssl) and the second one is the quadratic stack (zscp). After plotting both data files, one can see that the final stacked seismograms are aligned much better in comparison with the initially stacked traces and that in case of the final stack (*asf0411150.aq*), the linear and quadratic stacks are narrower and better defined than in the initial stack (*asi0411150.aq*).

The file *RE0411150.ttr* contains the travel-time residuals and the error estimates. The beginning of the file is shown in *Tab. II.3.1*. First eight lines contain the information about the event (number of stations, localization of the epicentre, trace start time, number of seconds between the origin time of an event and the trace start time (dummy value in this example), the sampling interval in seconds and the name of the phase) and number of iterations. Lines with results of individual stations follow in a series: a station number, a station name; a final time shift $\{\tau_i\}$

required to achieve the final alignment (relative time residual), an error estimate, an initial time shift obtained from the propagation model (moveout) and an indicator whether the trace was (1) or was not (0) used in the computation.

Table II.3.1 **Example of *.ttr file**

```
          33
   4.7000    -77.5100     25.000
  2004    11    15
     9    18   57.1000
 999.9900
 0.0500
 P
          5
   1   ANZR  -0.3000   0.1934    2.6108   1
   2   BOB   -0.2500   0.1416    8.6973   1
   3   CAIR  -0.4000   0.1088    3.0734   1
   4   CING   0.3000   0.0712   -4.8989   1
   5   CLLR   0.6000   0.1408    2.8488   1
   6   CRER   0.5500   0.0653   -0.4463   1
   7   CSNR   0.4000   0.0250    1.8765   1
   8   CSTR  -0.6000   0.0762    2.9998   1
   9   CUTR   0.3500   0.1136    3.9139   1
  10   ELBR  -0.1000   0.0608    5.6525   1
```

In addition to *tcas* program, the package for the Adaptive Stacking procedure also involves a program intended for plotting the traces saved in the AQ file. The program is called *aqplot* and uses the PGPLOT graphics subroutine library which can be downloaded free of charge from

http://www.astro.caltech.edu/~tjp/pgplot/.

Program *aqplot* requires an input file called *aqplot.in* that includes the name of the plotted file (e.g., *asf0411150.aq*), format of the output file (*ps* – landscape postscript, *vps* – portrait postscript, etc.) and several parameters determining the plotting pen. Program *aqplot* plots the seismograms into an output file called *pgplot.ps* by default.

II.3.3. Dataset and its conversion to AQ format

Implementation of the Adaptive Stacking semi-automatic picker into the picking routine would notably shorten the time needed for present manual procedure. Thus, we decided to test out the Adaptive Stacking program on a small subset from the dataset collected during the passive seismic experiment RETREAT (see *chapter I.2.*). In order to learn quickly and without difficulties manipulation with the program, we chose 8 different events (*Tab. II.3.2*) characterized by different sharpness of the onsets and signal-to-noise ratios.

Table II.3.2 **List of selected events to test the Adaptive Stacking program**

DAY – number of days from the start of recording; **EVENT** – event code compiled of the origin date and time; **DATE** – origin date [yy/mm/dd]; **OT** – origin time [hhmmss.ss]; **LAT** – latitude [º]; **LON** – longitude [º]; **D** – depth [km]; **MAG** – moment magnitude; **BACK** – back-azimuth [º]; **DIST** – epicentral distance [º]

DAY	EVENT	DATE	OT	LAT	LON	D	MAG	BAZ	DIST
250	0406280949	04/06/28	094947.00	54.80	-134.25	20	6.8	340.1	77.0
251	0406290701	04/06/29	070130.90	10.74	-87.04	9	6.3	283.0	88.0
319	0409051007	04/09/05	100707.82	33.07	136.62	14	7.2	42.6	88.8
320	0409062329	04/09/06	232935.09	33.21	137.23	10	6.6	42.1	89.0
333	0409192026	04/09/19	202604.10	52.21	174.03	25	6.2	10.1	83.0
390	0411150906	04/11/15	090656.56	4.70	-77.51	15	7.2	272.0	85.3
403	0411281832	04/11/28	183214.13	43.01	145.12	39	7.0	31.6	84.2
411	0412061415	04/12/06	141511.89	42.90	145.23	35	6.8	31.5	84.4

The AQ data format is an ASCII format including information about the event in the heading followed by the time series for each station. We show several beginning lines of an AQ file in *Tab. II.3.3* as an example of the format. The first five lines contain general information about the event: a number of stations that recorded the signal; latitude, longitude and depth of the event; date (year, month, day) of the trace start; trace start time (hours, minutes and seconds), followed by a number of seconds between the origin time and the trace start time (not the same value as the travel time!!); sampling interval in seconds (must be the same across whole array) and the name of picked phase. In practice, program *tcas* doesn't use all these values during the calculations. It really employs only the number of stations that recorded the signal and the sampling interval. The other stated numbers are dummy values which are not required by *tcas*. Nevertheless, presence of all that information makes the file well-arranged.

After the heading describing the event, the station specifications and the records of the arriving waves follow. The sixth line contains a number that denotes whether we want (1) or do not (0) the trace to be involved in the computation; a count of samples in the time series (unless this number is same for all stations, the running program collapses!!); a moveout correction in seconds and an identifier of the station. From next line, the values of the time series recorded at the given station are placed in sequence.

Table II.3.3 **Example of an AQ file**

```
33
4.7000     -77.5100     15.00
2004     11     15
9      18     57.099998       999.99999
 0.050   P
 1     1834       2.61078     ANZR
85881760.       87252480.       87992912.       82715032.
81056272.       78194080.       78805808.       62055920.
47730260.       53460520.       58650920.       41162660.
26694150.       14894330.      -11834340.       2178240.0
7443158.0       26090960.       12971670.      -19977350.      -
37934200.      -61934992.      -84292040.      -69664784.      -
61521780.      -46568180.      -37626128.      -42031328.      -
68081424.      -49948140.      -29881610.      -29606230.      -
38148320.      -29515230.      -3389742.0      -44175760.      -
74153632.      -76601424.      -53152568.      -41428140.      -
48047872.      -38709688.       3396099.0       30878750.
41321408.       12508680.      -3774684.0       16251500.
27448130.       44261940.       22080430.      -1123377.0      -
8441422.0       16553090.       35440340.       33420200.
78588736.       90367952.
```

The RETREAT data are stored in miniSEED format in the GFÚ, thus the selected data had to be converted from the miniSEED into the AQ format. The conversion is feasible in the Seismic Handler software (Stammler, 1993). After loading the event into Seismic Handler and selecting the segment containing the signal, it is necessary to resample all the traces to the same sampling interval. To unify the sampling interval at 50ms, we must type '*resample all 0.05*' in the command line. After that, the displayed segment of traces can be saved using command '*writea/npl=1 0411150906.ascii all station start*'. The data will be written into the ASCII file called *0411150906.ASCII* (number *0411150906* indicates the event according to *Tab. II.3.2*). The file contains a short heading (the sampling interval, number of samples, code of the station, trace start time) and the measured values for each station.

A moveout correction is a time interval that expresses the difference in the theoretic travel time at a given station and the theoretic travel time at a reference point according to a specific velocity model. A station in the centre of the array is usually selected as the reference site. Applying the moveout correction, we remove the part of the travel time caused by different epicentral distances across the array and we get a rough alignment of the traces. The corrections must be evaluated separately, apart from the main computing procedure, and inserted into the AQ file. In the case of RETREAT experiment (see *chapter I.2.*), we used IASP91 (Kennett, 1991) as the 1D velocity model and station SFIR (see *Fig. I.2.1*) as the reference station, because it is located approximately in the centre of the array. We calculated the travel times for all the stations in the array using program *TauP* (Crotwell et al., 1999) and determined the moveout corrections. Finally, we can create the AQ file *RE0411150906.aq* (see *Tab. II.3.3*) by putting together the ASCII file with the data and the file containing the moveout corrections.

II.3.4. Application of the Adaptive Stacking picker on the selected events from the RETREAT dataset

In this chapter, we show results (*Attachment 4*) of the Adaptive Stacking procedure applied on the selected data (see *Tab. II.3.2*) from the RETRAT experiment (see *chapter I.2.*) and we discuss them. All the figures in *Attachment 4*, computed with *tcas* and plotted with *aqplot* from the *asi*.aq* and *asf*.aq* files, represent broadband (BB) seismograms (CMG-40T) except for the event No. 0406280949, of which there is also a short-period (SP) filtered record – WWSSN-SP response. We added red vertical lines drawn according to the first onset in the linear stack into the final stack figures. It shows how well the first onset alignment is achieved. We remind that the linear stack is a waveform typical across the whole array, i.e., an average of all seismograms for the event. The blue vertical line marks the first extreme right after the first onset in the final linear stack. Such extreme is usually picked manually at each trace (correlated extreme) and the first onset is picked at only one station and computed consequently at the rest of the stations. This process is similar to aligning the first extreme after the first onset in the traces and the blue line shows the quality of this alignment.

The aim of stacking is to align the first onsets. Comparing the initial and the final stack, we can see that the traces are really well aligned. Looking in detail, some events are evidently better aligned than the others, e.g., event No. 0411150906 is aligned very precisely. It is a good example of waveforms that *tcas* can align perfectly. There is one strong period with a weak signal before and after it. Nevertheless, even in these exemplarily stacked traces we can see in detail that the seismograms with a little different shape of the signal (e.g., VLC, RONR, PIZR, MURB, FNVD, CRER) are moved slightly to one side.

Seismograms generated by the event No. 0412061415 are similar to those from the previous event; there is also one strong period. But in this case, the shape of the period differs much more from a station to another, thus the final stack is evidently less exact than in the previous case. E.g., stations SFIR, SCUR, RAVR, MTVR, CSTR, CLLR, BOB etc., are shifted out of the correct alignment of the first onsets about ~ 0.1 s.

In the case of event No. 0411281832, which contains a very strong period as well, the final stack is good except for the RSMR station. Stations SFIR, SCUR, RONR, RAVR, PIZR, MTVR, MNGR, CLLR and CSTR are shifted about ~ 0.1 s like in the previous case. RSMR station was shifted much more to the right instead of to the left by the procedure. It seems that the anomaly of RSMR should not be due to the short stack window, because the stack window appears to be wide enough to include the whole strong period at RSMR station (see the initial linear stack for the width of the stack window). It is not clear, why the trace at RSMR station was moved totally out of the correct area.

In the picture of initial stack belonging to the event No. 0409062329, we can see that the traces are evidently more chaotic comparing with other initial stacks though the moveout corrections were already applied to this event. In this case, it is impossible to select a **short** stack window in which the onset and the first period after the onset for all stations would fit in the selected time interval. Thus, there is still long signal after the first period (see the final linear stack belonging to this event) that unfortunately differs quite a lot across the stations and badly influences

the results. The final stack of the onsets is not exact in cases of the stations, e.g., ZOCR, VOLR, PIIR. When the data is picked manually, the first extreme after the first onset is usually marked. We can see that these three stated stations are incorrectly aligned not only in case of the first onsets but also the extremes after the onset are not aligned well. And both, the first onset and the extreme after the first onset, are shifted to the same side.

On the other hand, this event is a very instructive illustration of an improvement between the linear/quadratic initial stack and linear/quadratic final stack. The characteristic waveform (one clear period after the first onset in the final linear stack) suddenly appears after a few iterations out of the ill-defined initial linear stack. Nevertheless, comparing this very nice final linear stack with casually elected trace from, e.g., ZOCR, VOLR, SFIR, PIIR, CING, BOB, BARR stations, we will see by eye that they differ very much. Especially the shape of the maximum after the first onset is different from the final linear stack. This fact certainly contributes to not very precise alignment of the first onsets.

Comparing the pictures of initial and final stack from the event No. 0409192026, we can see that the Adaptive Stacking procedure improved the alignment of the first onsets significantly. The traces in the initial stack seem to be chaotic just like in the case of the previous event (No. 0409062329). Thus, it was also necessary to select a little wider stack window than it was appropriate. Then the very strong maximum after the first onset was correlated, which evidently influenced the final stack, as it is visible in the picture of the final quadratic stack. The second peak, belonging to the maximum, is much stronger than the first one of the minimum. But in fact, manually we would pick the minimum and it seems that it would move the traces (VOLR, RSMR, PIIR) to the correct side so that the alignment of the first onsets would be better.

In the record of event No. 0406290701, there is a strong period following the first onset. The shape of this period does not differ very much across the array and there is requirement of only slight improvement of the alignment; initial stack is not bad. Observe that the initial and the final linear stack do not change notably. On the other hand, it is interesting to realize that the final quadratic stack transformed from two interfused peaks into two well separated peaks.

The event No. 0409051007 generated complicated and long-continuing seismograms. The strongest extreme does not arrive immediately after follow the first onset but more than 10 seconds later. Therefore, we carried out the Adaptive Stacking procedure twice with a different stack window width each time. In the first step, the stack window was 10 seconds wide and it contained the first minimum and a part of the following maximum. The second stack window was 20 seconds wide and it included also the strongest extreme in the signal. Final alignments are very good at both examples and they differ barely perceptibly one from the other. Such similarity is probably due to the weak widening of the signal across the array, the shape resemblance of the stacked part of the traces and also due to the good initial alignment after the application of moveout corrections. It is worth paying attention to the linear and especially quadratic final stacks in both cases. Comparing the final quadratic stack of the example with the shorter stack window with that of the longer stack window, we can clearly see to which part of the stack window was given priority in each case. In the first example, it is obvious that the main importance was assigned to the first minimum after the first onset. In the second

example, the first minimum is not as important as the minimum one period later which is much stronger. But fortunately, the time between the first onset and the strongest minimum is evidently nearly the same at all stations so the final alignment was not destroyed in the case of longer stack interval (no widening of the signal across the array).

And finally, we tested event No. 0406280949 with two different gain-frequency characteristics of the traces. Originally, all seismograms we work with are BB records (CMG-40T). But we decided to test the Adaptive Stacking procedure with the SP data as well and thus simulated the recordings of event No. 0406280949 with the WWSSN-SP response.

We can see that the alignment of BB waveforms is not bad in general, but looking in detail, it is not exact enough (e.g., stations MAON, RSMR, PIIR, etc.). The signal is complicated and the shape of the period after the first onset changes across the array. However, the alignment is still much better here than in the picture of the final stack processed by the Adaptive Stacking from the SP record. There is obviously no alignment; the traces are shifted one to the others over one or more periods. But this wrong result should not be very surprising because the Adaptive Stacking method is based on the correlation between the waveforms and in the SP record just one frequency prevails. Thus, it seems nearly impossible to align the first period after the first onset correctly, especially when the initial alignment is not very good. In case of manual picking, it would be also difficult to measure the arrival time correctly in this record.

II.3.5. Discussion about the Adaptive Stacking software

To obtain accurate results, it is important, besides other factors, to choose properly the input parameters in the file *tcas.cmd* (see *chapter II.3.2.*). All these parameters can be changed arbitrarily. Nevertheless, the parameters (d) and (f) mostly influence the final alignment. Concerning the parameter (f), *max and min diff time*, it is not useful to allow a large interval to the travel-time residuals because in that case, the values of the residuals tend to move to the width of the interval. Then, the average of the travel-time residuals is close to one of the edge values of the interval. It is more suitable that the average of the residuals over the stations is not far from the zero in conformity with formulas (I.3.2) and (I.3.3), i.e., the average of the relative residuals should be zero.

The choice of the parameter (d), *stack window*, is very important for accurate final alignment as well. First, we have to plot the seismograms and look through them to define the stack interval. The window should contain a small part of the trace before the onset and approximately one period of the signal after the onset. The interval should not be larger because another signal away from the onset would be stacked in that case. The misfit tends to be minimal when the strongest extreme in the stack window is aligned. The strongest extreme is not necessarily the first maximum or minimum after the onset. In case of an inappropriately wide stack window, we could obtain some untrue values of the travel-time residuals due to a strong signal situated far from the first onset but still involved in the large stack window. For example, the signal can widen across the array due to a large area of the array. The more significant widening of the signal across the array is and the further from the onset the strong extreme involved in the stack window is

situated, the worse the onsets are aligned. We can also obtain inaccurate results when the signal is not uniform at the stations (e.g., events No. 0409062329, 0406280949).

Incorrect results are also obtained in case of some periodic signal after the first onset and a large stack window (SP record from the event No. 0406280949). The periodicity might cause a shift of a trace over the whole period, so called cycle skipping effect. Such inconveniences occur when the frequency spectrum of the waveform is narrow, e.g., after applying a narrow-band filter to the dataset.

The results seem to be the best in case of a very simple waveform with low noise before the onset, then a high peak and a low minimum or vice-versa and only weak signal after the distinctive period. The Adaptive Stacking procedure can align such a record with high accuracy (e.g., event No. 0411281832).

Another factor that influences the accuracy of the final alignment is the quality of the initial alignment. If the traces keep being chaotic and not only very slightly shifted one to the others after applying the move out corrections, i.e., the initial stack, a long stack window must be selected. However, then a signal that we are not interested in will be correlated as well and it might negatively influence the final alignment (e.g., events No. 0409062329, 0409192026). In case of a good initial alignment (e.g., event No. 0406290701), the final alignment is just an improvement of the initial stack, thus a short stack window can be selected and only a small interval around the first onsets will be correlated then.

II.3.6. Conclusions on the Adaptive Stacking software

Program *tcas* aligns well the records with a simple signal, e.g., one strong period that does not change its shape significantly across the array. In the case of more complicated and changing waveforms, the final alignment of the first onsets is not as precise as in the simpler cases.

The quality of a final alignment depends also on the initial stack. The more aligned the traces are after the initial stack, the more precise final alignment we obtain. Adaptive Stacking just slightly improves the initial stack. However in practice, it is not rare that the travel-time residuals from some events are scattered significantly. The value of a residual depends on physical characteristics of material through which the wave passes and also the direction from which the wave comes is decisive. In case of a young active region with anisotropic structure, the travel-time residuals differing a lot across the array might occur. Regrettably, the Adaptive Stacking procedure is not successfully applicable on such recordings.

For some scientific purposes, one needs to measure the absolute travel-time residuals, not only the relative values. Unfortunately, it is not feasible to mark an absolute residual at a trace in *tcas* program, which is a practical complication for usage of this program.

Concerning the full automation of *tcas* program, its application on the RETRAT data does not seem feasible, because each event must be opened and looked through to determine the input parameters (especially the '*stack window*') and in addition, the Adaptive Stacking procedure is not sufficient for complicated records that unfortunately form the majority of the whole dataset in tectonically complicated provinces. Therefore, the software does not safe time, neither provides more precise measurements than the manual picking.

II.4. Autopick

The third semi-automatic picking programme that we have tested, is named Autopick (Vecsey, personal communication). It is a set of MatLab, Shell and Seismic Handler scripts created by Luděk Vecsey (GFÚ AV ČR). Autopick is not still in the final stage of its development and it has not been published yet. Even the name Autopick is preliminary and it has been used only in this work until now. Therefore, we will discuss the programme only very briefly in this section.

II.4.1. Data pre-processing

Before the main picking procedure, an automatic pre-processing routine, which estimates the quality of each individual event, was done in MatLab. The purpose of this procedure is the examination whether there is a signal with sufficient signal-to-noise ratio in the records of an event and whether it is worth loading and further processing.

The main idea of the pre-processing is application of STA/LTA (Bormann, 2002) method on the seismograms and also on an artificial trace named MEAN which is calculated for each event. The MEAN trace is similar to the linear stack in the Adaptive Stacking method (see *chapter II.3.1.*) - a sum of aligned traces. The alignment is achieved here with a cross-correlation of a few selected traces. It is preferred to compute the MEAN trace out of only a few and not all the recordings, because the cross-correlation takes a long time and we need the MEAN trace only for an approximate estimation of the signal quality. The output file of this procedure contains two quality numbers for each event. One quality number comes from STA/LTA analysis of the MEAN trace and the other is an average of the quality numbers computed for each trace of the event.

II.4.2. Picking procedure

The picking of the arrival times is performed in the Seismic Handler (Stammler, 1993). The Seismic Handler is a very powerful software package with many possibilities of signal processing and used as a standard software in data processing in the GFÚ. Until now, we have used it especially for manual picking of the first maximum or minimum coming after the first onset - correlated extreme - and an absolute arrival time at a station where the first onset is clearly visible. But the Seismic Handler is also able to correlate traces and to perform other useful procedures. In addition to that, Luděk Vecsey has come up with several ideas how to make the picking routine faster. Apart from the pre-processing procedure that points out the events worth picking, he prepared several scripts (written in shell; using Seismic Handler commands as well) that make faster loading and saving the event.

After opening the Seismic Handler software, we enter the first command (*go1*) that loads an event from a list containing the event numbers (one per row). Besides loading, the seismograms are automatically filtered and also re-sampled all to the same frequency. The filter type and the sampling frequency are defined in the shell script *go1.sh*. Then, we have to load the additional information pertaining to the event (in the toolbar: *save* → *recover evt file*; *locate* → *external locations*)

and we can also calculate theoretical arrival times of the waves of our interest (*locate → theo tables*) or sort the seismograms according to the epicentral distance (*trace list → sort distance*). At this moment, we look through the seismograms and if a trace is damaged, it should be deleted.

Now, the correlation of the traces proceeds. At an arbitrary trace, we determine a correlation window around the phase we want to pick and mark a maximum or minimum after the first onset of the phase of our interest. After the correlation (*array → correlation pick*), the correlated pick is indicated in each seismogram. We must revise them and change, if necessary. The correlated extremes need not to be marked in the most precise manner because the picking procedure does not end here. Now, we align the traces according to the correlated picks (*array → align*). Above the seismograms, a new trace appears. The trace is called ALIGN and it is a sum of all the aligned seismograms. We delete the auxiliary picks and the seismograms remains aligned.

In a trace (e.g., ALIGN), we delimit the first well apparent extreme after the first onset. An interval of half a period width around the extreme is enough. Then, Seismic Handler marks the maximum or minimum value of the selected time interval in each trace (*array → min/max pick*). If the seismograms were aligned with sufficient accuracy, the extreme we want to pick at each seismogram, would be situated somewhere in the selected time interval and consequently, it should be found and marked by *min/max pick* procedure. These picks are the final ones, therefore it is important to check them carefully, shift some picks to the right position if needed (flat extremes!!) and assign a different weight number in the cases where the pick is of worse quality than 1 (the best and default weight number, with an accuracy of one sample). And finally, we must determine an absolute pick in an arbitrary seismogram. As the noise is suppressed in the ALIGN trace, it is usually possible to mark the absolute pick in that trace.

Now, we can save the picks (*work → final parameters*) or cancel them if they are not good enough to be saved (*work → cancel parameters*). The output file containing the picks is saved in a directory determined by Seismic Handler. Command *go2* renames and moves the output file to a directory defined in the script *go2.sh*. If we enter the *go1* command at that moment, the event which is next in the list of events is loaded and prepared to be picked.

II.4.3. Application of picker Autopick on the RETREAT dataset

As in the cases of the previous pickers (see *chapters II.2.* and *II.3.*), we picked the arrival times of the P-waves in the seismograms from the RETREAT experiment (see *chapter I.2.*) with programme Autopick. This time, it was not only a subset but the whole dataset (938 teleseismic events) that we checked with the pre-processing routine (see *chapter II.4.1.*) and picked the P-wave first arrivals where it was possible.

Seismic Handler reads data in the AH, the GSE and the Q-file format. Q-file is a format designed particularly for the Seismic Handler. Therefore, we converted the data into the Q-file format. We decided to use the WWSSN-SP (see *chapter Y.2.*) filter and the re-sampling frequency of 100Hz. These both parameters are defined in the script *go1.sh* (see *chapter II.4.2.*).

We present 5 events picked with the Autopick (*Tab. II.4.1* and *Attachment 5*), as a few examples of all the picked events (312 earthquakes - *Attachment 2*). The events in *Tab. II.4.1* are sorted according to the quality number derived from the pre-processing. All the five events were also picked with the Adaptive Stacking (see *chapter II.3.*). Nevertheless, the direct comparison of the results from both methods is difficult because of different filters used in each of the procedures (Adaptive Stacking - broadband CMG40-T; Autopick - short period WWSSN-SP).

Table II.4.1 **List of discussed events picked with the Autopick**

QUAL – sequential number of the event in the list of events sorted according to the quality number; **DAY** – number of days from the start of recording; **EVENT** – event code compiled of the origin date and time; **DATE** – origin date [yy/mm/dd]; **OT** – origin time [hhmmss.ss]; **LAT** – latitude [°]; **LON** – longitude [°]; **D** – depth [km]; **MAG** – moment magnitude; **BACK** – back-azimuth [°]; **DIST** – epicentral distance [°]

QUAL	DAY	EVENT	DATE	OT	LAT	LON	D	MAG	BAZ	DIST
1	411	0412061415	04/12/06	141511.89	42.90	145.23	35	6.8	31.5	84.4
21	403	0411281832	04/11/28	183214.13	43.01	145.12	39	7.0	31.6	84.2
55	333	0409192026	04/09/19	202604.10	52.21	174.03	25	6.2	10.1	83.0
76	320	0409062329	04/09/06	232935.09	33.21	137.23	10	6.6	42.1	89.0
106	251	0406290701	04/06/29	070130.90	10.74	-87.04	9	6.3	283.0	88.0

The event No. 0412061415 originated a high-quality signal (the best according to the pre-processing procedure). Comparing with the picture from Adaptive Stacking (broad band; see *Attachment 4*), it seems that the short period filter suppressed the noise effectively and that the beginning part of the signal is more consistent across the stations in case of Autopick (short period). The correlated minimums were picked accurately and the absolute pick was marked in the ALIGN trace.

The short period filtration altered the record of event No. 0411281832 distinctly comparing with the broadband seismograms from Adaptive Stacking (see *Attachment 4*). But again the first minimum after the first onset is more consistent across the stations and therefore better for picking the correlated extremes which Autopick managed precisely. The absolute pick is picked in the ALIGN trace again.

In the case of event No. 0409192026, the signal is evidently worse for picking (55^{th} according to the quality number) than in the previous cases but the signal is still clear. After the short period filtration, the very slightly changing, nearly constant part right after the first onset (see *Attachment 4*) changed into rapidly oscillating signal but still consistent across the stations. This enabled us to pick the correlated extreme (maximum) which is closer to the absolute arrival time (picked in the RSMR trace in this case). In Seismic Handler, it is possible to put an arbitrary trace (e.g., ALIGN) on another and compare the differences. This can be very helpful when any doubts about the correct correlated extreme occur. It was used in case of, e.g., RAVR, BARR or VLC stations where the signal is slightly inconsistent with the other stations.

The event 0409062329 seems to be picked in the best possible manner. The beginning of the signal is not very strong but the moderate maximum after the first onset is clear and picked accurately in each trace.

The record of the event No. 0406290701 is very noisy, but in spite of that there is just one very strong amplitude in the signal, the minimum of which we picked as a correlated extreme. It is very difficult to determine the absolute arrival time at a station, because it is hidden in the noise. In the ALIGN trace, the noise should be suppressed comparing with the other stations as it is a sum of all the seismograms (see *chapter II.4.2.*) and it is really so in the case of event No. 0406290701. The ALIGN trace is also a little bit noisy but nevertheless, a sudden first onset is obvious and can be marked reliably there.

II.4.4. Discussion about the Autopick software

The benefit of the data pre-processing is evident. For each event, the quality of the signal-to-noise ratio is evaluated and thus we have a possibility to load and to pick preferentially the events with high quality numbers. The command *go1* loads the events into Seismic Handler in an order according to a list of event quality numbers (see *chapter II.4.2.*). In this manner, we reduce the number of loaded and opened events that could seem to be suitable for picking according to their magnitude, but their signal-to-noise rations are low in reality.

Picking the events in the order of their quality numbers made the measuring really faster, especially at the beginning of the picking. During the first day, we picked 60 high-quality events. The next days, the number of measured events (events of lower quality) decreased to ~ 35 events/day but it is still approximately three times more than with pure manual picking. And what should also be appreciated, is that among the first hundred events there was no event which we would not be able to pick at all! Afterwards, it was approximately 1 unsuitable per 15 good events and it was becoming worse gradually up to 1 bad per 5 good events after approximately 250 events. To finish the picking procedure in the most effective manner, we assorted the events according to the epicenter location - 16 segments comprising different epicentral distances (from 25° to 50° and from 50° to 105°) and back azimuths (from 0° to 360° after 45°) - and we focused on picking the events from the segments where the earthquakes were scarce to get the best possible ray coverage (see *Fig. I.2.2*).

In contrast to the two previous pickers (XPICK - *chapter II.2.*; Adaptive Stacking - *chapter II.3.*), where the process of waveform comparison is performed just once, the Autopick applies also, apart from the correlation by which a rough alignment is achieved, the *min/max pick* procedure that marks the maximum or minimum value in the selected interval (see *chapter II.4.2.*). This maximum or minimum is the correlated extreme that we usually want to pick. The *min/max pick* procedure improves the accuracy of the measuring (see the pictures of the picked seismograms; XPICK - *Figs. II.2.1-3*, Adaptive Stacking - *Attachment 4*, Autopick - *Attachment 5*).

The Seismic Handler is widely used and well developed picking software that provides a very comfortable work environment. Therefore, it was easy and fast to perform the manual corrections of the picks marked automatically by the Autopick in the seismograms, where it was necessary, especially in the cases of flat extremes,

for which the maximum or minimum was not obvious. There was a need for manual repicking from time to time in case of all the three tested semi-automatic pickers. No absolutely accurate (semi-)automatic picking program was probably invented up to now, therefore, it is very important whether the picking software includes a possibility of manual corrections of the picks or not.

II.4.5. Conclusions on the Autopick software

The picking of the whole dataset from the RETREAT experiment (see *chapter I.2.*) took less than two weeks of everyday eight-hour work. We marked the correlated extremes and an absolute pick at seismograms from 312 events (see *Fig. I.2.2* and *Attachment 2*) selected according to signal-to-noise ratio (quality number) and back-azimuth from 938 events in the event-oriented database from the RETREAT experiment.

However, considering the total time needed, apart from the main picking procedure (see *chapter II.4.2.*), one has to consider also to the pre-processing (see *chapter II.4.1.*), during which the quality of the records was estimated as well as the data re-formating.

The Autopick program (including MatLab pre-processing, shell scripts for a fluent data opening and saving and Seismic Handler rough correlation and *min/max pick* procedure) is a very fast, accurate and user-friendly semi-automatic picking software that is still under the development.

We consider the robust Autopick as the most accurate picking software of the three tested programs. Therefore, we employed the arrival times picked with the Autopick in the analysis of P-wave anisotropy in the Northern Apennines (see *Part I*).

Attachments

Attachment 1 - List of seismic stations involved in the RETREAT experiment

STA – station code; **LAT** – latitude [°]; **LON** – longitude [°]; **ALT** – altitude [km]

STA	LAT	LON	ALT	STA	LAT	LON	ALT
ANZR	44.5760	11.1500	0.039	MNGR	44.5070	10.7850	0.404
ARCI	42.8519	11.4754	1.080	MSTR	43.9130	10.4920	0.230
BADR	43.5100	12.2440	0.441	MTVR	44.4680	11.0910	0.274
BARR	44.2828	12.0797	0.079	MURB	43.2630	12.5246	0.845
BOB	44.7679	9.4478	0.910	PDCR	43.7810	10.5800	0.083
CAIR	44.2940	11.0030	0.848	PESR	43.9410	12.8400	0.152
CING	43.3756	13.1954	0.626	PIIR	43.7219	10.5250	0.066
CLLR	43.6680	11.0300	0.220	PIZR	44.1310	10.8620	1.236
CORR	44.4760	10.0890	0.702	PNTR	44.0110	10.8200	0.827
CRER	43.6190	11.9520	1.246	POPR	43.0220	10.5340	0.016
CSNR	43.4731	11.2902	0.636	PRUR	44.0100	10.3090	0.479
CSTR	44.4380	11.0320	0.310	PTCR	44.2440	10.9710	0.901
CUTR	44.1000	10.7560	0.691	RAPR	43.2890	11.6090	0.337
ELBR	42.7470	10.2110	0.146	RAVR	44.7559	11.1188	0.015
FIRR	44.1890	11.4340	0.721	RONR	44.2150	10.9230	1.048
FNVD	44.1678	11.1229	0.950	RSMR	43.9303	12.4497	0.645
FOSR	44.1350	10.0200	0.520	SACS	42.8491	11.9097	0.845
FSSR	43.6930	12.7770	0.480	SASR	43.2570	10.6900	0.431
GABR	43.5000	10.4130	0.246	SCUR	44.4156	9.5361	0.817
GRFR	43.1470	10.9760	0.741	SFIR	43.9048	11.8469	0.548
GROG	43.4262	9.8920	0.118	USOR	43.9810	10.6850	0.864
GUSR	44.3510	10.5880	0.666	VLC	44.1594	10.3864	0.562
MAON	42.4283	11.1309	0.237	VOLR	43.5478	10.8572	0.325
MASR	43.8611	11.3808	0.500	VRGR	43.6400	10.4700	0.011
MCUR	44.0050	11.1797	0.726	ZOCR	44.3508	10.9765	0.700

Attachment 2 - List of events used for P-wave directional-term analysis

DAY – number of days from the start of recording; **EVENT** – event code compiled of the origin date and time; **DATE** – origin date [yy/mm/dd]; **OT** – origin time [hhmmss.ss]; **LAT** – latitude [º]; **LON** – longitude [º]; **D** – depth [km]; **MAG** – moment magnitude; **BACK** – back-azimuth [º]; **DIST** – epicentral distance [º]

DAY	EVENT	DATE	OT	LAT	LON	D	MAG	BAZ	DIST
1	0310231054	03/10/23	105439.68	51.40	176.69	33	5.6	8.6	84.1
3	0310251241	03/10/25	124135.25	38.40	100.95	10	5.8	60.0	64.8
3	0310251247	03/10/25	124758.83	38.38	100.97	10	5.8	60.0	64.9
6	0310282148	03/10/28	214821.02	43.84	147.75	65	6.1	29.5	84.5
9	0310310106	03/10/31	010628.28	37.81	142.62	10	7.0	35.9	87.7
11	0311021335	03/11/02	133531.09	44.58	150.33	33	5.5	27.5	84.7
14	0311050058	03/11/05	005851.11	4.97	-77.77	33	6.0	272.4	85.3
18	0311091952	03/11/09	195236.81	-0.67	-19.69	10	6.6	219.7	51.9
21	0311120826	03/11/12	082643.74	33.17	137.07	384	6.4	42.3	89.0
23	0311141843	03/11/14	184351.14	36.40	141.07	41	5.7	37.7	88.2
26	0311170643	03/11/17	064306.80	51.15	178.65	33	7.8	7.5	84.6
26	0311170712	03/11/17	071242.55	51.28	177.61	33	5.8	8.1	84.3
27	0311180212	03/11/18	021222.57	51.10	178.12	33	5.5	7.8	84.6
27	0311180750	03/11/18	075010.66	51.04	178.89	33	5.8	7.3	84.7
35	0311261925	03/11/26	192507.34	28.52	-43.73	10	5.6	269.2	45.5
40	0312010138	03/12/01	013831.96	42.90	80.51	10	6.0	65.2	49.3
44	0312052126	03/12/05	212609.48	55.54	165.78	10	6.7	14.0	78.6
48	0312091244	03/12/09	124401.68	51.33	-179.27	33	6.2	6.1	84.6
58	0312190011	03/12/19	001158.23	19.85	95.70	10	5.6	78.5	73.0
60	0312210740	03/12/21	074045.83	-0.77	-20.60	10	6.6	220.7	52.5
61	0312220847	03/12/22	084707.35	42.28	144.60	37	5.8	32.3	84.7
62	0312230558	03/12/23	055837.19	-0.70	-20.33	10	5.8	220.4	52.3
65	0312260156	03/12/26	015652.44	29.00	58.31	10	6.8	94.9	40.6
68	0312290130	03/12/29	013054.70	42.42	144.61	33	6.1	32.2	84.5
81	0401110432	04/01/11	043247.79	-36.70	53.35	5	6.2	147.0	89.3
81	0401111931	04/01/11	193132.81	55.60	165.68	21	5.5	14.0	78.5
86	0401161807	04/01/16	180755.66	7.64	-37.70	10	6.2	244.0	55.3
89	0401190722	04/01/19	072252.91	84.47	105.21	10	5.6	7.5	47.0
94	0401241301	04/01/24	130145.70	52.12	-30.18	10	5.9	301.8	28.1
96	0401261027	04/01/26	102707.65	51.13	178.08	36	5.6	7.8	84.5
97	0401270950	04/01/27	095052.17	56.81	-156.76	75	5.6	352.9	78.9
100	0401301751	04/01/30	175144.81	44.73	150.06	30	5.5	27.6	84.5
111	0402102033	04/02/10	203351.27	59.37	-152.03	65	5.6	350.9	75.9
115	0402141030	04/02/14	103022.18	34.77	73.22	11	5.5	78.3	48.2
123	0402220646	04/02/22	064627.04	-1.56	100.49	42	6.3	91.2	91.1
126	0402250856	04/02/25	085606.50	54.62	162.81	19	5.5	15.9	78.9
138	0403082339	04/03/08	233911.34	10.48	-43.92	10	6.0	251.8	57.4

DAY	EVENT	DATE	OT	LAT	LON	D	MAG	BAZ	DIST
142	0403122245	04/03/12	224519.00	36.40	70.77	218	5.8	77.7	45.7
146	0403162123	04/03/16	212319.86	37.56	96.67	14	5.5	63.0	62.6
147	0403170321	04/03/17	032107.91	-21.12	-65.59	289	6.1	245.4	95.0
149	0403192042	04/03/19	204200.31	-34.50	55.28	10	5.7	144.5	88.2
150	0403200853	04/03/20	085315.11	53.83	160.47	52	5.8	17.5	79.1
156	0403261520	04/03/26	152006.62	41.86	144.21	22	5.8	32.7	84.9
157	0403271847	04/03/27	184729.20	33.95	89.18	8	6.0	70.3	59.7
166	0404052124	04/04/05	212404.00	36.51	71.03	187	6.6	77.4	45.8
170	0404090155	04/04/09	015550.71	-1.55	100.54	65	5.5	91.1	91.1
175	0404140154	04/04/14	015409.22	55.23	162.66	51	6.2	15.8	78.3
175	0404142307	04/04/14	230739.94	71.07	-7.75	12	6.0	347.8	28.8
197	0405061343	04/05/06	134312.89	42.53	145.02	28	5.6	31.9	84.6
202	0405110828	04/05/11	082848.28	0.41	97.82	21	6.2	91.6	87.8
202	0405112358	04/05/11	235854.41	12.70	-44.49	10	5.5	254.1	56.2
219	0405281238	04/05/28	123844.47	36.29	51.61	17	6.3	89.2	32.0
220	0405290347	04/05/29	034710.77	37.75	141.88	29	5.8	36.5	87.4
226	0406040148	04/06/04	014803.17	54.46	-163.85	72	5.6	356.7	81.7
232	0406101519	04/06/10	151957.75	55.68	160.00	188	6.9	17.1	77.3
249	0406271251	04/06/27	125150.35	-40.92	43.31	10	5.6	155.8	89.6
250	0406280949	04/06/28	094947.00	54.80	-134.25	20	6.8	340.1	77.0
251	0406290701	04/06/29	070130.90	10.74	-87.04	9	6.3	283.0	88.0
253	0407010920	04/07/01	092044.14	54.13	-35.26	10	5.6	305.8	31.2
260	0407081030	04/07/08	103049.16	47.20	151.30	128	6.4	25.7	82.7
269	0407170610	04/07/17	061018.07	34.75	140.22	46	5.6	39.2	89.2
271	0407190801	04/07/19	080149.46	49.62	-126.97	23	6.4	333.6	79.6
273	0407210011	04/07/21	001129.78	40.97	143.08	30	5.5	33.9	85.2
274	0407220945	04/07/22	094514.90	26.49	128.89	20	6.1	52.0	89.9
277	0407251435	04/07/25	143519.06	-2.43	103.98	582	7.3	89.4	94.2
281	0407290144	04/07/29	014406.91	12.45	95.00	22	5.9	84.7	77.5
281	0407291323	04/07/29	132303.28	12.44	95.00	24	5.6	84.7	77.5
290	0408070930	04/08/07	093016.94	51.75	-166.31	8	6.3	358.0	84.5
290	0408071418	04/08/07	141835.23	-6.24	95.67	20	5.8	97.9	90.8
293	0408100147	04/08/10	014732.81	36.44	70.80	207	6.0	77.6	45.7
293	0408100613	04/08/10	061333.24	39.63	141.96	69	5.7	35.4	85.8
307	0408241005	04/08/24	100534.47	32.54	92.19	10	5.7	70.0	62.6
313	0408301223	04/08/30	122321.60	49.54	157.28	11	5.7	21.0	82.3
319	0409051007	04/09/05	100707.82	33.07	136.62	14	7.2	42.6	88.8
319	0409051457	04/09/05	145718.61	33.18	137.07	10	7.4	42.3	89.0
320	0409062329	04/09/06	232935.09	33.21	137.23	10	6.6	42.1	89.0
321	0409071836	04/09/07	183620.27	33.24	137.09	10	5.6	42.2	88.9
322	0409081458	04/09/08	145825.83	33.14	137.20	21	6.2	42.2	89.1
323	0409091633	04/09/09	163321.73	17.76	-81.55	25	6.0	284.4	79.3
327	0409130300	04/09/13	030012.85	44.00	151.41	8	6.1	27.1	85.6
329	0409151910	04/09/15	191050.59	14.22	120.41	115	6.0	66.0	93.9
332	0409180707	04/09/18	070748.43	23.11	-67.61	10	5.7	279.6	65.9
333	0409192026	04/09/19	202604.09	52.21	174.03	25	6.2	10.1	83.0

DAY	EVENT	DATE	OT	LAT	LON	D	MAG	BAZ	DIST
350	0410061440	04/10/06	144039.92	35.95	139.92	64	5.8	38.8	88.0
351	0410072146	04/10/07	214620.30	37.12	54.48	34	5.6	85.9	33.7
352	0410081436	04/10/08	143606.11	13.93	120.53	105	6.5	66.1	94.2
359	0410150408	04/10/15	040850.24	24.53	122.69	94	6.7	57.5	87.8
366	0410221200	04/10/22	120012.43	14.17	40.30	10	5.5	130.1	39.0
367	0410230856	04/10/23	085600.86	37.23	138.78	16	6.6	38.8	86.5
367	0410230903	04/10/23	090312.53	37.32	138.82	10	6.1	38.7	86.4
367	0410230911	04/10/23	091157.42	37.24	138.61	18	5.8	38.9	86.4
367	0410230934	04/10/23	093404.99	37.32	138.81	10	6.3	38.7	86.4
368	0410242104	04/10/24	210457.06	37.31	138.70	11	6.0	38.8	86.4
370	0410260211	04/10/26	021133.44	31.02	81.15	10	6.0	77.7	55.8
371	0410270140	04/10/27	014050.26	37.28	138.88	14	6.0	38.7	86.5
379	0411041403	04/11/04	140311.67	43.62	146.81	61	5.9	30.2	84.3
383	0411081555	04/11/08	155501.16	24.10	122.54	29	6.3	57.9	88.0
386	0411111002	04/11/11	100247.33	42.14	144.34	32	6.1	32.5	84.7
390	0411150906	04/11/15	090656.56	4.70	-77.51	15	7.2	272.0	85.3
391	0411161157	04/11/16	115728.14	53.06	160.13	48	5.5	18.0	79.8
392	0411172058	04/11/17	205822.31	39.19	71.86	20	5.8	73.6	45.1
395	0411200807	04/11/20	080722.08	9.60	-84.17	16	6.4	280.2	86.7
396	0411211141	04/11/21	114107.76	15.68	-61.71	14	6.3	269.5	66.5
401	0411262242	04/11/26	224237.31	42.38	142.90	58	5.7	33.3	83.9
403	0411281832	04/11/28	183214.12	43.01	145.12	39	7.0	31.6	84.2
411	0412061415	04/12/06	141511.89	42.90	145.23	35	6.8	31.5	84.4
419	0412140556	04/12/14	055610.04	44.12	141.79	10	5.8	33.0	82.0
419	0412142320	04/12/14	232013.36	18.96	-81.41	10	6.8	285.2	78.4
426	0412211534	04/12/21	153428.12	42.96	145.41	37	5.7	31.4	84.4
431	0412260308	04/12/26	030844.21	13.74	93.01	30	5.9	85.0	75.2
431	0412260324	04/12/26	032454.94	4.47	94.07	26	5.8	91.2	82.2
431	0412261019	04/12/26	101931.73	13.46	92.74	26	6.3	85.4	75.2
431	0412261448	04/12/26	144844.27	13.59	92.91	30	5.8	85.2	75.2
432	0412270032	04/12/27	003216.48	5.48	94.47	33	6.1	90.2	81.8
432	0412270049	04/12/27	004928.59	12.98	92.39	23	6.1	86.0	75.2
432	0412270939	04/12/27	093906.80	5.35	94.65	35	6.2	90.2	82.1
432	0412271446	04/12/27	144646.48	12.35	92.47	19	5.8	86.5	75.7
433	0412281117	04/12/28	111743.87	4.73	95.21	36	5.8	90.2	82.9
434	0412290139	04/12/29	013941.24	8.38	93.16	34	5.9	89.0	78.9
434	0412290150	04/12/29	015052.57	9.11	93.76	8	6.1	88.0	78.8
434	0412290556	04/12/29	055647.54	8.79	93.20	12	6.2	88.6	78.7
434	0412292112	04/12/29	211259.47	5.23	94.62	29	5.7	90.3	82.1
435	0412301758	04/12/30	175811.19	12.24	92.51	30	5.8	86.5	75.8
436	0412311438	04/12/31	143846.62	5.11	94.86	49	5.6	90.2	82.4
437	0501010403	05/01/01	040310.99	5.47	94.40	36	5.8	90.3	81.8
437	0501010625	05/01/01	062544.82	5.10	92.30	11	6.7	92.0	80.5
437	0501011908	05/01/01	190807.80	7.34	94.46	55	6.1	88.8	80.6
437	0501012228	05/01/01	222813.78	7.19	92.76	10	5.5	90.1	79.4
438	0501020827	05/01/02	082741.89	3.24	95.46	8	5.9	91.2	84.1

DAY	EVENT	DATE	OT	LAT	LON	D	MAG	BAZ	DIST
438	0501021535	05/01/02	153556.72	6.36	92.79	30	6.4	90.7	80.0
440	0501040913	05/01/04	091312.25	10.67	92.36	23	6.1	87.8	76.8
441	0501051454	05/01/05	145404.81	5.49	94.39	48	5.9	90.3	81.8
442	0501060011	05/01/06	001117.10	5.60	93.25	30	5.5	91.0	80.9
442	0501060056	05/01/06	005629.91	5.32	94.83	49	6.1	90.1	82.2
443	0501071049	05/01/07	104914.33	8.77	93.56	30	5.5	88.4	78.9
445	0501092212	05/01/09	221256.52	4.93	95.11	40	6.1	90.2	82.7
448	0501120840	05/01/12	084003.65	-0.88	-21.19	10	6.8	221.3	52.8
454	0501180659	05/01/18	065903.74	57.05	-33.81	10	5.7	311.6	30.6
454	0501181409	05/01/18	140906.22	42.95	144.87	42	6.3	31.7	84.2
456	0501200259	05/01/20	025910.50	49.83	156.18	38	5.5	21.6	81.8
460	0501240416	05/01/24	041647.44	7.33	92.48	30	6.3	90.2	79.1
463	0501272009	05/01/27	200952.16	5.51	94.31	30	5.6	90.3	81.7
473	0502060424	05/02/06	042418.63	13.85	93.58	35	5.6	84.6	75.5
480	0502130122	05/02/13	012209.31	5.08	94.79	48	5.7	90.3	82.3
481	0502142338	05/02/14	233808.66	41.73	79.44	22	6.2	67.0	49.1
483	0502162027	05/02/16	202752.48	-36.32	-16.56	10	6.6	201.7	83.7
484	0502170531	05/02/17	053128.08	4.70	95.16	47	5.9	90.3	82.9
485	0502181933	05/02/18	193346.41	5.45	94.42	48	5.8	90.3	81.8
489	0502220225	05/02/22	022522.92	30.75	56.82	14	6.5	93.8	38.5
492	0502252304	05/02/25	230404.02	38.11	72.71	114	6.1	74.6	46.2
493	0502261237	05/02/26	123740.69	40.73	142.38	68	5.8	34.5	85.1
493	0502261256	05/02/26	125652.62	2.91	95.59	36	6.8	91.3	84.4
501	0503060521	05/03/06	052143.43	84.95	99.39	10	6.3	7.0	46.4
505	0503100028	05/03/10	002826.36	85.25	92.89	10	5.5	6.6	45.8
508	0503130331	05/03/13	033123.08	27.09	61.89	54	6.0	94.5	44.2
508	0503132212	05/03/13	221245.81	5.49	94.60	52	5.5	90.1	81.9
511	0503161323	05/03/16	132332.56	43.47	146.89	39	5.6	30.2	84.5
512	0503171337	05/03/17	133737.11	15.14	-91.38	197	6.1	289.1	87.9
512	0503172320	05/03/17	232049.34	4.86	95.09	60	5.7	90.2	82.7
515	0503200153	05/03/20	015341.83	33.81	130.13	10	6.7	46.5	85.0
520	0503250104	05/03/25	010452.96	5.49	94.37	39	5.9	90.3	81.8
523	0503281609	05/03/28	160936.53	2.09	97.11	30	8.6	90.8	86.1
523	0503281830	05/03/28	183044.56	0.92	97.87	36	6.1	91.2	87.4
523	0503281902	05/03/28	190219.91	1.01	97.82	30	5.8	91.1	87.3
523	0503282313	05/03/28	231300.95	0.17	97.04	38	5.7	92.3	87.4
526	0503310723	05/03/31	072353.79	1.70	97.12	22	5.8	91.1	86.4
528	0504021252	05/04/02	125236.59	78.61	6.10	10	6.1	358.5	34.9
529	0504030059	05/04/03	005921.42	0.37	98.32	30	6.0	91.3	88.2
529	0504030310	05/04/03	031056.47	2.02	97.94	36	6.3	90.3	86.7
533	0504072004	05/04/07	200441.06	30.49	83.66	11	6.3	76.8	57.9
535	0504091516	05/04/09	151627.89	56.17	-154.52	14	6.0	351.6	79.3
536	0504101114	05/04/10	111419.62	-1.71	99.78	30	6.5	91.8	90.6
536	0504102222	05/04/10	222215.70	35.60	140.40	43	6.1	38.6	88.5
540	0504141129	05/04/14	112952.55	-1.91	99.95	33	5.8	91.8	90.9
543	0504172123	05/04/17	212350.83	-1.63	99.62	21	5.8	91.8	90.5

DAY	EVENT	DATE	OT	LAT	LON	D	MAG	BAZ	DIST
570	0505140505	05/05/14	050518.48	0.59	98.46	34	6.8	91.0	88.1
570	0505141804	05/05/14	180455.06	30.69	56.86	10	5.5	93.8	38.6
577	0505210511	05/05/21	051135.39	-3.29	-80.99	39	6.3	268.7	93.4
577	0505212301	05/05/21	230116.05	5.28	94.80	55	5.9	90.1	82.2
587	0505310229	05/05/31	022931.29	5.24	94.43	30	5.5	90.4	82.0
588	0506012006	05/06/01	200641.45	28.88	94.63	25	6.1	71.8	66.5
597	0506100350	05/06/10	035007.88	51.19	179.55	40	5.6	6.9	84.6
599	0506120417	05/06/12	041713.49	52.79	143.87	10	5.6	27.0	75.5
600	0506132244	05/06/13	224433.91	-19.99	-69.20	115	7.8	248.6	96.6
601	0506141710	05/06/14	171012.28	51.24	179.31	17	6.8	7.0	84.5
601	0506142249	05/06/14	224917.81	50.98	179.43	27	5.6	7.0	84.8
602	0506150250	05/06/15	025054.19	41.29	-125.95	16	7.2	328.8	86.4
604	0506170621	05/06/17	062142.59	40.77	-126.57	12	6.6	328.9	87.1
606	0506191615	05/06/19	161515.23	35.61	140.48	48	5.7	38.6	88.6
614	0506271135	05/06/27	113545.60	18.78	-107.30	20	6.2	302.7	95.6
618	0507010348	05/07/01	034828.69	36.57	71.32	63	5.6	77.2	46.0
621	0507041136	05/07/04	113605.65	-42.28	42.37	10	6.3	157.0	90.6
622	0507050152	05/07/05	015202.95	1.82	97.08	21	6.8	91.1	86.3
623	0507060824	05/07/06	082441.95	69.00	-16.64	10	5.6	340.2	28.9
626	0507092337	05/07/09	233711.14	33.42	140.82	55	5.8	39.5	90.5
637	0507202154	05/07/20	215405.72	43.07	109.02	6	5.5	51.8	66.8
640	0507230734	05/07/23	073456.77	35.50	139.98	61	6.1	39.0	88.4
640	0507231440	05/07/23	144025.02	36.39	70.72	209	5.5	77.7	45.6
640	0507232253	05/07/23	225335.08	5.11	94.80	48	5.6	90.2	82.3
641	0507241542	05/07/24	154206.20	7.92	92.19	16	7.5	90.0	78.5
642	0507251602	05/07/25	160207.56	71.11	-7.43	10	5.5	348.0	28.8
643	0507260408	05/07/26	040837.16	45.37	-112.61	12	5.7	323.0	77.6
643	0507261217	05/07/26	121714.27	52.87	160.10	27	5.8	18.1	79.9
643	0507261411	05/07/26	141136.39	-15.35	-72.96	110	5.9	254.4	96.0
644	0507270239	05/07/27	023922.57	33.26	142.32	33	5.5	38.6	91.4
646	0507290500	05/07/29	050030.09	52.91	-168.65	50	5.6	359.5	83.4
646	0507292033	05/07/29	203340.03	2.86	93.56	32	5.8	92.8	83.0
647	0507301513	05/07/30	151320.12	5.18	94.48	38	5.8	90.4	82.1
651	0508031103	05/08/03	110315.13	11.25	-85.54	14	6.5	282.3	86.6
653	0508050056	05/08/05	005653.72	51.24	-178.25	23	5.8	5.5	84.7
654	0508060402	05/08/06	040232.96	85.26	97.16	10	5.5	6.6	46.2
655	0508070217	05/08/07	021746.04	-47.09	33.62	10	6.2	164.5	93.1
664	0508160246	05/08/16	024628.40	38.28	142.04	36	7.2	36.1	87.0
673	0508252108	05/08/25	210813.03	36.94	79.17	17	5.5	72.6	51.3
685	0509060116	05/09/06	011602.35	24.08	122.19	32	6.1	58.1	87.8
689	0509101657	05/09/10	165747.27	4.86	95.04	41	5.8	90.3	82.7
692	0509131432	05/09/13	143257.81	8.07	91.91	30	5.5	90.1	78.2
699	0509202123	05/09/20	212337.56	12.71	40.53	10	5.5	131.1	40.3
700	0509210225	05/09/21	022508.11	43.89	146.15	103	6.1	30.5	83.9
702	0509231348	05/09/23	134831.41	16.13	-87.49	29	5.9	287.1	84.5
703	0509241924	05/09/24	192402.66	12.47	40.63	11	5.6	131.1	40.6

DAY	EVENT	DATE	OT	LAT	LON	D	MAG	BAZ	DIST
705	0509260155	05/09/26	015537.67	-5.68	-76.40	115	7.5	263.8	91.7
710	0510012154	05/10/01	215409.34	-23.61	-63.63	547	5.7	242.3	95.5
717	0510080350	05/10/08	035040.80	34.54	73.59	26	7.7	78.3	48.6
717	0510081046	05/10/08	104628.79	34.73	73.10	8	6.4	78.4	48.1
717	0510081225	05/10/08	122520.18	34.77	73.12	10	5.8	78.3	48.1
717	0510082113	05/10/08	211331.86	34.73	73.18	10	5.9	78.3	48.2
718	0510091920	05/10/09	192037.44	34.35	73.70	10	5.5	78.5	48.8
720	0510111505	05/10/11	150539.66	4.82	95.10	30	6.0	90.3	82.8
721	0510122023	05/10/12	202338.23	34.86	73.11	10	5.6	78.2	48.1
724	0510151006	05/10/15	100617.01	46.82	154.11	42	6.1	24.1	83.9
724	0510151551	05/10/15	155107.20	25.32	123.36	183	6.5	56.5	87.6
726	0510171923	05/10/17	192302.20	-17.77	-69.49	123	5.8	250.4	95.3
728	0510190233	05/10/19	023328.31	34.75	73.04	5	5.6	78.4	48.1
728	0510191144	05/10/19	114442.79	36.40	140.84	32	6.5	37.9	88.1
729	0510201526	05/10/20	152631.95	52.21	-169.04	35	5.7	359.7	84.1
731	0510221312	05/10/22	131247.81	37.15	140.93	53	5.6	37.4	87.5
732	0510231008	05/10/23	100814.74	37.38	134.56	380	6.0	41.4	84.4
732	0510231504	05/10/23	150420.89	34.85	73.04	10	5.6	78.3	48.0
737	0510282230	05/10/28	223058.23	11.07	-62.04	64	5.5	266.1	69.8
749	0511091133	05/11/09	113313.19	-1.02	-76.94	248	5.9	267.5	88.9
750	0511101929	05/11/10	192954.14	57.47	120.59	6	5.9	34.4	63.3
754	0511142138	05/11/14	213851.42	38.11	144.90	11	7.0	34.2	88.3
760	0511201253	05/11/20	125302.95	53.84	-164.09	30	6.2	356.8	82.3
761	0511211536	05/11/21	153630.98	31.02	130.00	145	6.2	48.3	87.1
767	0511271022	05/11/27	102219.19	26.77	55.86	10	6.1	99.7	40.1
767	0511271630	05/11/27	163037.56	26.84	55.81	10	5.5	99.6	40.0
772	0512021313	05/12/02	131309.52	38.09	142.12	29	6.5	36.1	87.2
775	0512051219	05/12/05	121956.62	-6.22	29.83	22	7.2	155.7	52.9
781	0512111554	05/12/11	155413.91	57.44	120.76	10	5.7	34.4	63.4
782	0512122101	05/12/12	210140.62	43.21	139.33	26	5.7	35.0	81.8
782	0512122147	05/12/12	214746.06	36.36	71.09	224	6.5	77.5	45.9
791	0512211432	05/12/21	143239.30	6.62	-82.75	10	6.0	277.0	87.8
793	0512232147	05/12/23	214728.00	-1.39	-77.52	192	6.1	267.6	89.5
800	0512301826	05/12/30	182643.91	7.53	-82.27	10	6.1	277.4	86.8
802	0601010847	06/01/01	084713.35	4.74	95.14	51	5.7	90.3	82.8
808	0601070223	06/01/07	022343.59	52.42	173.61	30	5.7	10.3	82.8
821	0601200853	06/01/20	085352.94	31.07	-41.42	10	5.7	270.7	42.4
822	0601210407	06/01/21	040704.74	13.03	93.27	52	5.8	85.4	75.8
824	0601232050	06/01/23	205044.98	6.86	-77.79	14	6.2	273.8	84.1
854	0602222219	06/02/22	221907.80	-21.32	33.58	11	7.5	156.9	68.4
860	0602280731	06/02/28	073102.65	28.12	56.87	18	6.2	97.2	40.0
875	0603151419	06/03/15	141948.69	-21.14	33.72	10	5.6	156.7	68.3
880	0603201740	06/03/20	174044.52	34.76	73.75	10	5.6	78.0	48.6
885	0603250728	06/03/25	072857.65	27.57	55.69	18	5.9	98.8	39.5
885	0603250955	06/03/25	095512.38	27.54	55.78	10	5.5	98.8	39.6
885	0603251000	06/03/25	100036.60	27.47	55.80	15	5.5	98.9	39.6

DAY	EVENT	DATE	OT	LAT	LON	D	MAG	BAZ	DIST
891	0603310117	06/03/31	011700.96	33.50	48.78	7	6.1	95.9	31.3
892	0604011002	06/04/01	100219.57	22.87	121.28	9	6.2	59.5	88.1
906	0604152240	06/04/15	224054.09	22.80	121.36	17	5.9	59.5	88.2
911	0604202325	06/04/20	232502.16	60.95	167.09	22	7.6	11.6	73.6
912	0604210432	06/04/21	043243.82	60.53	165.82	9	6.3	12.4	73.8
912	0604211114	06/04/21	111415.33	61.35	167.52	12	6.1	11.3	73.3
913	0604220721	06/04/22	072157.95	61.20	167.32	10	5.8	11.4	73.4
916	0604251826	06/04/25	182617.16	1.99	97.00	21	6.3	91.0	86.1
920	0604291658	06/04/29	165806.31	60.49	167.52	11	6.6	11.5	74.1
921	0604300043	06/04/30	004310.59	44.50	102.39	10	5.7	53.8	62.1
931	0605100242	06/05/10	024251.03	52.51	-169.26	18	6.4	359.9	83.8
932	0605111722	06/05/11	172254.14	23.31	94.32	48	5.7	76.6	69.8
934	0605130311	06/05/13	031142.94	5.51	94.44	45	5.9	90.2	81.8
937	0605161528	06/05/16	152825.92	0.09	97.05	12	6.8	92.3	87.4
943	0605221112	06/05/22	111200.38	60.77	165.74	16	6.7	12.3	73.6
943	0605221308	06/05/22	130801.67	54.28	158.43	184	6.2	18.5	78.2
949	0605280900	06/05/28	090012.45	19.16	121.18	23	5.6	62.1	90.8
957	0606050627	06/06/05	062707.96	1.17	-28.07	10	6.0	229.9	54.6
957	0606050634	06/06/05	063431.80	1.02	-28.16	10	5.6	229.9	54.8
961	0606092317	06/06/09	231727.88	-47.75	32.61	22	5.9	165.3	93.5
963	0606112001	06/06/11	200126.31	33.13	131.14	139	6.3	46.3	86.0
966	0606140418	06/06/14	041842.51	51.75	177.08	14	6.4	8.3	83.8
967	0606150649	06/06/15	064948.83	45.39	97.35	9	5.8	55.2	58.7
968	0606161710	06/06/16	171040.30	40.35	143.71	30	5.6	33.9	86.0
970	0606181828	06/06/18	182802.25	33.03	-39.70	10	5.9	272.1	40.1
974	0606221053	06/06/22	105311.57	45.42	149.34	95	6.1	27.7	83.7
979	0606271807	06/06/27	180722.73	6.50	92.79	28	6.2	90.6	79.9
980	0606282102	06/06/28	210209.20	26.82	55.90	10	5.8	99.6	40.1
983	0607011934	06/07/01	193439.61	51.06	-179.31	41	5.5	6.2	84.8
984	0607021720	06/07/02	172025.78	51.10	-179.36	49	5.6	6.2	84.8
990	0607082040	06/07/08	204000.98	51.21	-179.31	22	6.6	6.2	84.7
991	0607090416	06/07/09	041620.11	51.04	-179.17	19	5.5	6.1	84.9
1011	0607291953	06/07/29	195343.05	23.59	-63.92	10	5.8	277.7	63.0
1019	0608061816	06/08/06	181640.17	26.12	144.01	23	6.0	41.2	98.2
1024	0608111430	06/08/11	143040.69	18.56	-101.06	60	6.1	298.1	91.8
1029	0608161839	06/08/16	183900.38	-28.82	61.74	13	5.9	136.8	86.4
1030	0608171111	06/08/17	111135.54	55.62	161.69	55	6.1	16.2	77.7
1037	0608242150	06/08/24	215036.66	51.15	157.52	43	6.5	20.2	80.9
1039	0608262340	06/08/26	234039.47	51.33	-179.57	35	5.8	6.3	84.5
1039	0608262346	06/08/26	234618.52	51.38	-179.54	35	5.7	6.3	84.5
1044	0608312258	06/08/31	225825.80	28.80	130.03	33	5.6	49.7	88.8
1045	0609011025	06/09/01	102517.13	53.26	159.70	51	5.7	18.2	79.5
1045	0609011204	06/09/01	120422.17	53.97	-166.39	75	5.9	358.2	82.3
1061	0609170730	06/09/17	073011.10	-17.69	41.83	10	5.5	147.7	67.8
1062	0609180346	06/09/18	034601.54	51.64	-173.90	53	5.8	2.8	84.6

Attachment 3 - List of events used for SKS splitting analysis

DATE – origin date [yy/mm/dd]; **OT** – origin time [hhmmss.ss]; **LAT** – latitude [º]; **LON** – longitude [º]; **D** – depth [km]; **MAG** – moment magnitude; **BACK** – back-azimuth [º]; **DIST** – epicentral distance [º]

DATE	OT	LAT	LON	D	MAG	BAZ	DIST
2003/10/31	01:06:28	37.81	142.62	10	7.0	36.3	87.5
2004/01/11	04:32:47	-36.70	53.35	5	6.2	147.2	89.0
2004/02/05	21:05:02	-3.62	135.54	16	7.1	67.1	116.9
2004/02/07	02:42:35	-4.00	135.02	10	7.5	67.9	116.8
2004/02/21	02:34:42	-58.42	-14.96	10	6.6	193.8	104.3
2004/04/23	01:50:30	-9.36	122.84	65	6.7	81.5	112.1
2004/04/29	00:57:21	10.81	-86.00	10	6.2	282.6	87.6
2004/05/03	04:36:50	-37.69	-73.41	21	6.6	238.0	111.4
2004/07/25	14:35:19	-2.43	103.98	582	7.3	89.7	93.8
2004/09/05	10:07:07	33.07	136.62	14	7.2	43.1	88.7
2004/09/05	14:57:18	33.18	137.07	10	7.4	42.7	88.8
2004/09/06	12:42:59	-55.37	-28.98	10	6.9	202.3	104.6
2004/10/09	21:26:53	11.42	-86.67	35	7.0	283.5	87.6
2004/11/11	21:26:41	-8.15	124.87	10	7.5	79.0	112.7
2004/11/15	09:06:56	4.70	-77.51	15	7.2	272.3	85.7
2004/11/26	02:25:03	-3.61	135.40	10	7.2	67.3	116.8
2005/02/05	12:23:18	5.29	123.34	525	7.1	70.4	102.1
2005/03/02	10:42:12	-6.53	129.93	201	7.1	73.9	115.2
2005/04/10	10:29:11	-1.64	99.61	19	6.7	92.1	90.1
2005/05/14	05:05:18	0.59	98.46	34	6.8	91.3	87.8
2005/06/13	22:44:33	-19.99	-69.20	115	7.8	249.0	96.9
2005/06/15	02:50:53	41.30	-125.97	10	7.2	329.0	86.7
2005/08/07	02:17:46	-47.09	33.62	10	6.2	164.7	92.9
2005/08/16	02:46:28	38.28	142.04	36	7.2	36.5	86.9
2005/09/26	01:55:37	-5.68	-76.40	115	7.5	264.1	92.0
2005/10/29	04:05:56	-45.21	96.90	8	6.5	127.7	116.9
2006/01/02	06:10:49	-60.92	-21.58	10	7.4	196.0	107.9

Attachment 4 - Application of the Adaptive Stacking software on the selected events from the RETREAT experiment

Event num. **0411150906** magnitude 7.2 back-azimuth 272.0° epicentral distance 85.3°

Initial stack

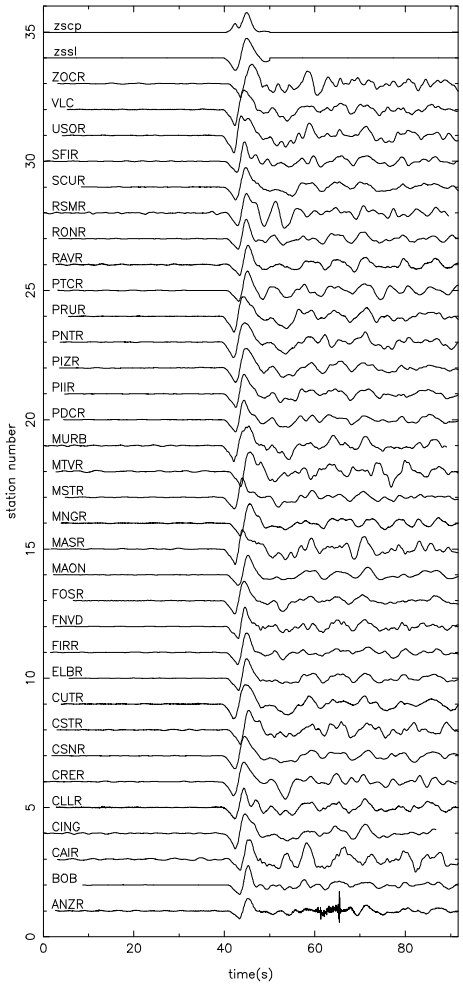

Final stack

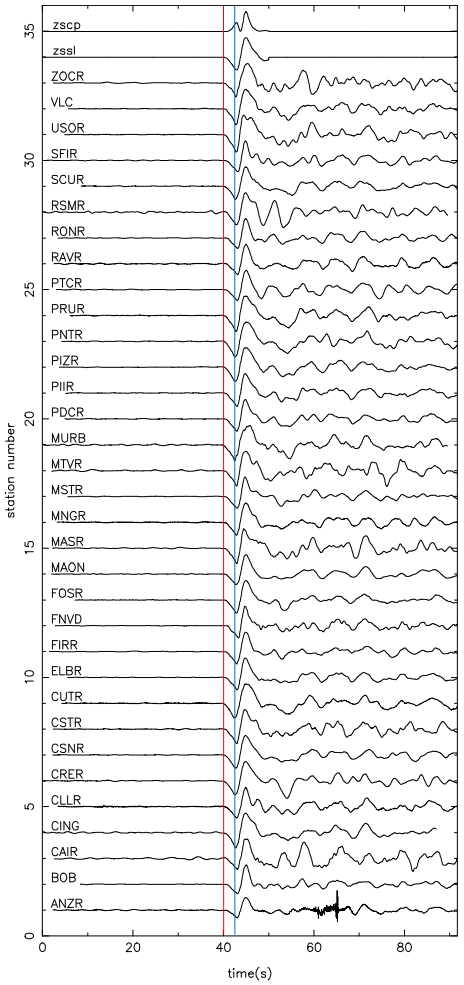

Final stack – detail

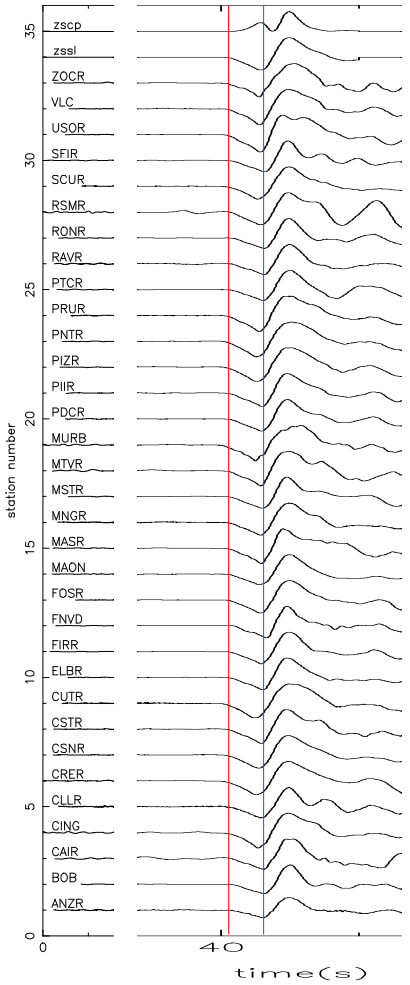

Event num. **0412061415** magnitude 6.8 back-azimuth 31.5° epicentral distance 84.4°

Initial stack

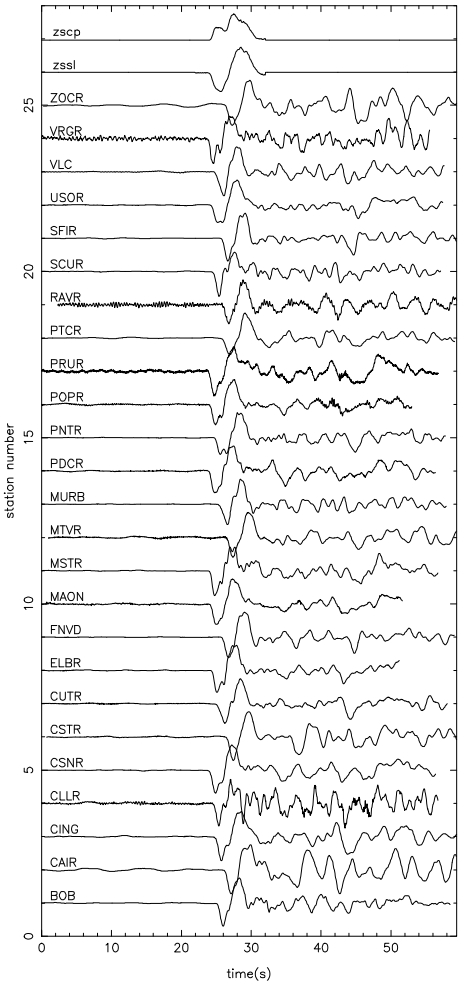

Final stack

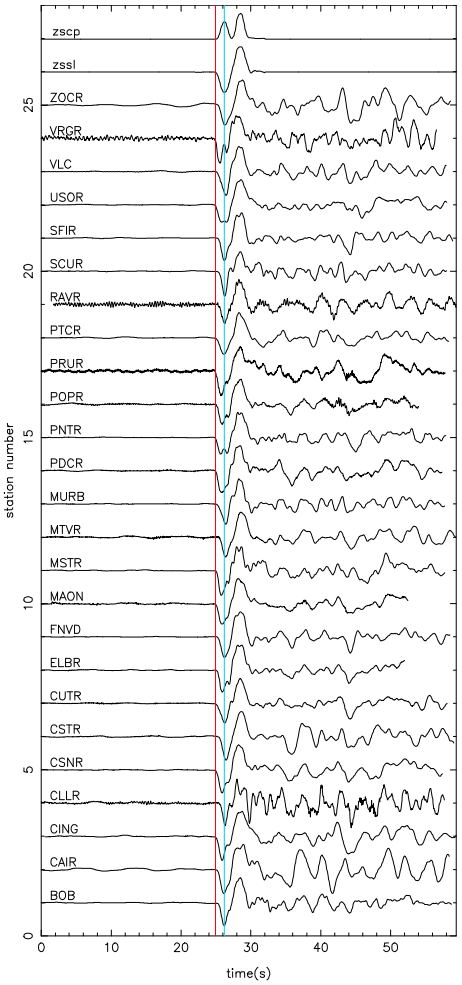

Final stack – detail

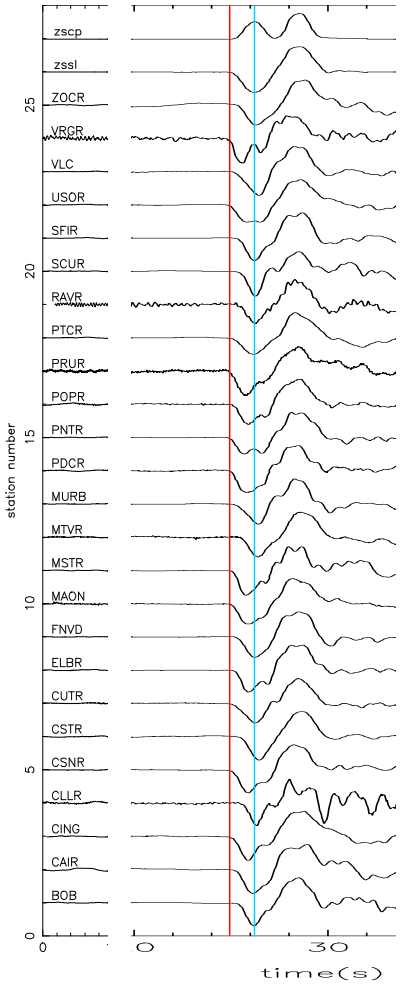

Event num. **0411281832** magnitude 7.0 back-azimuth 31.6° epicentral distance 84.2°

Initial stack

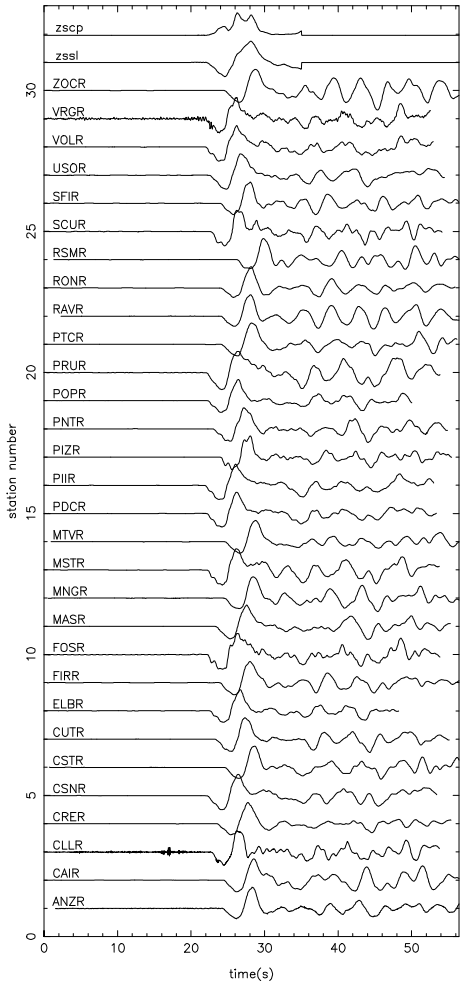

Final stack

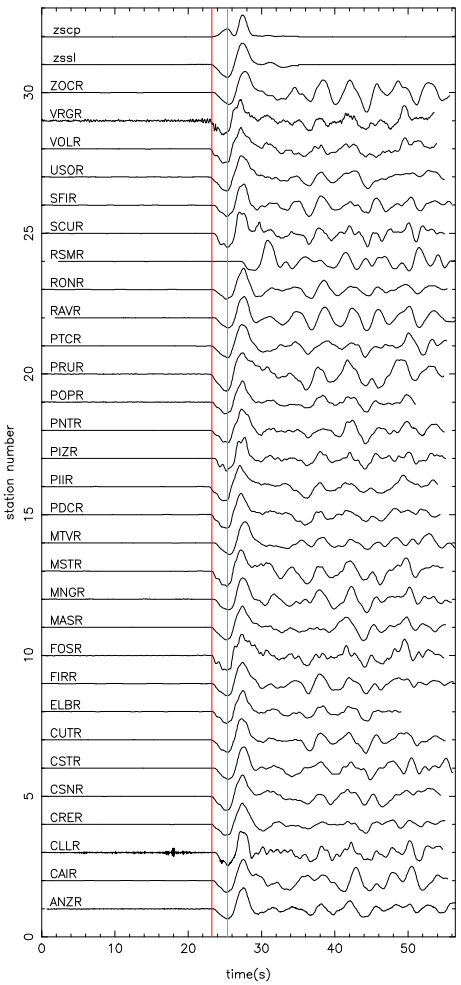

Final stack – detail

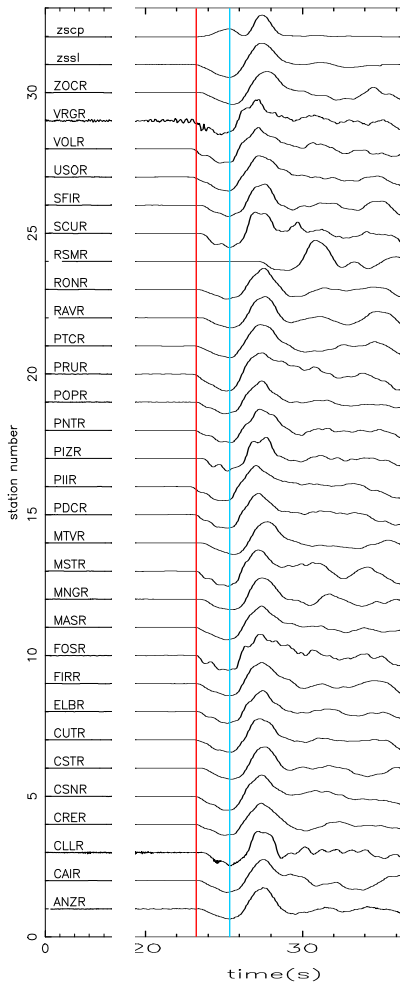

Event num. **0409062329** magnitude 6.6 back-azimuth 42.1° epicentral distance 89.0°

Initial stack

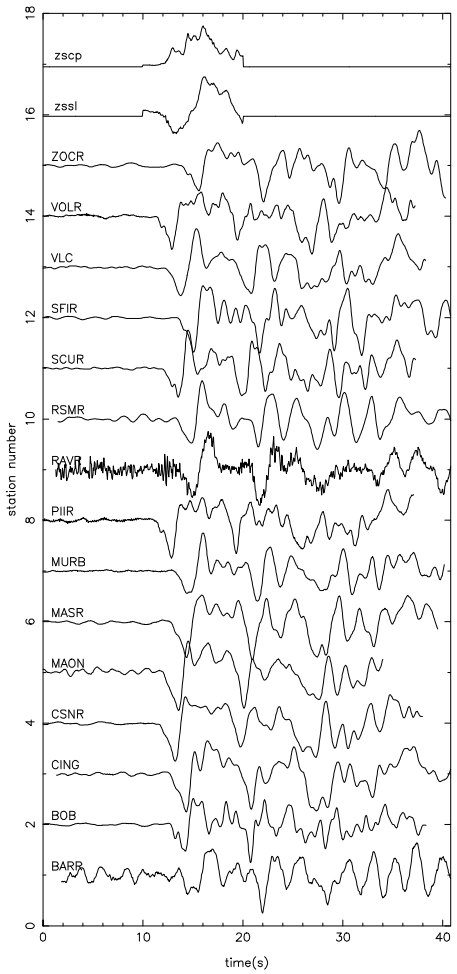

Final stack

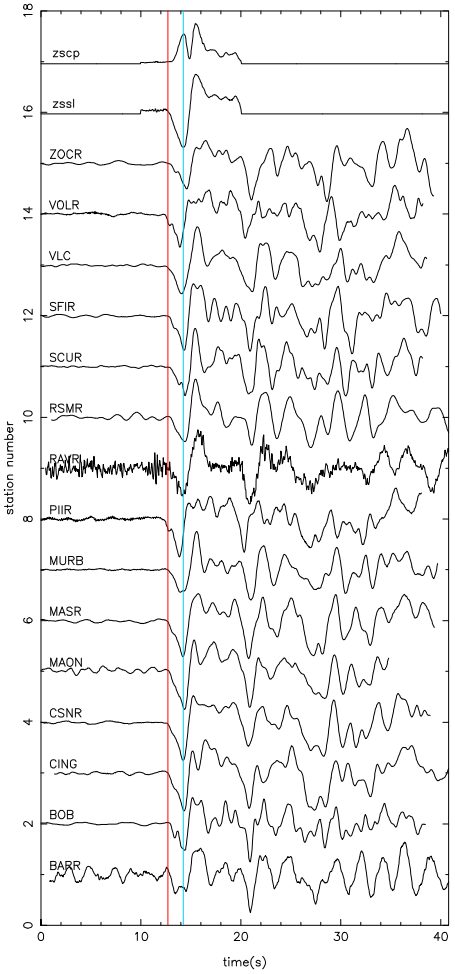

Final stack – detail

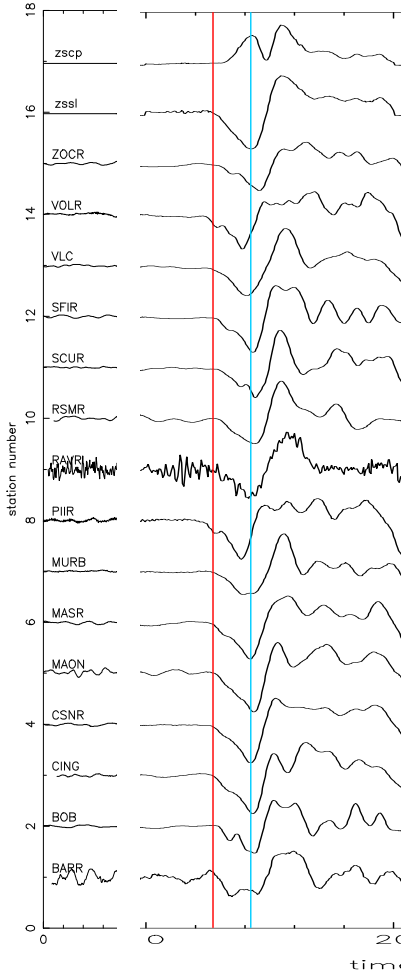

Event num. **0409192026** magnitude 6.2 back-azimuth 10.1° epicentral distance 83.0°

Initial stack

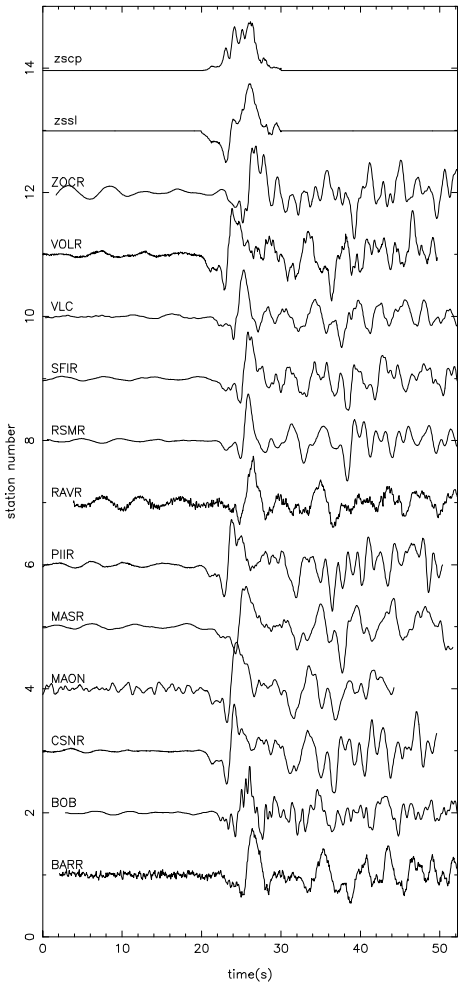

Final stack

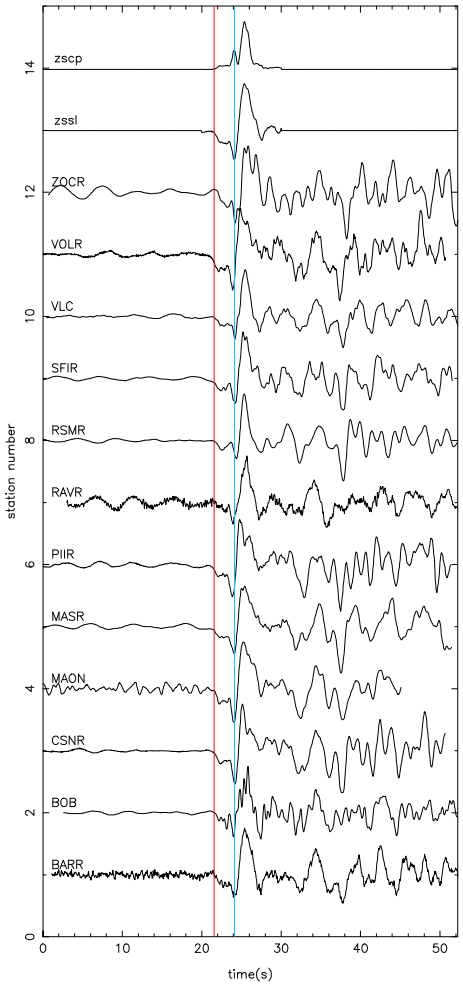

Final stack – detail

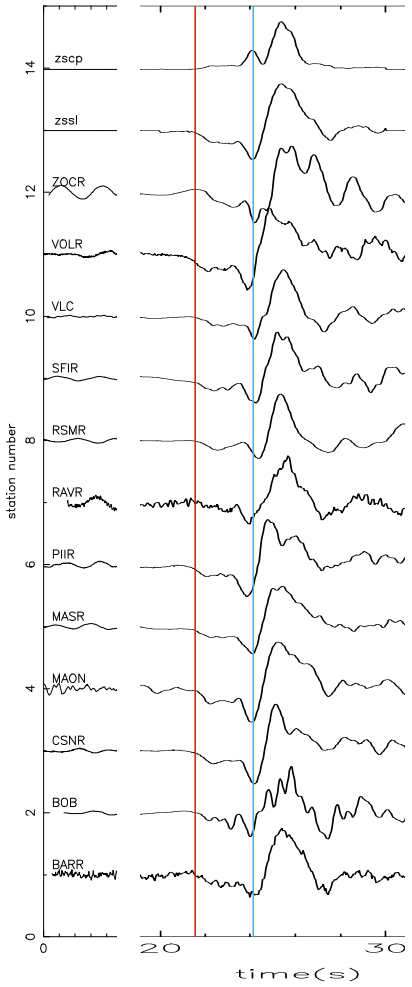

Event num. **0406290701** magnitude 6.3 back-azimuth 283.0° epicentral distance 88.0°

Initial stack

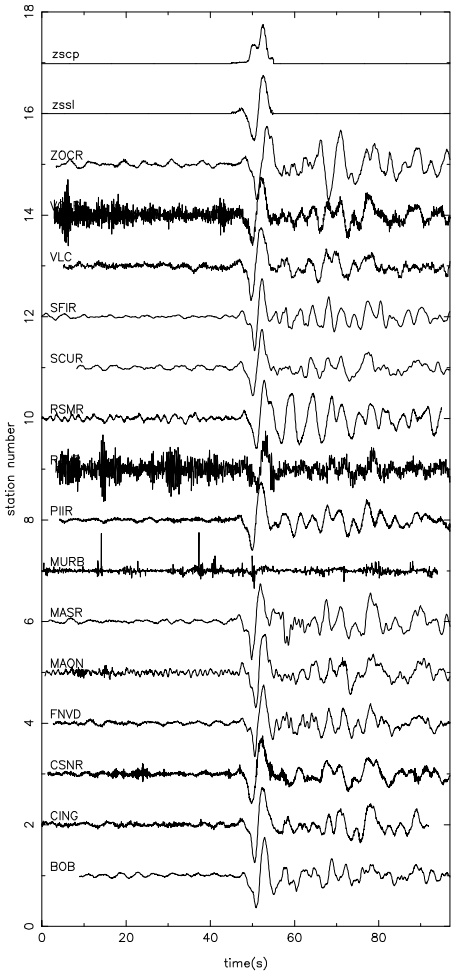

Final stack

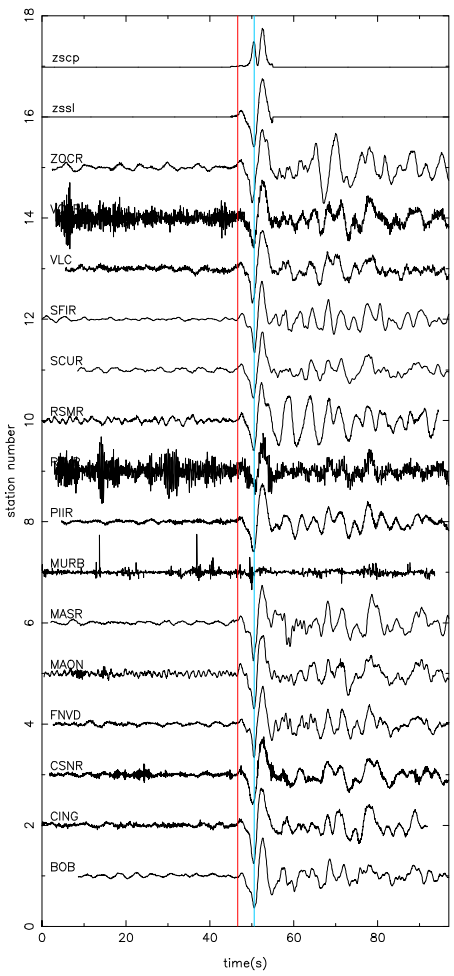

Final stack – detail

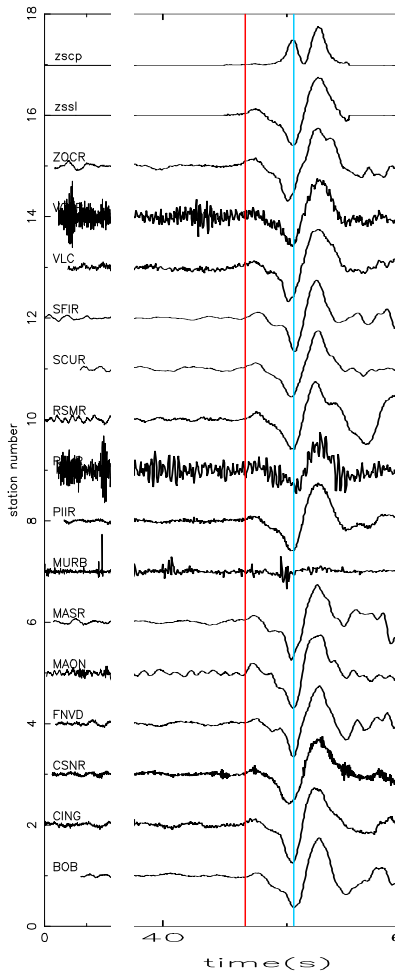

Event num. **0409051007 – short stack window** magnitude 7.2 back-azimuth 42.6° epicentral distance 88.8°

Initial stack

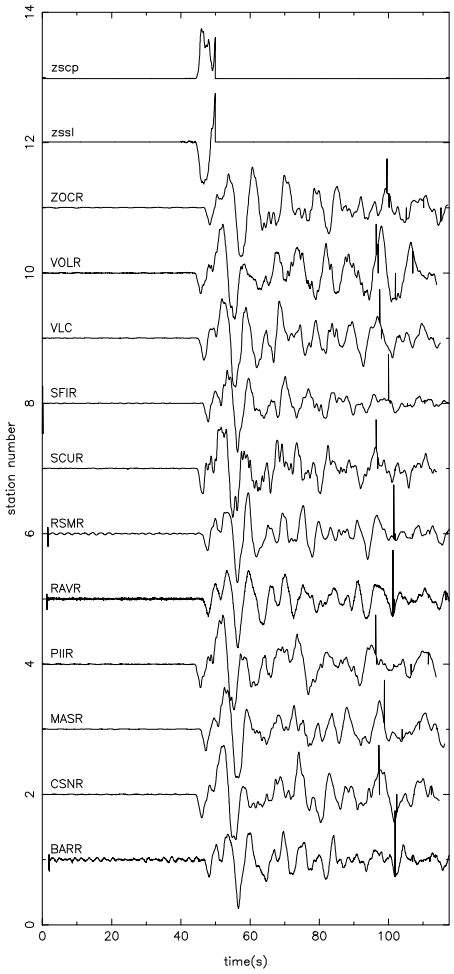

Final stack

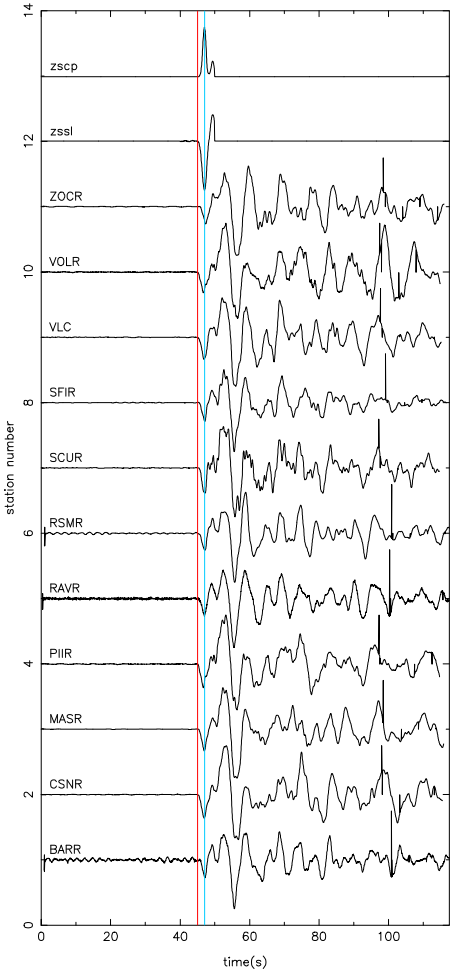

Final stack – detail

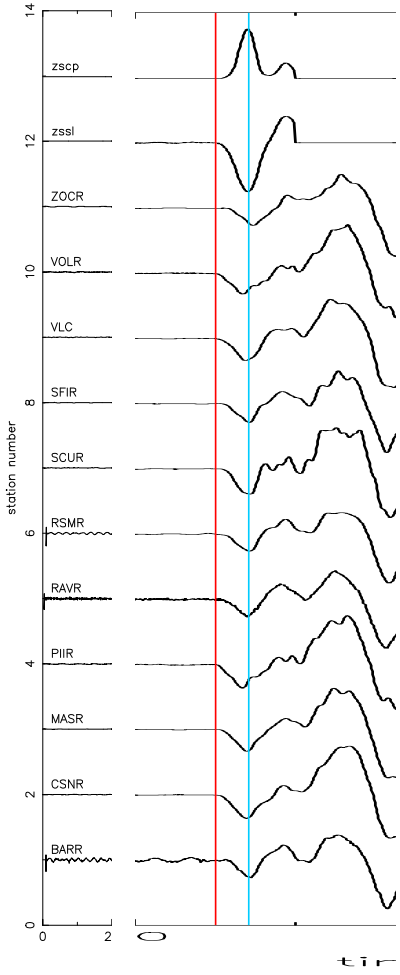

Event num. **0409051007 – long stack window** magnitude 6.3 back-azimuth 283.0° epicentral distance 88.0°

Initial stack

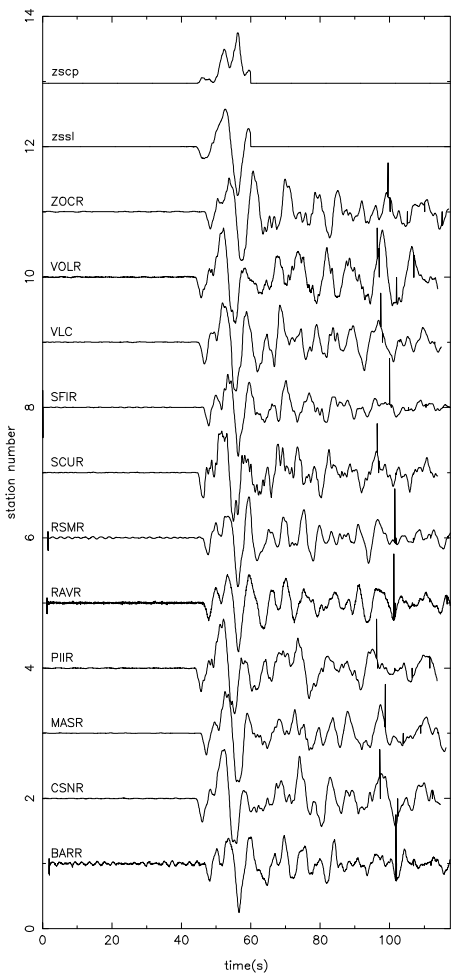

Final stack

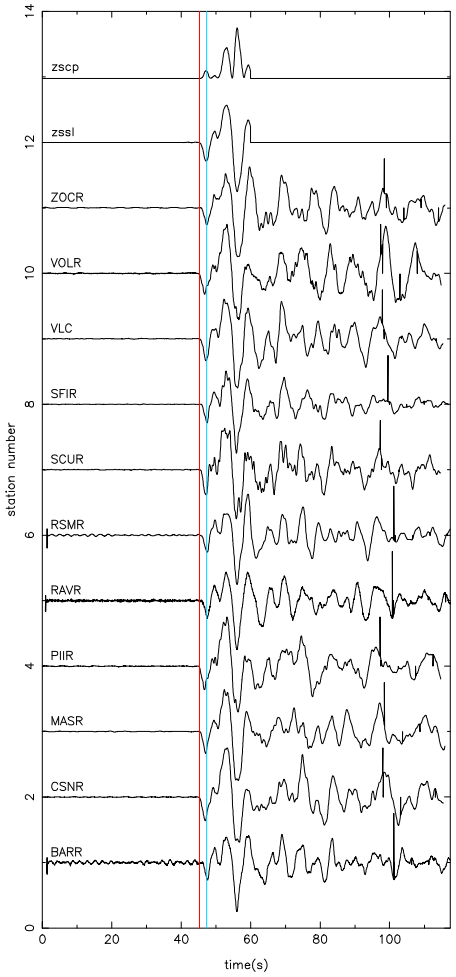

Final stack - detail

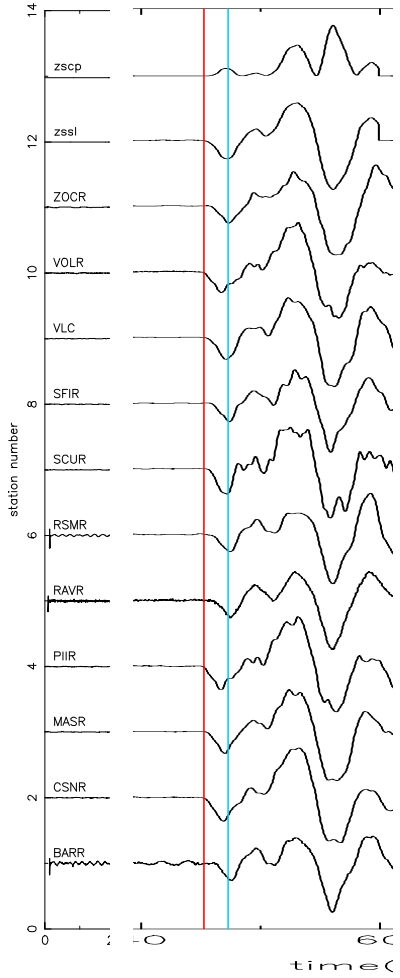

Event num. **0406280949** magnitude 6.8 back-azimuth 340.1° epicentral distance 77.0°

Initial stack

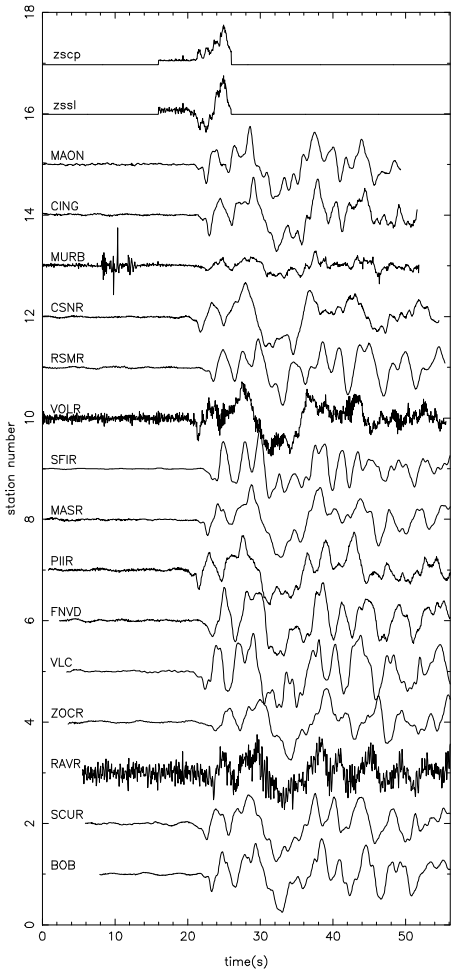

Final stack

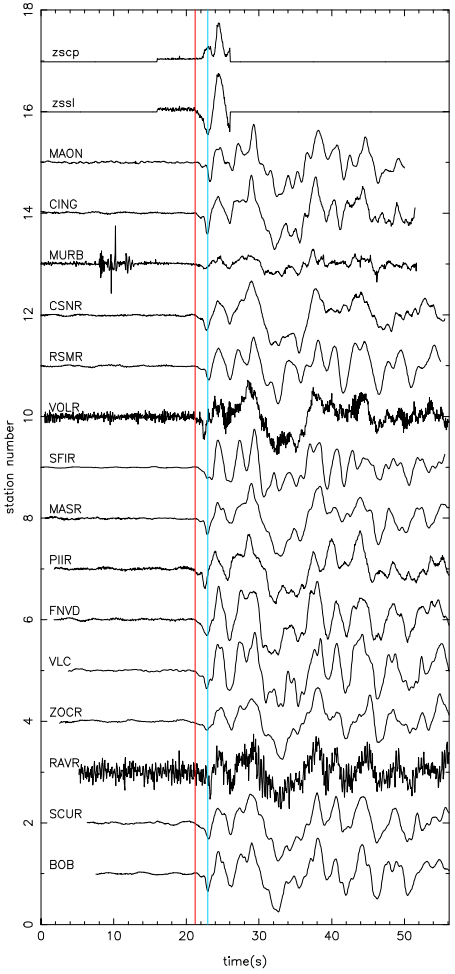

Final stack – detail

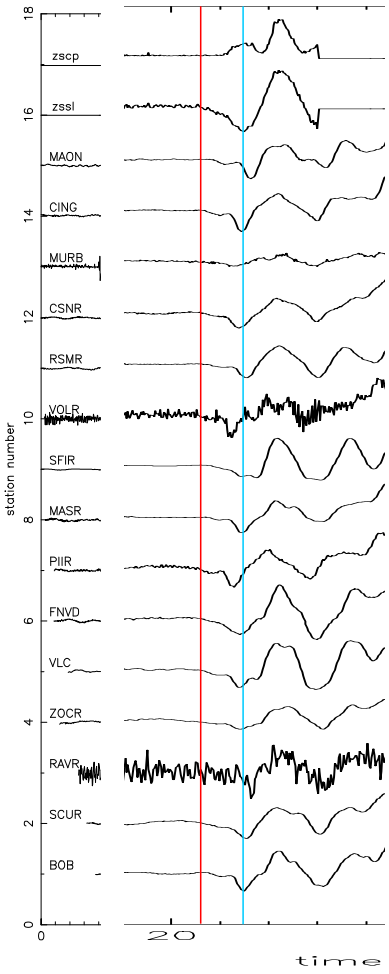

Event num. **0406280949 – short period** magnitude 6.8 back-azimuth 340.1° epicentral distance 77.0°

Initial stack

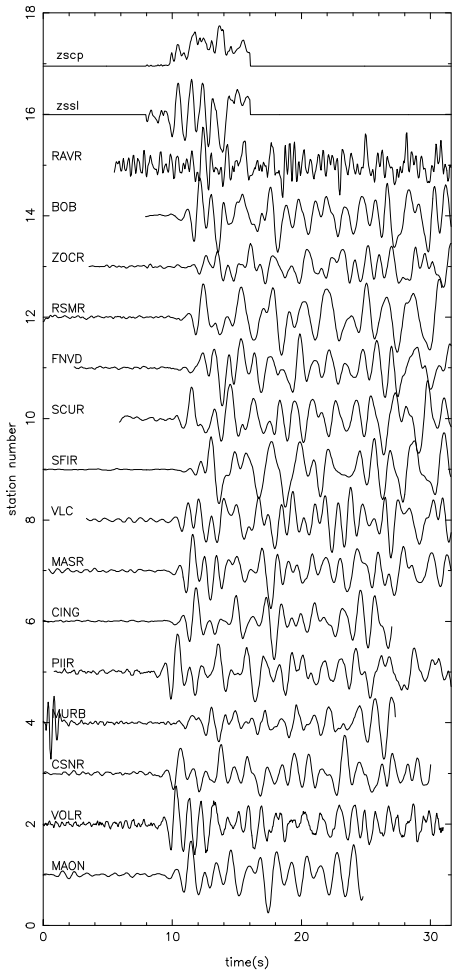

Final stack

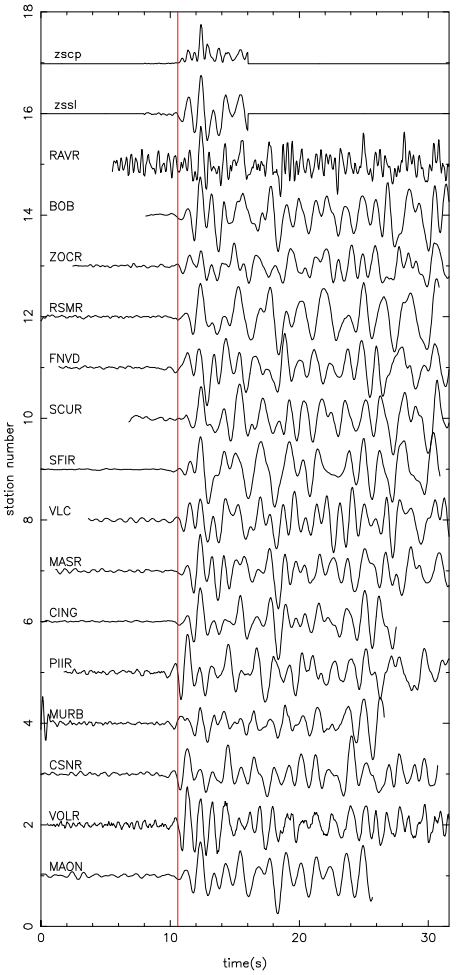

Final stack – detail

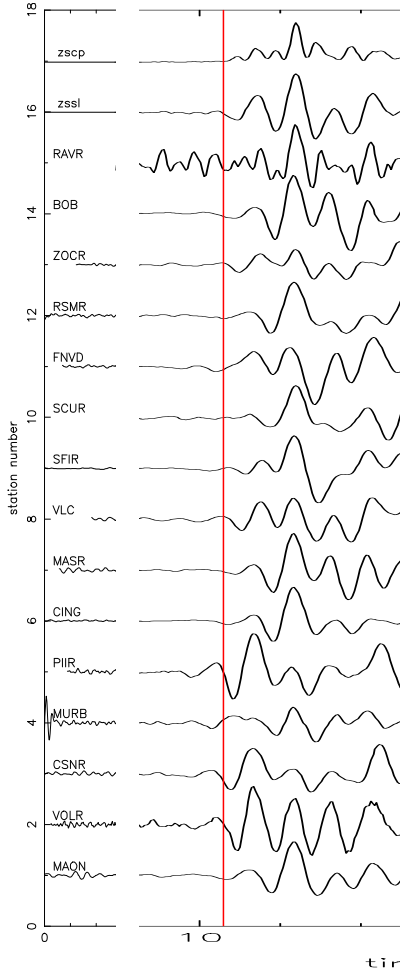

Attachment 5 - Examples of application of the Autopick software on the seismograms from the RETREAT experiment

Event num. **0412061415** 1st according to quality list

All stations

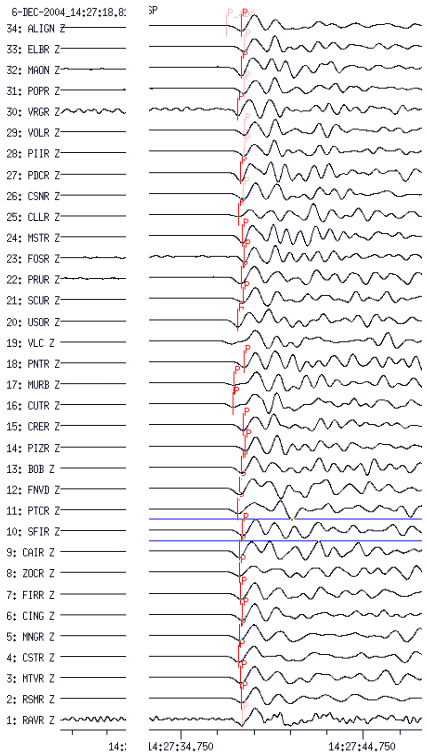

Detail

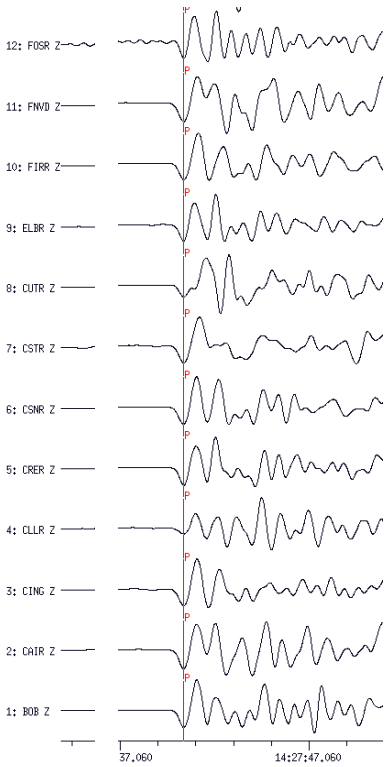

Trace ALIGN

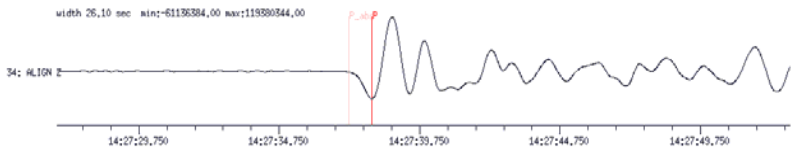

Event num. **0411281832** 21st according to quality list

All stations

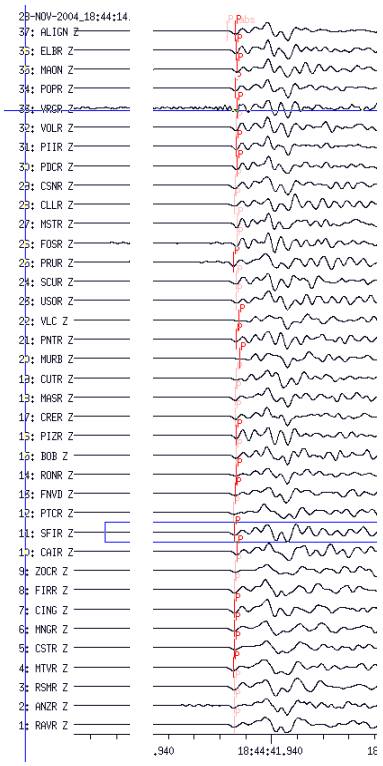

Detail

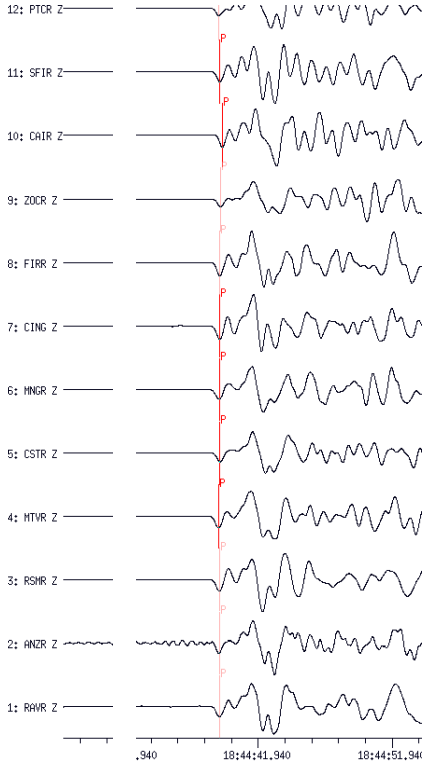

Trace ALIGN

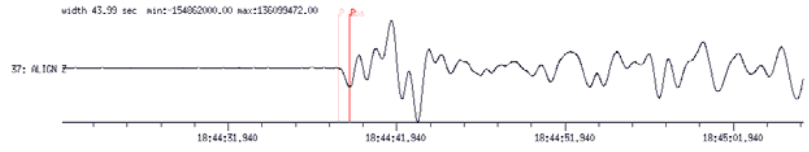

Event num. **0409192026** 55th according to quality list

All stations

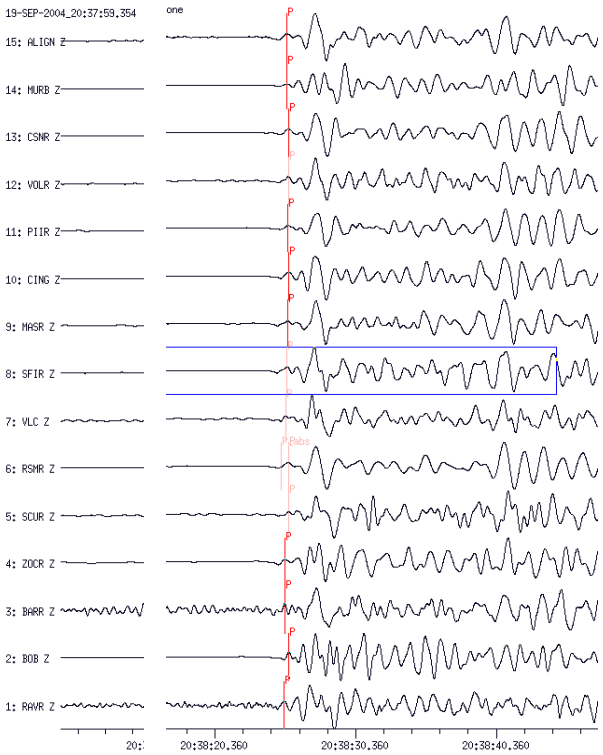

Trace ALIGN

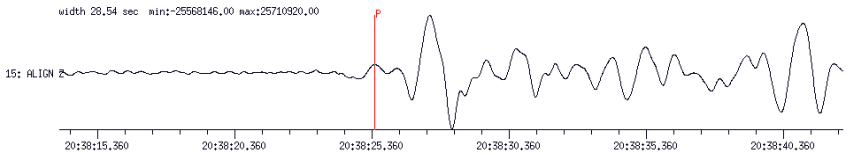

Event num. **0409062329** 76th according to quality list

All stations

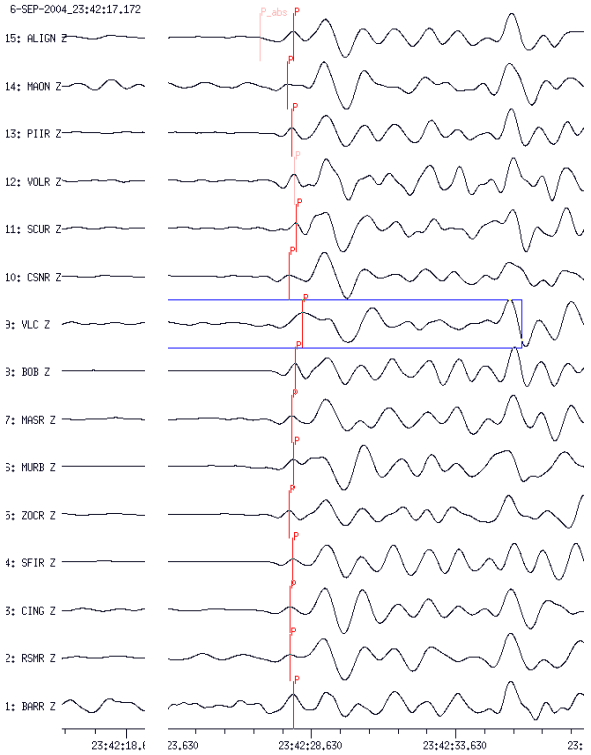

Trace ALIGN

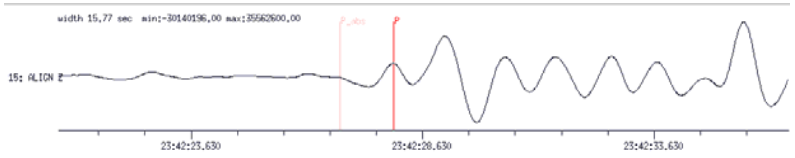

Event num. **0406290701** 106th according to quality list

All stations

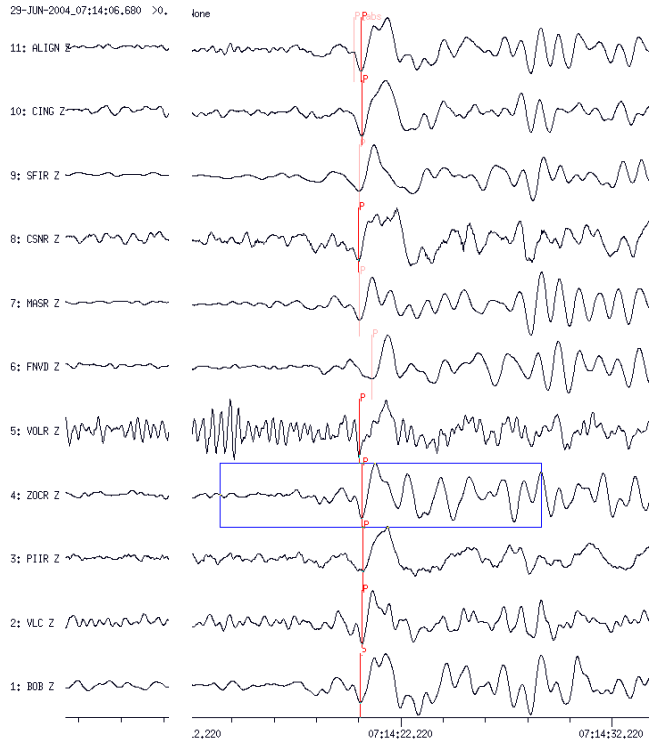

Trace ALIGN

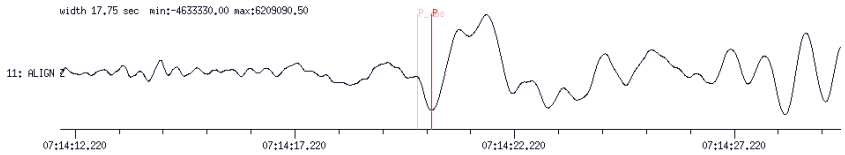

Bibliography

Ando M., Ishikawa Y. and Yamazaki F. (1983): Shear-wave polarization anisotropy in the mantle beneath Honshu, Japan. *J. Geophys. Res.* **88**, 5850-5864.

Ando M. (1984): ScS polarization anisotropy around Pacific Ocean. *J. Phys. Earth* **32**, 179-195.

Babuška V., Plomerová J. and Šílený J. (1984a): Spatial variations of P residuals and deep structure of the European lithosphere. *Geophys. J. R. Astron. Soc.* **79**, 363-383.

Babuška V., Plomerová J. and Šílený J. (1984b): Large-scale oriented structures in the subcrustal lithosphere of central Europe. *Ann. Geophys.* **2**, 649-662.

Babuška V. and Plomerová J. (1989): Seismic anisotropy of the subcrustal lithosphere in Europe: another clue to recognition of accreted terranes? In: Deep structure and past kinematics of accreted terranes, Hillhouse J.W. (editor). *Geophys. Monograph 50, IUGG* **5**, Washington DC, 209-217.

Babuška V. and Plomerová J. (1990): Tomographic studies of the upper mantle beneath Italian region. *Terra Nova* **2**, 569-576.

Babuška V. and Cara M. (1991): Seismic anisotropy in the Earth. Kluwer Academic Publishers, Dordrecht, 217 pp.

Babuška V. and Plomerová J. (1992): The lithosphere in central Europe - seismological and petrological aspects. *Tectonophysics* **207**, 141-163.

Babuška V. and Plomerová J. (1993): Lithosphere thickness and velocity anisotropy - seismological and geothermal aspects. *Tectonophysics* **225**, 79-89.

Babuška V., Plomerová J. and Šílený J. (1993): Models of seismic anisotropy in deep continental lithosphere. *Phys. Earth Planet. Inter.* **78**, 167-191.

Babuška V. and Plomerová J. (2000): Saxothuringian-Moldanubian suture and predisposition of seismicity in the western Bohemian Massif. *Studia geoph. et geodaet.* **44**, 292-306.

Babuška V. and Plomerová, J. (2001): Subcrustal lithosphere around the Saxothuringian-Moldanubian Suture Zone - a model derived from anisotropy of seismic wave velocities. *Tectonophysics* **332**, 185-199.

Babuška V., Plomerová J., Vecsey L., Granet, M. and Achauer U. (2002): Seismic anisotropy of the French Massif Central and predisposition of Cenozoic rifting and volcanism by Variscan suture hidden in the mantle lithosphere. *Tectonics* **21**, U407-U429.

Babuška V. and Plomerová J. (2006): European mantle lithosphere assembled from rigid microplates with inherited seismic anisotropy. *Phys. Earth Planet. Inter.* **158**, 264-280.

Babuška V., Plomerová J. and Vecsey L. (2008): Mantle fabric of western Bohemian Massif (central Europe) constrained by 3D seismic P and S anisotropy. *Tectonophysics* **462**, 149-163.

Benoit H.M., Torpey M., Liszewski K., Levin V. and Park J. (2011): P ans S wave upper mantle seismic velocity structure beneath the Northern Apennines: New evidence for the end of subduction. *Geochemistry, Geophysics, Geosystems* **12**, 1-19.

Bock G. and SVEKALAPKO Seismic Tomography Working Group (SSTWG) (2001): Seismic probing of Archean and Proterozoic Lithosphere in Fennoscandia. *EOS, Transactions, AGU* **82**, 621-629.

Bormann P., Grünthal G., Kind R. and Montag H. (1996): Upper mantle anisotropy beneath central Europe from SKS wave splitting: effects of absolute plate motion and lithosphere-asthenosphere boundary topography? *J. Geodynamics* **22**, 11-32.

Bormann P. (2002): New Manual of Seismological Observatory Practice. GFZ Potsdam.

Brechner S., Klinge K., Krüger F. and Plenefisch T. (1998): Backazimuthal variations of splitting parameters of teleseismic SKS phases observed at the broadband stations in Germany. *Pure and Appl. Geophys.* **151**, 305-331.

Christensen N. I. (1984): The magnitude, symmetry and origin of upper mantle anisotropy based on fabric analyses of ultramafic tectonites. *Geophys. J. R. Astron. Soc.* **76**, 89-111.

Civello S., Margheriti L. (2004): Toroidal mantle flow around the Calabrian slab (Italy) from SKS splitting. *Geophys. Res. Lett.* **31**, L10601.

Cimini G.B. and Marchetti A. (2006): Deep structure of peninsular Italy from seismic tomography and subcrustal seismicity. *Ann. Geophys.* **49** (Suppl. 1), 331-345.

Cotte N., Pedersen H.A. and TOR working group, 2002. Sharp contrast in lithospheric structure across the Sorgenfrei_Tornquist zone as inferred by surface wave analysis of TOR1. *Tectonophysics* **360**, 75-88.

Crotwell H. P., Owens T. J. and Ritsema J. (1999): The TauP Toolkit: Flexible seismic travel-time and ray-path utilities. *Seismological Research Letters* **70**, 154–160.

Dewey J.F., Helman M.L., Turco E., Hutton D.H.W. and Knott S. (1989): Kinematics of the Western Mediterranean. In: Coward, M.P., Dietrich, D. (editors.). *Alpine Tectonics. Geol. Soc. Lond.* Spec. Publ. **45**, 265–283.

Di Stefano R., Bianchi I., Ciaccio M.G., Carrara G. and Kissling E. (2011): Crustal thickness and 3D Moho geometry in Italy: new constraints from controlled-source seismology and receiver functions. Submitted.

Doglioni C. (1991): A proposal of kinematic modelling for W-dipping subductions possible applications to the Tyrrhenian–Apennines system. *Terra Nova* **3**, 423–434.

Eken T., Plomerová J., Roberts R., Vecsey L., Babuška V., Shomali H. and Bodvarsson R. (2010): Seismic anisotropy of the mantle lithosphere beaneath the Swedish National Seismological Network (SNSN). *Tectonophysics* **480**, 241-258.

Faccenna C., Jolivet L., Piromallo C. and Morelli A. (2003): Subduction and the depth of convection in the Mediterranean mantle. *J. Geophys. Res.* **107**, 2099.

Gregersen S, Voss P. and Tor Working Group (2002): Project TOR: on the sharpness of the deep lithosphere transition across Germany-Denmark-Sweden. *Tectonophysics*, 61-73.

Iyer H. and Hirahara K. (1993): Seismic tomography. Chapmann & Hall, London, 842 pp.

Judenherc S., Granet M., Brun J.P., Poupinet G., Plomerová J., Mosquet A. and Achauer U. (2002): Images of lithospheric heterogeneities in the Armorican segment of the Hercynian range in France. *Tectonophysics* **358**, 121-134.

Lucente F.P., Chiarabba G.B. and Giardini D. (1999): Tomographic constraints on the geodynamic evolution of the Italian region. *J. Geophys. Res.* **104**, 20307-20327.

Kennett B.L.N. (1998): Seismic wave propagation and seismic tomography. Research School of Sci., Australan National University, Canberra, 116 pp.

Kennett B.L.N. (1991): IASPEI 1991 Seismological tables. Research School of Sci., Australan National University, Canberra, 167 pp.

Koulakov I., Kaban M.K., Tesauro M. and Cloetingh S. (2009): P- and S-velocity anomalies in the upper mantle beneath Europe from tomographic inversion of ISC data. *Geophys. J. Int.* **179**, 345-366.

Kumazawa M. and Anderson O.L. (1969): Elastic moduli, pressure derivatives and temperature derivatives of single-crystal olivine and single crystal forsterite. *J. Geophys. Res.* **74**, 5961-5972.

Levin V., Menke W., Park J. (1999): Shear wave splitting in Appalachians and Urals: a case of multilayer anisotropy. J. Geophys. Res. 104, 17975-17994.

Lucente F.P., Margheriti L., Piromallo C. and Barruol G. (2006): Seismic anisotropy reveals the long route of the slab through the western–central Mediterranean mantle. *Earth Planet. Sci. Lett* **241**/3-4 517–529.

Makeyeva L., Plešinger A. and Horálek J. (1990): Azimuthal anisotropy beneath the Bohemian Massif from broad-band seismograms of SKS waves. *Phys. Earth Planet. Inter.* **62**, 298-306.

Margheriti L., Nostro C., Cocco M. and Amato A. (1996): Seismic anisotropy beneath the Northern Apennines (Italy) and its tectonic implications. *Geophys. Res. Lett.* **23**, 2721–2724.

Margheriti L., Lucente L. and Pondrelli S. (2003): SKS splitting measurements in the Apenninic–Tyrrhenian domain (Italy) and their relation with lithospheric subduction and mantle convection. *J. Geophys. Res.* **108**, 2218.

Margheriti L., Pondrelli S., Piccinini D., Agostinetti N.P., Giovani L., Salimbeni S., Lucente F.P., Amato A., Baccheschi P., Park J., Brandon M., Levin V., Plomerová J., Jedlička P., Vecsey L., Babuška V., Fiaschi A., Carpani B. and Ulbricht P. (2006): The subduction structure of the Nothern Apennines: results from the RETREAT seismic deployment. *Annals of geophysics* **49**, 1119-1131.

Munzarová H. (2009): Automatizace měření časů seismických vln zaregistrovaných při pasivních experimentech (RETREAT, Itálie). Bachelor thesis, Charles University, Department of Geophysics, Prague.

Park J. and Levin V. (2002): Seismic anisotropy: tracing plate dynamics in the mantle. *Science* **296**, 485-489.

Piromallo C. and Morelli A. (2003): P wave tomography of the mantle under the Alpine-Mediterranean area. *J. Geophys. Res.* **108**, 2065.

Plomerová J., Šílený J. and Babuška V. (1996): Joint interpretation of upper mantle anisotropy based on teleseismic P-travel time delays and inversion of shear-wave splitting parameters. *Phys. Earth. Planet. Int.* **95**, 293-309.

Plomerová J., Babuška V., Šílený J. and Horálek J. (1998): Seismic anisotropy and velocity variations in the mantle beneath the Saxothuringicum-Moldanubicum contact in central Europe. *Pure and Appl. Geophys.* **151**, 365-394.

Plomerová J., Arvidsson R., Babuška V., Granet M., Kulhánek O., Poupinet G. and Šílený J. (2001): An array study of lithospheric structure accross the Protogine Zone, Varmland, south-central Sweden - signs of a paleocontinental collision. *Tectonophysics* **332**, 1-21.

Plomerová J., Babuška V., Vecsey L., Kouba D. and TOR working group (2002): Seismic anisotropy of the lithosphere around the Trans-European Suture Zone (TESZ) based on teleseismic body-wave data of the Tor experiment. *Tectonophysics* **360**, 89-114.

Plomerová J., Babuška V., Vecsey L., Kozlovskaya E., Raita T. and SSTWG (2006a): Proterozoic-Archean boundary in the upper mantle of eastern Fennoscandia as seen by seismic anisotropy. *J. Geodyn.* **41**, 400-410.

Plomerová J., Margheriti L., Park J., Babuška V., Pondrelli S., Vecsey L., Piccinini D., Levin V., Baccheschi P. and Salimbeni S. (2006b): Seismic Anisotropy beneath the Northern Apennines (Italy): Mantle Flow or Lithosphere Fabric? *Earth Planet. Sci. Lett*. **247,** 157-170.

Plomerová J. and Babuška V. (2010): Long memory of mantle lithosphere fabric - European LAB constrained from seismic anisotropy. **Lithos** *120*, 131-143.

Rawlinson N. and Kennett B.L.N. (2004): Rapid estimation of relative and absolute delay times across a network by Adaptive Stacking. *Geophys. J. Inter*. **157**, 332-340.

Salimbeni S., Pondrelli S., Margheriti L., Levin V., Park J., Plomerová J. and Babuška V. (2007): Abrupt change in mantle fabric across Northern Apennines detected using seismic anisotropy. *Geophys. Res. Letters* **34**, L07308.

Salimbeni S., Pondrelli S., Margheriti L., Park J. and Levin V. (2008): SKS splitting measurements beneath Northern Apennines region: A case of oblique trench-retreat. *Tectonophysics* **462**, 68-82.

Sandvol E. and Hearn T. (1994): Bootstrapping shear-wave splitting errors. *Bull. Seismol. Soc. Am.* **84**, 1971-1977.

Savage M.K. and Silver P.G. (1993): Mantle deformation and tectonics: constraints from seismic anisotropy in western United States. *Phys. Earth Planet. Inter.* **78**, 207-227.

Savage M.K. (1999): Seismic anisotropy and mantle deformation: what have we learned from shear wave splitting? *Rev. Geophys.* **37**, 65-106.

Serpelloni E., Anzidei M., Baldi P., Casula G. and Galvani A. (2005): Crustal velocity and strain-rate fields in Italy and surrounding regions: new results from the analysis of permanent and non-permanent GPS networks. *Geophys. J. Int.* **161**, 861-880.

Silver P.G. and Chan W.W. (1991): Shear wave splitting and subcontinental mantle deformation. *J. Geophys. Res.* **96**, 16429-16454.

Silver P.G. and Savage M.K. (1994): The interpretation of shear-wave splitting parameters in the presence of two anisotropic layers. *Geophys. J. Int.* **119**, 949-963.

Silver P.G. (1996): Seismic anisotrpy beneath the continents: probing the depths of geology. *Annu. Rev. Earth Planet. Sci.* **24**, 385-432.

Sobolev S.V., Zeyen H., Granet M., Achauer U., Bauer Ch., Werling F., Altherr R. and, Fuchs K. (1997): Upper mantle temperatures and lithosphere–asthenosphere system beneath the French Massif Central constrained by seismic, gravity, petrological and thermal observations. *Tectonophysics* **275**, 143–164.

Spakman W. and Wortel R. (2004): A tomographic view on Western Mediterranean Geodynamics, The TRANSMED Atlas, The Mediterranean Region from Crust to Mantle. Cavazza W., Roure F., Spakman W., Stampfli G.M., Ziegler P. (editors). 31-52.

Stammler K. (1993): Seismichandler programmable multichannel data handler for interactive and automatic processing of seismological analyses. *Computers & geosciences* **19**, 135-140.

Stampfli G. and Borel G. (2002): A plate tectonic modelfor the Paleozoic and Mesozoic constrained by dynamic plate boundaries and restored synthetic oceanic isochrones. Earth Planet. Sci. Lett. 196, 17-33.

Šílený J. and Plomerová J. (1996): Inversion of shear-wave splitting parameters to retrieve three-dimensional orientation of anisotropy in contitnental lithosphere. *Phys. Earth Planet. Inter.* **95**, 277-292.

Van Decar J.C. and Crosson R.S. (1990): Determination of teleseismic relative phase arrival times using multi-channel cross correlation and least squares. *Bull. seism. Soc. Am.* **80**, 150-169

Vecsey L., Plomerová J. and Babuška V. (2008): Shear-wave splitting measurements - Problems and solutions. *Tectonophysics* **462**, 178-196.

Vinnik L.P., Kosarev G.L. and Makeyeva L.I. (1984): Anisotropy of the lithosphere from the observation of SKS and SKKS. *Proc. Acad. Sci. USSR* **278**, 1335-1339 (in Russian).

Vinnik L.P., Makeyeva L.I., Milev A. and Usenko A.Y. (1992): Global patterns of azimuthal anisotropy and deformations in the continental mantle. Geophys. J. Int. 111, 433-447.

Vinnik L.P., Krishna V.G., Kind R. Bormann P. and Stammler K. (1994): Shear wave splitting in the records of the German regional seismic network. Geophys. Res. Lett. 21, 457-460.

Wortel M. and Spakman W. (2000): Subduction and slab detachment in the Mediterranean–Carpathian region. *Science* **290**, 1910–1917.